Università Campus Bio-Medico di Roma

Corso di dottorato di ricerca in
Bioingegneria e Bioscienze
XXXI ciclo a.a. 2015-2016

Patient-tailored bidirectional interfaces for rehabilitation and assistive robots

Clemente Lauretti

Coordinatore
Prof. Giulio Iannello

Tutore
Prof. Loredana Zollo

28/05/2019

Dedicata ai miei nonni,

Clemente, Rita, Tullio e Franca.

Abstract

Bidirectional interfaces, which combine recording and stimulating systems in so-called closed-loop devices, are the new generation of interfaces. In order to guarantee attentive usage and fine control of the device, they are typically tailored on the users' particular needs and are designed by taking into account users' residual physical and cognitive abilities.
Ambition of this thesis is to design and develop a patient-tailored bidirectional interface for rehabilitation and assistive robots that i) is adaptable to the user's residual functional and motor capabilities and ii) works well in unstructured environments and with different robot types (e.g. manipulators, exoskeletons or prostheses).
The developed bidirectional interface is composed of two main modules, namely the human-machine interface for the device control and the interface for sensory feedback.
The human-machine interface for the device control was designed to be used by patients with different level of disabilities to drive their rehabilitation or assistive robot, e.g. an upper-limb prosthesis, a robotic manipulator or an upper-limb exoskeleton, both continuously and by means of a trigger-based approach.
The interface proposed in this work is based on the coupled use of myoelectric and magneto-inertial sensors. It was first designed to be used by trans-humeral amputees to control their prosthetic device. In particular, with the proposed approach the user could operate the elbow flexion-extension, wrist prono-supination and hand opening-closing by exploiting the residual stump motions combined to the myoelectric activity of two target muscles, i.e. biceps and triceps. The proposed control interface was tested by eight healthy subjects who were asked to drive a trans-humeral prostesis in a virtual environment. A comparative analysis between the proposed control and the traditional myoelectric control used in literature to drive commercially available prostheses was carried out. Results demonstrated that the user, by using the proposed method, could manage simultaneous movements and more physiological reaching tasks compared to the traditional myoelectric control that enables only sequential movements.
Subsequently, adaptability of the proposed control interface to patients with different levels of disability and different robot types were demonstrated. It was tested on people with severe motor disability to control their robotic rehabilitation/assistive device, such as a manipulator

or an upper-limb exoskeleton, both continuously and by means of a trigger-based approach. Two experimental sessions were carried out.

The first experimental session was aimed to compare the proposed interface, based on magneto inertial sensors and myoelectric electrodes, to a standard interface made of the voice recognizer. Sixteen healthy subjects were asked to continuously control the motion of a robotic manipulator, by using the two control interfaces, for assistive purposes. The obtained results pointed out that performance and level of acceptance were higher for the proposed interface with respect to the voice control.

The second experimental session was aimed to evaluate user's preferences related to the amount of his/her intervention in the robot control. Two control modalities were implemented in order to modulate the frequency of the user's intervention in the robot control depending on the user's cognitive/physical state. They are the continuous control and the trigger control. They were compared in terms of effectiveness of the task fulfillment and user's personal feelings related to the interface usage. The obtained results demonstrated a high patient involvement in using the continuous control, but better performance, in terms of effectiveness of the task fulfillment, has been achieved with the trigger-based control.

Differently from the continuous control, the trigger-based control requires only a few actions to the user in order to start the robot movement. Hence, a motion planning system was developed in order to allow the robot autonomously accomplish the task in a way that is completely safe and accepted by the user. In this work a motion planning system for rehabilitation and assistive robotics, grounded on a Learning by Demontration (LbD) approach, was proposed. The LbD algorithm presented in this work is grounded on Dynamic Movement Primitives (DMPs) as in [49], but it is improved in terms of i) accuracy of the trajectory reconstruction, ii) adaptability of the DMPs to different subjects' anthropometry and robotic devices (e.g. manipulators or exoskeletons) ii) ability to reproduce human-like movements, iii) ability to solve orientation singularity in the DMP equations and iv) generalization capabilities with respect to different target positions. This was confirmed by four experimental sessions that were carried out in order to assess the motion planner performance. The experiments involved healthy subjects and patients with Limb girdle muscular dystrophys who were asked to perform activities of daily living with the aid of different robot types, i.e. robotic manipulators and upper-limb exoskeletons.

The interface for sensory feedback was designed and developed to improve user postural control during robot-aided daily living activities, both in standing and in sitting position.

In particular, the proposed vibrotactile stimulation feedback was employed, during robot-aided rehabilitation, to correct patients' spine posture. Three inertial sensors were used in order to measure trunk and neck flexion/extension (F/E) and information about user's incor-

rect posture were provided by two lightweight vibrating actuators located on the user's arms. The proposed stimulation feedback was compared to a typical approach used in literature to warn users about incorrect posture, i.e. visual feedback, in terms of i) effectiveness to improve the posture of the subject, ii) acceptability and iii) user's comfort. Ten healthy subjects were asked to perform 3D reaching movements with the aid of a robotic manipulator attached to their right wrist. During the rehabilitation session, they were provided with visual and vibrotactile feedback to retain their trunk and neck in a correct posture. Additionally they were asked to perform the tasks without any information about the correctness of their posture. The obtained results demonstrated that the users had a significant improvement in the spine posture when the task was performed with the aid of the visual and vibrotactile feedback compared to a no feedback condition.

Table of contents

List of figures vii

List of tables xii

1 Introduction 1

2 Non-invasive interfaces for the control of upper-limb prostheses 9
- 2.1 Introduction . . . 9
- 2.2 The proposed approach . . . 11
- 2.3 Experimental validation . . . 14
  - 2.3.1 Experimental setup . . . 14
  - 2.3.2 Experimental protocol . . . 16
  - 2.3.3 Results and discussion . . . 18

3 Non-invasive interfaces for the control of robot manipulators and exoskeletons 21
- 3.1 Input device and human-robot allocation of functions . . . 21
  - 3.1.1 Introduction . . . 21
  - 3.1.2 The proposed approach . . . 25
  - 3.1.3 Experimental validation 1 . . . 26
    - 3.1.3.1 Experimental setup . . . 28
    - 3.1.3.2 Experimental protocol . . . 30
    - 3.1.3.3 Results and discussion . . . 32
  - 3.1.4 Experimental validation 2 . . . 35
    - 3.1.4.1 Experimental setup and protocol . . . 35
    - 3.1.4.2 Results and discussion . . . 39
- 3.2 Motion planning of robot manipulators and exoskeletons . . . 41
  - 3.2.1 Introduction . . . 41
  - 3.2.2 The proposed approach . . . 48
    - 3.2.2.1 1^{st} variation to the DMP original formulation . . . 50

3.2.2.2 2^{nd} variation to the DMP original formulation 51
3.2.2.3 3^{rd} variation to the DMP original formulation 54
3.2.2.4 4^{th} variation to the DMP original formulation 59
3.2.3 Experimental validation 1 65
3.2.3.1 Experimental setup and protocol 65
3.2.3.2 Results and discussion 71
3.2.4 Experimental validation 2 78
3.2.4.1 Experimental setup 83
3.2.4.2 Experimental protocol 84
3.2.4.3 Results and discussion 91
3.2.5 Experimental validation 3 94
3.2.5.1 Experimental setup 95
3.2.5.2 Experimental protocol 96
3.2.5.3 Results and discussions 102
3.2.6 Experimental validation 4 104
3.2.6.1 Experimental setup 104
3.2.6.2 Experimental protocol 105
3.2.6.3 Results and discussion 108

4 Sensory feedback for robot-aided rehabilitation 111
4.1 Introduction 111
4.2 The proposed approach 117
4.3 Experimental validation 118
4.3.1 Experimental setup and protocol 118
4.3.2 Results and discussion 121

5 Conclusions and future work 127

References 132

List of figures

1.1 Block scheme of a bidirectional interface for rehabilitation and assistive robots 2

2.1 Block scheme of the proposed control strategy for trans-humeral upper-limb prostheses 12
2.2 Block scheme of the traditional emg control for trans-humeral prostheses . 13
2.3 Experimental setup 15
2.4 Virtual Reality developed in Labview environment 17
2.5 Experimental results for Elbow and Wrist angle achieved by a representative subject during tasks 1 19
2.6 An example of the sensor fusion (task 1) 20

3.1 Block scheme of the proposed control strategy for robotic manipulators and upper-limb exoskeleton 27
3.2 Block scheme of the platform components outlining the information flow among the subsystems. 29
3.3 Combined M-IMU/EMG (a) and Voice control (b) for assistive robots: Experimental setup 31
3.4 M-IMU data recorded for a representative subject during the execution of the task with the Combined M-IMU/EMG interface. 34
3.5 EMG data recorded for a representative subject during the execution of the task with the Combined M-IMU/EMG interface. 35
3.6 Robot position recorded for a representative subject during the execution of the task with the Combined M-IMU/EMG interface. ϕ is the end-effector rotation about z'-axis. 36
3.7 Voice states recorded for a representative subject during the execution of the task with the Voice control interface. 36

3.8 Robot position recorded for a representative subject during the execution of the task with the Voice control interface. ϕ is the end-effector rotation about z'-axis. 37
3.9 Study design of the M-IMU/EMG trigger control for drinking and pouring tasks (up) and reaching-grasping-moving tasks (down). 39
3.10 Frame of the visual interface for the continuous control. 40
3.11 Block scheme of the proposed motion planning for rehabilitation and assistive robotics 49
3.12 c and σ function in the two different modality to allocate the Gaussian Kernels. The trajectories computed with equally spaced and optimised kernel distribution are outlined in red and blue, respectively. X* and T* are the state and time corresponding to the critical point. 52
3.13 Block scheme of the proposed motion planning for upper-limb exoskeletons 53
3.14 Structure of the adopted neural network 54
3.15 Block scheme of the recursive method used to adjust the NN outputs for different subject anthropometries 55
3.16 Block scheme of the proposed motion planning for anthropomorphic robots 56
3.17 Grafical illustration of ϕ_1 for three different values of the dynamic parameterization factor (k=0,1,2) 64
3.18 Grafical illustration of ϕ_2 for three different values of the dynamic parameterization factor (k=0,1,2) 65
3.19 Grafical illustration of ϕ_3 for three different values of the dynamic parameterization factor (k=0,1,2) 66
3.20 Grafical illustration of $\|\phi\|$ for three different values of the dynamic parameterization factor (k=0,1,2) 67
3.21 Experimental setup. 68
3.22 Human-robot workspace (delimited by the black line). The positions in which the objects are moved in the considered workspace with respect to a initial recording position (red dot) are outlined with black dots. 70
3.23 Joint 3: (a) trajectory and (b) reconstruction error computed for a representative subject. 72
3.24 Joint 5: (a) trajectory and (b) reconstruction error computed for a representative subject. 73
3.25 Cartesian coordinate trajectories executed by the robotic arm during the drinking task with 24 glass different positions. (a) X coordinate, (b) Y coordinate. The recorded trajectory is outlined in red. 77

3.26 Cartesian coordinate trajectories executed by the robotic arm during the eating task with 24 plate different positions. (a) X coordinate, (b) Y coordinate. The recorded trajectory is outlined in red. 78
3.27 NESM upper-limb exoskeleton with the wrist-hand exoskeleton 79
3.28 NEMS reference frames positioning according to the Denavit-Hartenberg (D-H) convention 82
3.29 Block scheme of the platform 84
3.30 A representative subject performing the task (the subject signed an informed consent document to authorize publication of this picture) 85
3.31 The workspace reached during the assistive tasks is delimited by the black line. Object positions during training are indicated by black dots (the glass in the drinking task in (a), the bottle in the pouring task in (b) and the initial position of the sphere in the SHAP task in (c)). Conversely, the glass positions during the pouring task and the sphere final positions in the SHAP task are indicated by red dots in (b) and (c), respectively. 86
3.32 (a) a graphical representation of the end-effector and the base reference frame is shown; (b) the α angle for task 1-1, 2-1 is shown; (c) the α angle for task 3 is shown; (d) The base reference frame and bottle, end-effector and glass reference frames are shown; (e) the β angle for task 2-2 is shown. 89
3.33 Experimental results obtained for CA. The red lines denote the range within which the task is considered successfully accomplished. 92
3.34 Experimental setup. 95
3.35 A graphical illustration of the 9 points reached by the recruited subjects (on the left) and reached by the kuka robot (on the right). The red dot is the position reached by the subjects that was used to computed the DMPs parameters during the Generalization Capability assessment. 96
3.36 A graphical illustration of the objects positions for the pouring task performed by the recruited subjects (on the left) and by the kuka robot (on the right). Blue and black dots illustrate the 9 positions of the bottle and the glass, respectively, during the task fulfilment. Red and yellow dots are the positions of the bottle and the glass, respectively, used to compute the DMPs parameters during the Generalization Capability assessment. 97
3.37 Convex hull created by the human arm (blue line) and the robot arm (red line). 100
3.38 Joint motion during the fulfilment of task 1 105

3.39 Graphical illustration of the path tracked by the 4^{th} robot joint with and without the presence of an obstacle (red and blue lines, respectively). The path tracked by the 7^{th} robot joint with and without the presence of an obstacle are also shown in black and green lines. The red and green dots are the obstacle and the target position, respectively. 106
3.40 A graphical illustration of the robot joint configuration while performing the pouring task when the traditional approach (left) and the hybrid Joint/Cartesian DMP (right) is adopted. 107
3.41 Users feelings related to the robot motion 108
3.42 Experimental setup. 109
3.43 A graphical illustration of the objects positions for the pouring task during the offline database building 110

4.1 The proposed platform: during the rehabilitation session performed with the aid of the robotic platform, the subject posture is monitored by means of M-IMU sensors. The obtained information are used to provide visual/vibrotactile feedback to the user if an incorrect posture is assumed. 115
4.2 Positioning of the M-IMU sensors on the subject body. Sensor S1 is positioned on the chair and acts as a reference, sensors S2 and S3 are positioned on the trunk and on the head of the subject, respectively. 116
4.3 Head and Trunk F/E angles considered to provide feedback 116
4.4 The proposed VR module with nine target positions on three different levels and with angles of 0.21 rad with respect to the starting position (circled in red). 118
4.5 A representative subject is performing the required tasks with the aid of the rehabilitative platform. He is receiving information about his posture by means of A) Visual Feedback, B) Vibrotactile Feedback. 119
4.6 Trend of trunk and head F/E angles during task execution without feedback. The angle behaviour is shown in blue, the angle thresholds (i.e. 0 and 0.17 rad) are in black. 121
4.7 Trend of trunk and head F/E angles reached by one representative subject belonging to Group 2 during task execution with VF. The angle behaviour is shown in blue, the angle thresholds (i.e. 0 and 0.17 rad) are in black and the VF provided to the subjects when they exceed the thresholds is outlined in red. 122
4.8 Trend of trunk and head F/E angles reached by one representative subject belonging to Group 1 during task execution with VF. The angle behaviour is shown in blue, the angle thresholds (i.e. 0 and 0.17 rad) are in black and the VF provided to the subjects when they exceed the thresholds is outlined in red. 122

4.9 Trend of trunk and head F/E angles reached by one representative subject belonging to Group 2 during task execution with VtF. The angle behaviour is shown in blue, the angle thresholds (i.e. 0 and 0.17 rad) are in black and the VF provided to the subjects when they exceed the thresholds is outlined in red. 123
4.10 Trend of trunk and head F/E angles reached by one representative subject belonging to Group 1 during task execution with VtF. The angle behaviour is shown in blue, the angle thresholds (i.e. 0 and 0.17 rad) are in black and the VF provided to the subjects when they exceed the thresholds is outlined in red. 123
4.11 Normalized Incorrect Posture Time (NIPT) of subject head. 124
4.12 Normalized Incorrect Posture Time (NIPT) of subject trunk. 124
4.13 Reaction time for VF and VtF reported for the head and trunk. 125

List of tables

2.1 Values of performance indices for traditional EMG control and combined M-IMU/EMG control . . . 19

3.1 Voice control interface for moving a robot . . . 28
3.2 Performance results . . . 34
3.3 Questionnaire . . . 38
3.4 Results of Mann–Whitney test for the NASA-TLX test. . . . 41
3.5 Results of Mann–Whitney test for the NASA-TLX test. . . . 42
3.6 Joint NDE % obtained in session I . . . 75
3.7 Cartesian NDE % obtained in session I . . . 76
3.8 Number of kernels (N_G) obtained in session I . . . 76
3.9 Motion style index (MSI) obtained in session I . . . 76
3.10 Tasks description . . . 87
3.11 Experimental results obtained for GCA . . . 93
3.12 Experimental results obtained for comparative analysis . . . 104
3.13 Experimental results obtained for generalization capability . . . 104
3.14 Experimental results obtained for robustness against perturbation . . . 105
3.15 Questionnaire . . . 106

4.1 The administered questionnaire to evaluate the platform. . . . 120
4.2 Mean and std of NIPT for head in trunk in the three described conditions. . 124
4.3 Users' answers to the questionnaires, Strongly Disagree (SD) = 1 , Disagree (D) = 2, Neither agree nor disagree (N) = 3, Agree (A) = 4, Strongly Agree (SA) = 5. Results are reported as a percentage of the total subjects. . . . 126

Chapter 1

Introduction

Reducing the risk of injury, fatigue and discomfort are some of the key aspects to be taken into account when designing and developing a Human Machine Interface (HMI) for rehabilitation and assistive robots. This may have an impact on the performance of the task execution, quality of the interaction, patient involvement and user's acceptance [1]. There is in fact a great evidence in literature showing that interfaces which neglect these aspects are more likely to give rise to injuries, operating errors in the task performing and devices use abandonment [43].

Bidirectional interfaces, which combine recording and stimulating systems in so-called closed-loop devices, are the new generation of interfaces. They are composed of two main modules, namely the control and sensory feedback modules. The former is intended to detect the user's movement intention and to drive the rehabilitation/assistive device accordingly; conversely, the latter is meant to provide the user with a sensory feedback that provides him/her with important information about the task performing and hence to improve device effectiveness and acceptance. In order to guarantee attentive usage and fine control of the device and hence a more patient involvement, bidirectional interfaces are conveniently shaped on the user's particular needs. They are therefore designed by taking into account user's residual physical and cognitive abilities.

Emerging evidence suggests in fact that integration of patient-tailored closed-loop interfaces into intentional motor behaviours has paramount synergistic roles to replace or restore lost functionality in disabled people [50].

In this perspective, the design and development of bidirectional interfaces for rehabilitation and assistive robotic devices that are completely tailored on the patient's particular needs constitutes the main ambition of this work. The main features addressed in this thesis are: i) to make the system customized on the user's particular needs and adaptable to the user's residual functional and motor capabilities, ii) to

make the system work in unstructured environments and with different robot types (e.g. manipulators, exoskeletons or prostheses).
In Fig.1.1 a block scheme of a typical bidirectional interface for rehabilitation and assistive robotic devices is shown.

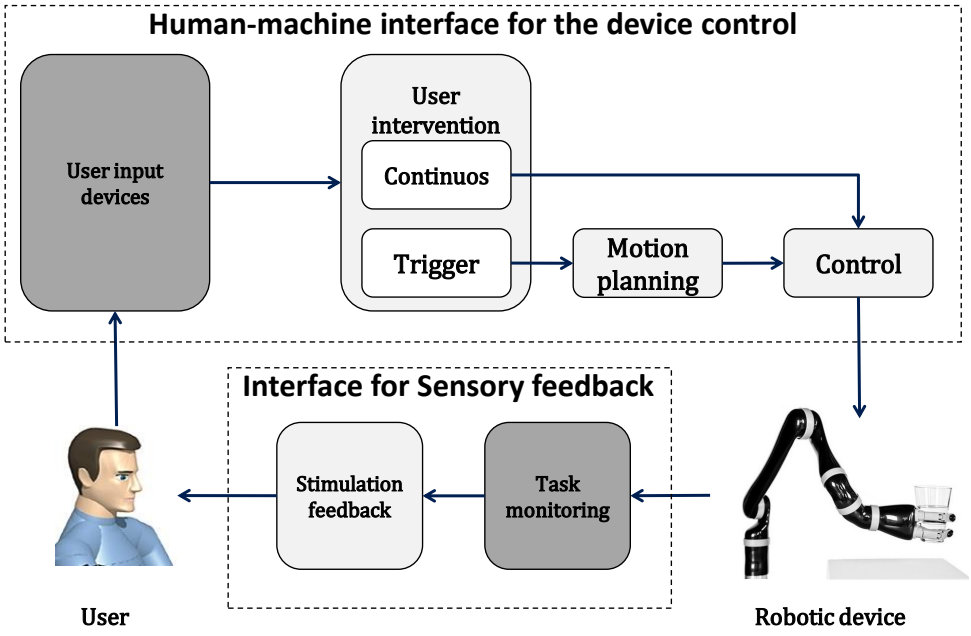

Fig. 1.1 Block scheme of a bidirectional interface for rehabilitation and assistive robots

In the following, the modules of human-machine interface for the control of rehabilitation and assistive robots and interface for sensory feedback are treated.

Human-machine interface for the control of rehabilitation and assistive robots

When designing a human-machine interface for the control of rehabilitation and assistive robots it is crucial to choose the user-device communication channels that are best suited to the residual cognitive and physical disability of the patient. To this end, many solutions including acoustic [73], optics [55], bionics [116], motion [80] and tactile [124] technologies have been proposed in the literature in order to detect the user's movement intention. Likewise, it is paramount to determine the proper user's amount of intervention in the device control that foster an active usage of the rehabilitation/assistive device and guarantee a successful accomplishment of the activity [68]. The more frequent is the required user's intervention the more fine is the device control and hence patient involvement in the device usage. However,

this can cause an increase of the physical and cognitive workload for the patient. Therefore, the proper balance between user's involvement and cognitive/physical workload needs to be achieved by purposely tuning the frequency of user's intervention in the device control according to the user's residual physical and cognitive abilities.

Solutions with a continuous user's intervention in the device control are best suited for people with a low level of disabilities. Take for instance the commercially available myoelectric interfaces used to drive upper-limb prostheses [130]. A continuous contraction of the amputee muscles is required in order to finely control the prosthesis movements. Likewise, solutions that can be used by subjects with upper-limb residual motor capabilities to drive assistive robotic manipulators, such as interfaces like joysticks [48] [75] or systems controlled by means of gesture recognition [91] or hand tracking [24], require a constant intervention of the patient in the system usage.

Conversely, solutions that require a less user's intervention in the device control are typically adopted by patients with a high level of disability to control rehabilitation/assistive robotic devices, such as robotic manipulators or upper-limb exoskeletons. The main advantage of these interfaces is that the task accomplishment is guaranteed with a less physical and cognitive demand. However, the higher is the required robot autonomy the more complex is the HMI to be designed. By means of these interfaces, the user can select the task to be performed and the robot will autonomously perform that task.

Typically, interfaces that require a less user's intervention in the device control integrate cameras [57] for detecting the position of the object to interact with. The robot motion is then properly planned [30] by guaranteeing an effective and safe interaction between human and robot and by improving robot acceptance and interface usability. Developing motion planning strategies that allow the robot moving like a human and permit untrained users to easily program and safely use the robotic system is therefore one of the main challenges to face when designing interfaces that require high robot autonomy in the task accomplishment. A typical approach used to plan the motion of rehabilitation/assistive robots in a way similar to humans in the point-to-point motion is the minimum-jerk trajectory [30]. However, it cannot be adopted to plan more complex tasks such the Activities of Daily Living (ADLs). Approaches that can face such a problem are grounded on replicated movements [5]. They use spline decomposition [53] or optimization of ad hoc developed objective functions [94] for replicating on the robotic system the trajectories executed by the subject. But their main drawback is that they cannot manage environment variability and external perturbations.

In this thesis a human-machine control interface was designed to be used by patients with different level of disabilities to drive their rehabilitation or assistive robotic device,

e.g. an upper-limb prosthesis, a robotic manipulator or an upper-limb exoskeleton, both continuously and by means of a trigger-based approach.

In particular, starting from a typical interface used to continuously control upper-limb prostheses and based on superficial EMG electrodes, M-IMUs were added in the prostheses control scheme with the aim to allow a simultaneous control of the prosthesis Degrees of Freedom (DoFs). In fact, one of the main drawback of the typical interface used to drive the commercially available multi-DoF prostheses is that only a single DoF could be operated at a time and a switch mode to manage transition among the various DOFs of the system is required. Hence, **the first contribution of this thesis is to propose a novel control strategy for multi-DoF prostheses, i.e. trans-humeral prostheses, that, based on the coupled use of myoelectric and magneto-inertial sensors, allows managing simultaneous movements and reaching tasks in a more natural way.** The EMG electrodes are placed on two antagonist muscles, i.e. biceps and triceps, in order to estimate the target muscles myoelectric activity; otherwise the M-IMUs are placed on the user's trunk and stump respectively, in order to evaluate shoulder flexion-extension and ab-adduction angles. Hence, with the proposed approach the user could operate the elbow flexion-extension, wrist prono-supination and hand opening-closing exploiting the residual stump motions combined to the myoelectric activity of two target muscles, i.e. biceps and triceps.

It is interesting to note that the proposed approach is easily adaptable to different level of user's disability since the sensors of the interface could be moved in different locations of the user's body with the aim to exploit user's residual motor abilities. Therefore, **the second contribution of this thesis is to propose an alternative version of the proposed combined M-IMUs/EMG interface to be used by people with severe motor disability to control their robotic device, such as a manipulator or an upper-limb exoskeleton.**

The M-IMU was positioned on the subject head. The head motion signals are translated into robust and quick commands for the robotic device. In order to avoid involuntary movement of the robot the M-IMUs were combined with EMG superficial electrodes positioned on the subject arm with the aim of enabling the robot motion. Two different control modalities were proposed in order to meet user's preferences and modulate the frequency of the user's intervention in the device control according to the user's residual physical and cognitive abilities. These control modalities will be named in the following M-IMUs/EMG continuous control and M-IMUs/EMG trigger control. Since there are no studies in literature aimed at assessing user's preferences in relation to the amount of the user's intervention in the robot control, a comparative analysis between the two control modalities proposed in this work to operate rehabilitation/assistive robotic devices was carried out in order to assess how the

balance between user's involvement and cognitive/physical workload is perceived by the user and influence the interface usability and acceptance.
Differently from the M-IMUs/EMG continuous control that require the user to continuously intervene in the device control, the M-IMUs/EMG trigger control require only a few actions to the user in order to start the robot movement. Hence, a motion planning system is needed in order to allow the robot autonomously accomplish the task in a way that is completely safe and accepted by the user. Therefore, **the third contribution of this work is to propose a motion planning system that i) can be easily trained by human subjects who have not technical skills to program the robot in performing daily living tasks, ii) can reproduce human-like movements that are safer and more accepted by the user compared to the ones typically used in literature to plan the motion of rehabilitation and assistive robots iii) can be adaptable to the environment change, such as different objects positions and user's anthropometries and iv) can manage external perturbations such as the presence of an obstacle along the path tracked by the robot.** The proposed motion planning is grounded on a Learning by Demonstration (LbD) approach with Dynamic Movement Primitives (DMPs): a set of nonlinear differential equations with a well-defined landscape attractor.
As for typical LbD approaches, LbD based on DMPs consist of two phases. In the first phase, namely the Motion Encoding, trajectories executed by a demonstrator are recorded during the execution of a task and distinctive features (called DMP parameters) are subsequently extracted from these trajectories using a Locally Weight Regression algorithm (LWR) in order to encode the robot motion. In the second phase, i.e. the Motion Decoding, DMPs are computed for each robot DoF, as a sum of Gaussian Kernels weighted by means of the previously computed DMP parameters. Generalization capability with respect to different robot initial configurations as well as convergence to different target positions is guaranteed when the motion is decoded by means of DMPs. Moreover, LbD-based motion planning drastically simplify the robot motion planning and make the interface accessible to non-expert people. In fact, LbD does not require an operator with technical skills to re-plan new movements for the robot: it just requires to observe a human demonstrator during the task execution and the robotic system to replicate the learnt movement. In this work modifications to the original formulation of DMPs proposed in [49] were applied in order to i) improve the accuracy of the trajectory reconstruction, ii) improve adaptabilities of the DMPs to different subjects' anthropometry and robotic device (e.g. manipulators or exoskeletons) ii) solve orientation singularity in the DMP equations and iii) improve generalization capabilities with respect to different target positions.

Interface for sensory feedback

The interface for sensory feedback has the aim to provide the user with important information related to the task performing and needs to be designed in order to exploit the user's residual sensory channels. In literature, many non-invasive solutions have been proposed to restore sensory information in disabled people, including visual, auditory, mechanical, electrotactile and vibrotactile stimuli. Vision is assessed to be the most important perceptive modality during interaction with the environment. For perceiving information with high resolution, vision dominates other senses [26]. However, visual feedback uses an important sensory channel which is essential for a successful accomplishment of the task. Hence, when the patient is focused on a complex task, visual feedback may be perceived as cumbersome or confusing since visual perceptual channel becomes overloaded [114].
To overcome this drawback, auditory feedback is a valuable means to convey important information to the patient related to the task performing. However, this kind of feedback could not be employed in many applications, such as prosthetics, since it is not accepted by users. Haptic feedback could be a worth solution to address this issue. Haptic refers to the sense of touch, and haptic interfaces refer to the communication of information through the sense of touch by the application of pressure, vibration, electricity, force etc.. Although a great number of haptic feedback devices could be employed to restore lost sensory feedback in patients or provide important information about the task performing there are some drawbacks that cannot be neglected. Electrotactile systems can cause pain and fatigue on the skin [54]. Force feedback systems can be cumbersome and have limited spatial resolution on the patient skin [29].
Vibrotactile feedback (VtF) systems can be considered to be safe and have an acceptable spatial resolution [67] in comparison to the other tactile solutions. Several studies in literature are focused on the development of vibrotactile balance prostheses for postural control in patients. They are mainly adopted and tested on patients with abnormal vestibular function and other sensory deficits [92] [126]. Based on the interesting results achieved in these studies, a few researches started to investigate the potential usage of these solutions in lower-limb amputees for improving their postural control functions during the gait [47] [86]. Additionally, a little research has attempted to asses whether VtF could be an effective tool to correct patients posture during the performing of activities in sitting positions [131].
Despite the wide use of VtF in many fields, this kind of feedback seems to be not suitable for applications that require long term usages [34]. Indeed, it is well known in the literature that an extended vibrotactile stimulation of the fast adapting sensory receptors on the user's skin induces sensory adaptation effects in the patient. However, this does not apply to rehabilitation sessions that may expose patients only to short and infrequent stimuli.

In this thesis the interface for sensory feedback was designed to improve user's postural control during robot-aided daily living activities, both in standing and in sitting position.

From an in-depth analysis of the literature emerged that VtF feedback can enhance motor learning and performance and is preferred by users over visual or auditory feedback [2] [59] [117]. However, there is poor attention to the type of feedback preferred by the users, in terms of acceptability and comfort, for correcting spine posture while performing activities in sitting positions [131]. Moreover, there are no previous studies in literature that investigate which type of feedback could be effectively and efficiently employed during robot-aided rehabilitation treatments to improve patient spine postures.

Therefore, **the fourth contribution of this work is to propose a vibrotactile stimulation feedback that can be effectively and efficiently employed in robot aided-rehabilitation, to correct patients' spine posture.**

The proposed stimulation feedback is based on the combined use of inertial sensors and vibrotactile actuators. Three inertial sensors were used. One was positioned on the chair the subjects were asked to seat during the treatment, one was located on the subject's trunk and the last one was fixed on the subject's head. The sensor placed on the chair acted as reference for the sensors positioned on the subject's trunk and head, and the other two sensors were used to measure trunk and neck flexion/extension (F/E), respectively. Information about user's incorrect posture is provided by two lightweight vibrating actuators located on the user's arms.

When the subject is not within the correct trunk posture Range of Motion (RoM) the motor located on the user's left arm start vibrating at the maximum intensity until the user corrects his/her posture. Likewise, when the user exceeds the neck F/E RoM limits the actuator placed on the user's right arm start vibrating, as well, in order to make the user adjust the neck posture.

It is worth observing that, as for the human-machine interface for the control of the robotic device, the developed stimulation feedback was designed to be completely adaptable to the user's needs. By moving the inertial sensors on different locations of the user's body, one can monitor the posture of different user's body parts, depending on the user's specific postural disorders and convey information about incorrect posture by means of vibrotactile stimulation on the user's most sensitive body parts.

Ten healthy subjects were asked to perform 3D reaching tasks with the aid of a robotic platform and correct their neck and trunk posture by exploiting information provided by visual a vibrotactile feedback. Then, a comparative analysis between the two feedback modalities was carried out in terms of effectively, user's acceptability and comfort.

Thesis organization

It is fair to point out that some of the contents included in this thesis are taken from conference and journal papers previously published by the author of this work. To summarize, the thesis is structured as follows.

- In Chapter 2, the state of art on the interfaces used to drive upper-limb prostheses is analyzed and a novel control strategy that overcome the limitations of the commercially available interfaces is proposed. Subsequently, the experimental setup and protocol used to validate the proposed approach is reported and experimental results are discussed. Part of the contents included in this chapter are already published in [66].

- In Chapter 3, the literature regarding the interfaces used to drive rehabilitation/assistive robotic devices such as, robotic manipulators and exoskeletons is analyzed, with a focus on the techniques adopted to plan the robot motion. Then, a novel control interface for robotic manipulators and upper-limb exoskeletons is proposed, and the experimental setup and protocol used to validate the approach is reported. Finally, experimental results are discussed. Part of the contents included in this chapter are already published in [64], [65] and [63]. Other contents are pending to be published in [62].

- In Chapter 4, the state of art regarding the stimulation feedback used to improve postural control during robot-aided rehabilitation treatments is examined. Subsequently, the proposed stimulation feedback to be employed to correct patients trunk and neck posture during robot aided-rehabilitation treatments is introduced and the experimental setup and protocol used to validate the approach is reported. Finally, experimental results are shown and discussed. Part of the contents included in this chapter are pending to be published in a journal paper [108].

In Chapter 5, conclusions and final considerations are reported.

Chapter 2

Non-invasive interfaces for the control of upper-limb prostheses

2.1 Introduction

Although the number of upper limb amputees is greatly less than lower ones, the seeking to address the issue of replicating the high number of complex functionalities, that natural upper limb exhibits, has aroused a more increasing interest in the upper-limb prosthetics during the recent years [18]. Commercially, such devices are available in two different types, i.e. body-powered and externally powered. Body-powered prostheses are driven by the user, throughout cables and restraint systems, exploiting residual movements of already active body sites; otherwise, the externally-powered embed electric motors to drive the D.o.f. (Degree Of Freedom) to be operated. Even though externally-powered prostheses exhibit higher performance in terms of motion accuracy and physical load required for the users, body-powered prostheses are still the most adopted for their simpleness and cheapness.

The most employed techniques to control externally-power prostheses are based on EMG recordings. In particular, most of such devices are driven by a relatively simple control strategy, i.e. amplitude-based control [130], whereby the amplitude of EMG signals recorded from two antagonist muscles are compared to a predetermined threshold and used to actuate one of the motors embedded in the prosthesis. This technique has the advantage to exhibit, for 1 DoF prostheses (e.g. most of the trans-radial prostheses), good performance in terms of motion accuracy and cognitive load required to the users [17].

Nevertheless, in multi-DoF devices, it allows only a single degree of freedom (DOF) to be operated at a time and requires a switch mode to operate transition among the various DOFs of the system [95]. Indeed, in most upper extremity amputees there are not enough muscle

groups that could be independently controlled by the amputees. As a consequence, in order to manage multi-DoFs devices (such as trans-humeral prostheses), amplitude-based control uses a cyclic selection process to choose the joint to be driven, thus enabling only sequential movements. Co-contraction of the two target antagonist muscles (e.g. biceps and triceps) is used as trigger signal to select the joint to move; on the other hand, the asynchronous isometric contraction of the two target muscles causes the movement of the selected joint in the two available directions. Natural limb control involves the simultaneous movement of multiple degrees of freedom (DOF), with the consequence of providing significant functionality during activities of daily living; unfortunately, due to the lack of muscle groups that could be independently controlled by the upper extremity amputees, amplitude-based control has the disadvantage of not recovering adequately this capability of simultaneously managing multiple DoFs. One way to solve this issue is resorting to the Target Muscle Reinnervation (TMR). TMR redirects residual nerves to muscles that have no biomechanical function due to amputation and makes independent myoelectric control sites available. However it has the clear disadvange to be invasive, since it require amputees to undergo surgery.

Pattern recognition applied to ElectroMyoGraphic (EMG) signals is another approach to control prosthetic devices. It is mainly a research technique (implemented in commercial devices only recently in USA) that tries to address the issue of simultaneous control of multiple joints. The classifier is previously trained on labelled EMG signals in order to select different classes of intended motions. In [8] a standard approach based on a single Linear Discriminant Analysis (LDA) classifier trained to recognize simultaneous movements and more complex organizations of multiple LDA classifiers have been evaluated. However, in most upper extremity amputees there are not enough muscle groups that could be independently controlled by the amputees; again TMR could be employed to solve this issue, since it is the sole surgical technique that could restore independent control sites in high-level amputees [60] and makes these sites available for pattern recognition approaches. Therefore, pattern recognition has the clear disadvantage of being difficult to apply in practice to high level upper limb amputees who are not subjected to TMR for simultaneously managing multiple DoFs [129] [130]. A hybrid solution could be employed, in order to allow upper limb amputees who do not undergo TMR surgery to manage simultaneous prosthesis movements. A body-powered cable could be used to drive the prosthetic elbow exploiting the residual user's neck or shoulder movements; otherwise EMG recordings could be employed to control the motor that drives the prosthetic wrist.

Progress beyond the SoA Our contribution is to propose a novel approach to EMG control of trans-humeral externally-powered prostheses that allows simultaneously managing mutiple

DoFs in a more natural way than the commercially available amplitude-based control, not resorting to pattern recognition. In the following the proposed approach will be named combined M-IMU/EMG control. It is interesting to note that it has the advantage of not being invasive, since it does not require a TMR surgery. Moreover, with respect to the amplitude-based control, it relies on a multi-modal interface consisting of two magneto inertial sensors and two EMG electrodes that allows an easier user's movement detection and a reduction of the user's cognitive load. Furthermore, with respect to the hybrid prosthetic solution, i.e. a combined externally powered and body powered prosthesis, it requires a less physical load for user interfacing.

The Combined M-IMU/EMG control has been validated by comparing it to the amplitude-based control. The experimental study that has been carried out involves eight healthy subjects. These subjects have been asked to direct a virtual prosthesis, using both the control strategies to be compared, in order to perform some activities of daily living.

2.2 The proposed non-invasive interfaces for the control of trans-humeral prostheses

The strategy presented in this work is based on the coupled use of Magneto-Inertial Measurement Units (M-IMUs) and EMG electrodes. Two versions of the strategy have been proposed. The former version, Combined M-IMU/EMG control v1.0, requires two M-IMUs and two EMG electrodes for detecting the user's movement intentions. The EMG electrodes should be placed on two antagonist muscles, i.e. biceps and triceps, in order to estimate the target muscles myoelectric activity; otherwise the M-IMUs should be placed on the user trunk and stump respectively, in order to evaluate shoulder flexion-extension and ab-adduction angles.

A flux diagram of this strategy is presented in Fig.2.1. The user can choose between two states. If biceps and triceps are not co-contracted (first state), elbow and wrist joints will not move. In this state the user could control grasp and release of the hand by contracting biceps and triceps, respectively. On the other hand, if biceps and triceps are co-contracted (second state) the user can control elbow and wrist movements by exploiting the two shoulder DoFs monitored by means of the M-IMUs. In other words, the flexion-extension movement of the user's shoulder causes the flexion-extension of the prosthetic elbow. Otherwise, the ab-adduction movement of the user's shoulder causes the prono-supination of the prosthetic wrist. It is obvious that such a strategy allows the user to manage two prosthesis DoFs simultaneously, i.e. elbow flexion-extension and wrist prono-supination.

Nevertheless, the proposed approach could look fatiguing and mentally cumbersome for the user if the required shoulder Range of Motion (RoM) to operate the prosthesis DoFs should be the same of the desired prosthetic joint RoM; first because of the long periods of co-contraction required to accomplish the task and second because of the changes of the endpoint position introduced by the additional residual limb movements necessary for the control of the prosthesis, that make the device use and the manipulation of items a bit difficult. In order to address these issues, the amplitude of the stump movements, required to control the prosthesis Dofs, could be significantly reduced as well as the time to accomplish the task, by introducing a gain factor in relating the user's shoulder movements and prosthetic ones. In other words, the prosthetic joint RoM is achieved by multiplying the shoulder RoM and the preset gain factor.

In the second version, the proposed combined M-IMU/EMG control v1.0 is extended to another pairs of muscles in addition to biceps and triceps, e.g. deltoid and trapezius, thus enabling the simultaneous motion of multiple DoFs of the prosthesis . This version of the proposed approach will be named Combined M-IMU/EMG control v2.0 and will not be tested in the following.

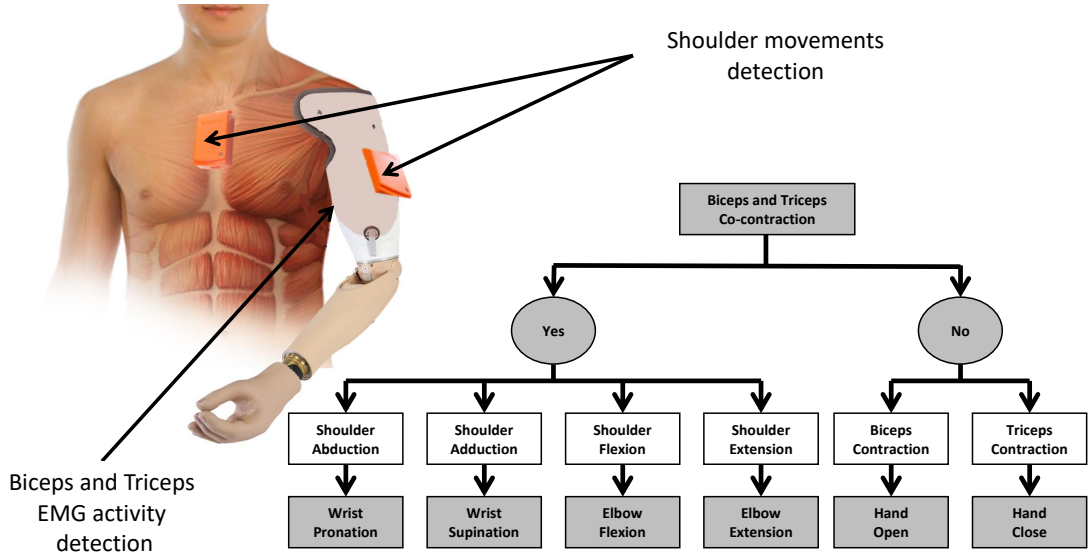

Fig. 2.1 Block scheme of the proposed control strategy for trans-humeral upper-limb prostheses

Traditional myoelectric interfaces for the control of trans-humeral prostheses

Conventional amplitude-based control consists of comparing the amplitude of the recorded EMG signals to a set of a predetermined thresholds [130]. These thresholds are generally chosen to be patient-tailored, such that they are set to certain percentages of the EMG data peak value, recorded from the subject during an initial calibration phase. The simplest form of the amplitude-based control uses a couple of EMG electrodes placed on two antagonist muscle pair in the residual limb [77]. In the following this approach will be named *traditional myoelectric control*.

In the traditional control, the muscle pair should be independently controlled by the amputee and free of EMG crosstalk. If the amplitude of EMG signals recorded by one of the two electrodes is higher than a predetermined threshold, a single DoF at a time is directed at a preset rate and the direction of its motion depends on which muscle is contracted. Typically biceps and triceps are used to flex and to extend the prosthetic elbow, respectively. Otherwise, they are used to direct pronation and supination of the prosthetic wrist, respectively, and hand opening and closing, as well. A flux diagram of the control strategy is presented in Fig.2.2.

Using more thresholds than one to compare the amplitude of EMG signal recorded, could be useful to control the joints rate motion proportionally to the amplitude of the target muscles myolectric activity.

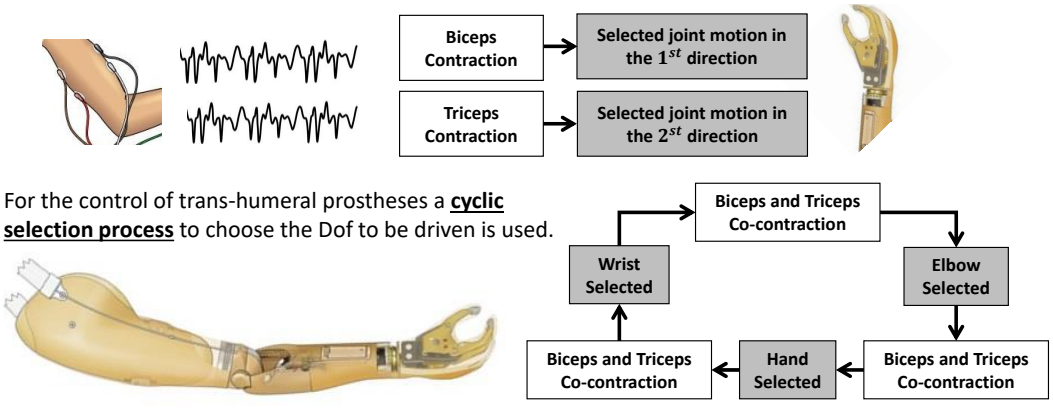

Fig. 2.2 Block scheme of the traditional emg control for trans-humeral prostheses

2.3 Experimental validation

2.3.1 Experimental setup

In the comparative analysis performed in this work, a conventional amplitude-based control that uses one threshold to drive the DoF at a single rate has been implemented. It has been compared to the combined M-IMU/EMG control v1.0.

The experimental setup (see. Fig.2.3) used to carry out the experimental trials includes the following components:

- Two double-differential EMG electrodes (Otto Bock 13E200=50 model) with an amplification gauge ranging in between 100 and 2000 have been used to acquire electromyographic activity of the target antagonist pair muscles. They were placed on the subject's arm along the longitudinal mid line of the target muscles by means of elastic bands.
- A National Instruments (NI) USB-6003 DAQ with a 16-bit ADC has been used for analog-to-digital conversion of the EMG signal.
- Two wireless M-IMUs (XSens MTw) have been used to detect shoulder flexion-extension and ab-adduction motion. Each sensor was applied onto the body of the subject by means of strap holders.
- An Awinda Station has been used to check the reception at 100 Hz of synchronised wireless data from the two wirelessly connected M-IMUs.
- A Virtual Reality (VR) purposely developed in Labview environment has been used to test the two control strategies on daily living tasks. The VR shows a virtual prosthesis closed to a table on which virtual objects, i.e. a bottle and a ball, are placed. The user can control the virtual prosthesis by means of the IMUs and EMG electrodes previously applied onto his body, using the traditional myoelectric control and the combined M-IMU/EMG control v1.0.
- Finally, a work station is used to run the VR and perform sensor fusion.

The EMG signals preprocessing for increasing the signal-to-noise ratio is already realized by the electronics integrated in the Myobock electrodes. Indeed, the EMG signals are pre-amplified with a gain factor of 2000 and are pre-filtered by a high pass filter with a cut-off frequency of 20 Hz.

The data recorded by the accelerometer, gyroscope and magnetometer embedded in the MTw motion trackers are internally processed by their integrated electronics too, in order

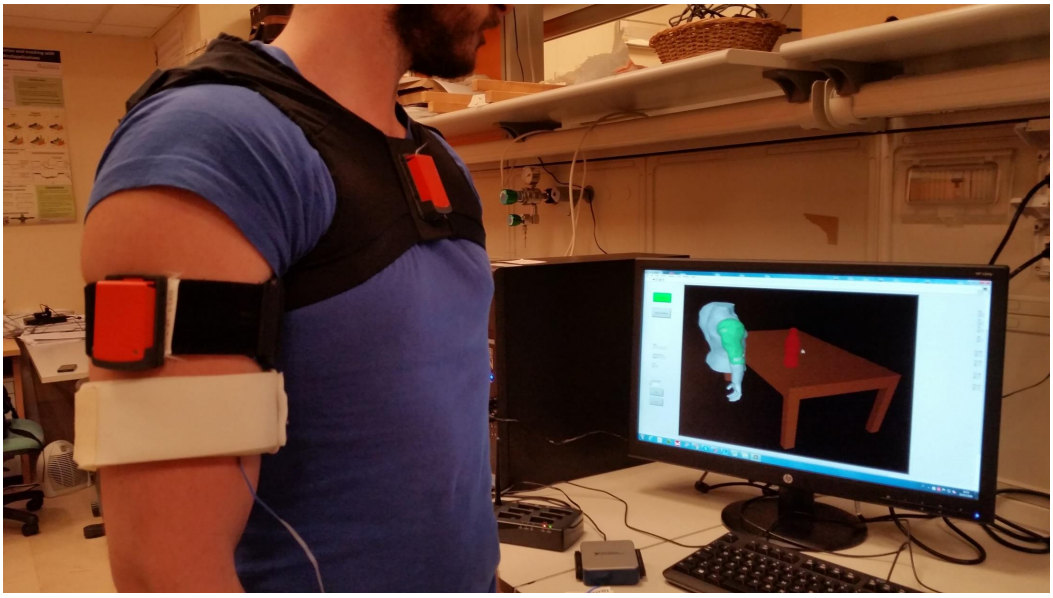

Fig. 2.3 Experimental setup

to provide a good output estimation of the sensor velocity and orientation. This orientation is calculated between the sensor-fixed co-ordinate system, S, and a earth-fixed reference co-ordinate system, G, and it is expressed in terms of matrix rotation. By default, the local earth-fixed reference co-ordinate system used is defined as a right handed cartesian co-ordinate system with: X positive when pointing to the local magnetic North, Y according to right handed co-ordinates (West), Z positive when pointing up. Denoting S_1 and S_2 the fixed co-ordinate system of the sensors placed on the subject trunk and arm respectively, the shoulder F-E and AB-AD angles, θ_1 and θ_2 , are evaluated as follows:

$$R_{S_1}^{S_2} = R_{S_1}^{G} R_{G}^{S_2} = \begin{bmatrix} r_{11} & r_{12} & r_{13} \\ r_{21} & r_{22} & r_{23} \\ r_{31} & r_{32} & r_{33} \end{bmatrix} \tag{1}$$

$$\theta_1 = -\arcsin(r_{31}) \tag{2}$$

$$\theta_2 = \tan\left(\frac{r_{21}}{r_{11}}\right) \tag{3}$$

The using of two M-IMUs to calculate the shoulder F-E and AB-AD angles is useful to reduce the orientation error due to the static ferromagnetic fields in the environment. Indeed, being the error that affect the orientation assessment of the two M-IMUs the same, the computing of the shoulder F-E and AB-AD angles as a relative orientation between the two M-IMUs causes a dejection of the error that affects the shoulder motions estimation.

The data recorded by EMG electrodes and M-IMUs are fused to detect user motion intention. If the shoulder Flexion-Extension (F-E) and Abd-adduction (AB-AD) angles estimated by the IMUs increase of $\Delta\theta_1$ and $\Delta\theta_2$, the virtual prosthetic elbow and wrist will rotate of $\Delta\theta_3$ and $\Delta\theta_4$, respectively, expressed as follows

$$\Delta\theta_3 = K\Delta\theta_1 \tag{4}$$

$$\Delta\theta_4 = K\Delta\theta_2 \tag{5}$$

where K is a proportional coefficient set to 2. The motion time interval starts when the amplitude of the EMG signals exceed a predetermined threshold (i.e. 1 V) and ends when this amplitude decreases under the threshold.

When the amplitude of the EMG signal from the biceps exceeds the threshold, the hand closing is commanded. Otherwise, if the amplitude of the triceps EMG signal exceeds the threshold the hand opening is controlled. In both cases the prosthetic elbow and wrist are not moved.

2.3.2 Experimental protocol

Eight volunteer able-bodied individuals have been recruited for this study. Before beginning the test, they were required to be in standing position, in order to carry out the calibration of the M-IMUs. Moreover, they were asked to perform biceps and triceps contraction, in order to set the thresholds depending on the amplitude of the acquired EMG data. Subsequently, they were trained to drive the virtual prosthesis by means of the traditional and the combined M-IMU/EMG control strategies, for a period of 1 second per control.

After the training, they were asked to perform four different tasks in the Virtual Environment (VE) with both controls. Each task was aimed to reach and grasp a virtual object properly placed in the VE. In particular, task 1 and 3 were aimed to reach and grasp a virtual bottle; otherwise, task 2 and 4 were aimed to reach and grasp a virtual ball. Fig.2.4 shows the position of the virtual objects during the performing of task 1 and 2. The position of these virtual objects was slightly changed during the performing of task 3 and 4, such that the objects were moved 0.1 m in front of the subject along the sagittal direction and 0.1 m on the right of the subject along the transverse direction, respectively. Five trials for each task were performed, starting from the neutral position of the virtual prosthesis shown in Figs. 2.4a 2.4c. Each task required the following actions to be accomplished: shoulder flexion-extension (SF,SE), shoulder ab-adduction (SAB,SAD), elbow flexion (EF), wrist pronation-supination (WP,WS), hand closure (HC). Visual feedback was provided by means

of the VE: the virtual arm and the object turned green when the arm was around the target with a tolerance band of ± 15 for each DoF. The task was completed when the subject held the virtual object with the virtual arm for 1 s.

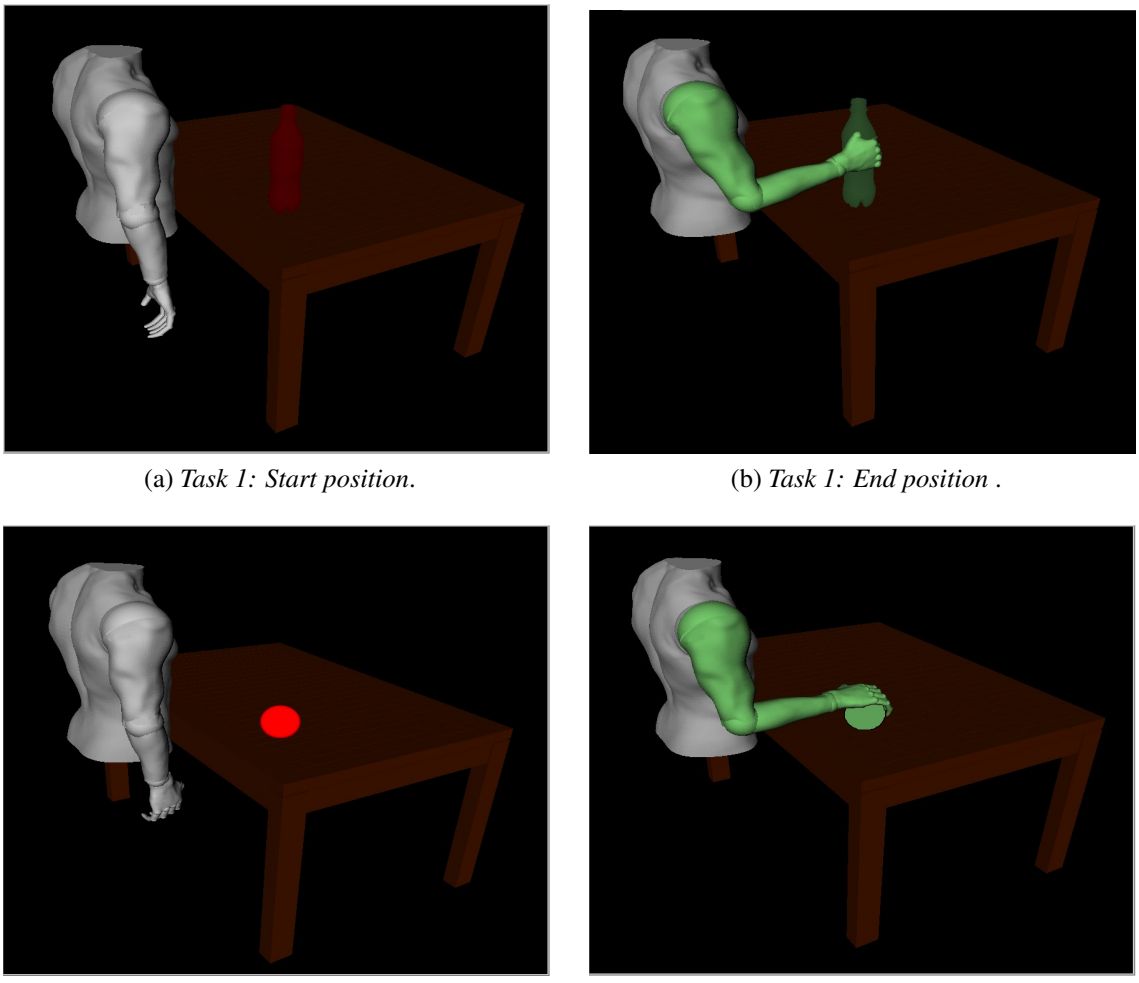

(a) *Task 1: Start position.* (b) *Task 1: End position .*

(c) *Task 2: Start position.* (d) *Task 2: End position .*

Fig. 2.4 Virtual Reality developed in Labview environment

The M-IMU data acquired for each trial were segmented from the time when the velocity of the monitored joint exceeded the 10% of the peak value up to the time when velocity decreased under the 10% of the peak value. The segmented signals were processed to extract quantitative indices capable of describing the subject's performance. They are:

Completion time and average rotational speed

Completion time and average rotational speed (AR speed) are typical parameters used for analysing the functional performance of a subject during real-time tests [115]. They

have been used to quantify the performance of subjects ability to complete the tasks. The completion time is the period of time that starts when the velocity grew up to the 10% of the peak value and ends when the velocity decrease to the 10% of the peak value.

The average rotational speed is calculated for each joint as the ratio between the angle by which the joint rotates during the completion time, and the completion time.

Success rate

Success rate refers to the number of successful trials performed by a subject. For each task a maximum completion time of 20 seconds has been set. If the subject accomplished the task within this time, the task was considered successfully completed. Otherwise, the task was considered unsuccessful.

A statistical analysis based on Student Test was performed for the two indices. Mean value and standard deviation (STD) of these indices, per task and per control strategy has been calculated. For each of these indices, in order to compare the results achieved for the two control strategy, a paired T-test was performed. The significant factor was reported for $p-VALUE = 0.05$.

2.3.3 Results and discussion

The experimental results of a representative subject are reported in Figs.2.5a and 2.5b for task 1, mean value and standard deviation (STD) have been calculated on 5 trials. Additionally in Fig.2.6 EMG and M-IMU data recorded during task 1 are reported for both the control strategies, as an example of the performed sensor fusion.

Fig.2.6a and Fig. 2.6c reports the EMG and the M-IMU data, respectively, for the Combined EMG/M-IMU control. During the performing of the first task, when the biceps EMG signal exceeded the threshold (a1), the elbow F-E was directed (c1). A double co-contraction of the target muscles was subsequently performed in order to switch the selected joint from elbow to wrist (a2). This one was driven when the biceps EMG signal exceeded the threshold (a3). Finally, a double co-contraction of the target muscles was performed in order to switch the selected joint from wrist to hand (a4), that is driven when the biceps EMG signal exceeded the threshold, as well (a5).

Fig. 2.6b and Fig. 2.6d reports the EMG and the M-IMU data, respectively, for the traditional EMG control. During the performing of the same task, when both the biceps and triceps EMG signals exceeded the threshold (b1), as well as the shoulder flexion and abduction was performed (d1), the elbow flexion and wrist supination was driven. The isometric contraction of the biceps (b2), drove the hand close at the end of the task.

Subsequently, in Tab. 2.1 the values of the aforementioned performance indices, with mean and STD calculated on the eight subjects, are reported for each control strategy. One can observe that higher performance is obtained with the combined M-IMU/EMG control for each task. When the combined M-IMU/EMG control was adopted, all the subjects performed the tasks by simultaneously moving elbow and wrist. On the other hand, with the traditional EMG control the tasks were performed with sequential movements.

Tab. 2.1 also shows if the difference between the two controls is significant by reporting the p-value for each index. It is worth noticing that significant difference was obtained ($p-VALUE < 0.05$) for both completion time and average rotational speed for each task.

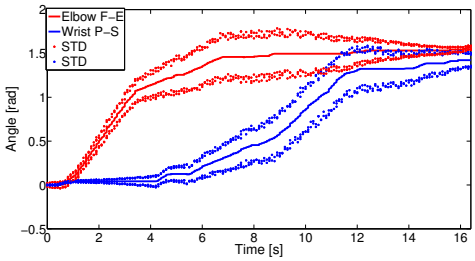

(a) *Traditional control: elbow F-E and wrist P-S during the task 1.*

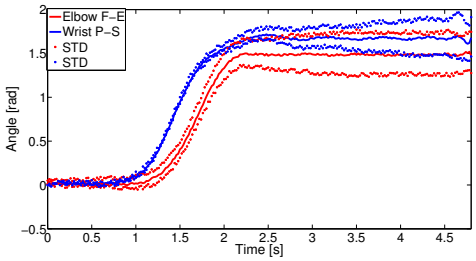

(b) *Combined M-IMU/EMG control: elbow F-E and wrist P-S during the task 1.*

Fig. 2.5 Experimental results for Elbow and Wrist angle achieved by a representative subject during tasks 1

Table 2.1 Values of performance indices for traditional EMG control and combined M-IMU/EMG control

Condition	Task	(1) Completion time [s]	P-VALUE (1)	(2) EF-EE AR speed [rad/s]	P-VALUE (2)	(3) WS-WP AR speed [rad/s]	P-VALUE (3)	Success rate [%]
Traditional	1	14 ± 4	0.009	$0,13 \pm 0,03$	0.008	$0,11 \pm 0,04$	0.008	80
	2	14 ± 4	0.007	$0,13 \pm 0,03$	0.021	$0,13 \pm 0,03$	0.07	72,5
	3	15 ± 4	0.008	$0,11 \pm 0,02$	0.012	$0,03 \pm 0,04$	0.09	70
	4	16 ± 4	0.007	$0,09 \pm 0,04$	0.022	$0,03 \pm 0,03$	0.006	77,5
Novel	1	9 ± 5	0.009	$0,22 \pm 0,08$	0.008	$0,23 \pm 0,08$	0.008	95
	2	8 ± 4	0.007	$0,3 \pm 0,1$	0.021	$0,26 \pm 0,09$	0.07	90
	3	9 ± 4	0.008	$0,2 \pm 0,1$	0.012	$0,21 \pm 0,05$	0.09	97,5
	4	8 ± 3	0.007	$0,19 \pm 0,07$	0.022	$0,22 \pm 0,07$	0.006	87,5

Elbow Flexion (EF), Elbow Extension (EE), Wrist Supination (WS), Wrist Pronation (WP), Average Rotational speed (AR speed)

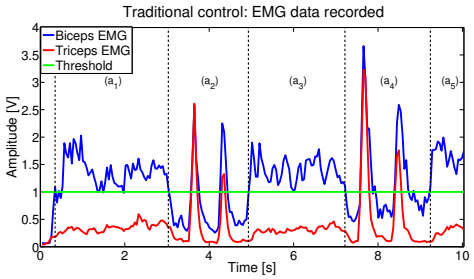

(a) *[a1]Biceps contraction to drive elbow flexion, [a2] two co-contraction to drive wrist supination, [a3] two co-contraction to switch the selected joint to wrist, [a4] biceps contraction to drive hand closing .*

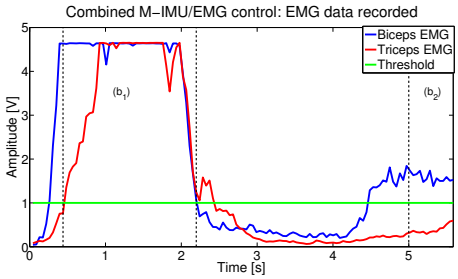

(b) *[b1] Co-contraction to drive elbow F-E and Wrist P-S, [b2] biceps contraction to drive hand closing .*

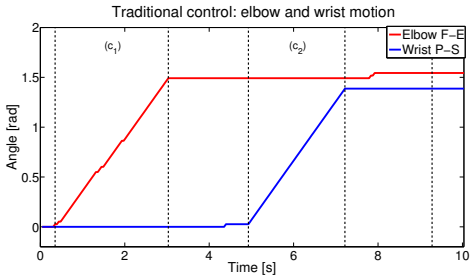

(c) *[c1] Elbow flexion, [c2] wrist supination.*

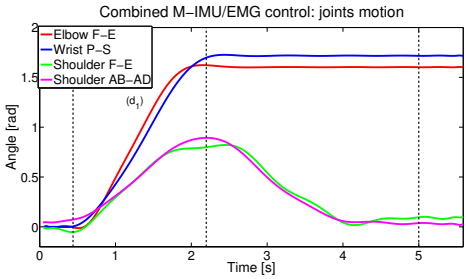

(d) *[d1] Shoulder flection and abduction to drive elbow flexion and wrist supination when biceps and triceps are co-contracted.*

Fig. 2.6 An example of the sensor fusion (task 1)

Chapter 3

Non-invasive interfaces for the control of robot manipulators and exoskeletons

3.1 Input device and human-robot allocation of functions

3.1.1 Introduction

Input devices for the detection of user intention

The commercially available robots, usually employed in rehabilitation and assistive field, are not enough capable to fully satisfy the demands of patients with severe motor disorders, since they lack the ability to adequately recognize patient actions and intentions [83].

A usual paradigm used in rehabilitation to detect patient movement intention is based on the interaction forces between the robot and the patient. Force sensors embedded in the robot are used to detect the user movement direction and sophisticated controllers like force, impedance or admittance controllers are employed in order to adequately assist the patient [111] [127]. However, this technique require the user to have residual motor capabilities in order to apply forces on the robot and trigger its movement. As a consequence, this solution could not be used to detect the movement intention of users with a high level of disability and could be efficiently employed only to control robots which require a thigh physical interaction with the patient, such as wearable robots.

In order to provide a solution that could be easily adaptable to the users' disability level, both cognitive and physical, multimodal information coming from different sensor types could be combined to obtain a more complete picture of the user [128] [35]. The use of multiple sensors that acquire information from the user has also the advantage to not require the user to apply forces on the robots for triggering its movement. This implies that this

solution could be used not only for rehabilitation wearable robots but also for assistive manipulators.
In order to record multimodal informaton from the users, many solutions have been proposed in the literature. They could be gathered into 5 categories, i.e. i) Acoustic devices ii) Optics devices iii) Bionics devices iv) Motion devices and v) Tactile devices.

Acoustic devices Acoustic or sound based technology is mainly focused on speech recognition, and can be used to convert spoken words to text, manipulate or control a device, or communicate with a machine. Generally, a human operator is required to speak towards a microphone and his/her voice is then converted into electrical signals to be processed by computers or microcontrollers. Using pattern recognition techniques important features from these electrical signals could be extracted and hence words can be recognized to provide the device to be controlled, e.g. a robotic system, with user commands. In [73] [46][101] speech recognition is used to control a assistive robots.

Another interesting application of acoustic technology in HMI is the myography, which consists of measuring the acoustic properties of muscles as they contract [12]; the more a muscle contracts the greater is the measured sound.

Optics devices Optic based technology does not usually require the user to physically interact with the device to be controlled. Therefore, hand gesture recognition and body tracking is one of the most popular applications of optic based technology, due to the freedom from the physical interaction between the robot and machine. Devices like cameras, laser and LEDs are commonly used to build optic based HMIs. Several works in literature, for instance, adopt RGDB cameras to teleoperate robotics manipulators in hazardous environment [69], robot-assisted surgery [84] and tele-rehabilitation [55]. Human arm motion is first recorded by means of cameras and subsequently replicated onto the robot kinematic chain throughout human to robot motion mapping methods [36]. As an alternative to camera based HMI, Laser and LEDs are also widely used for hand gesture recognition in portable solutions [91]. As the human hand is moved closed to the LED based HMI, the Infra Red (IR) light is reflected back and captured by the sensors. A laser system works in a similar way: light is emitted and tracked by the sensors embedded in the HMI.

Bionics devices Bionic technology includes any device that uses or monitors the biological signals from the human body, in order to perform a function. These biological signals are usually recorded via electrodes and are i) electroencephalographic (EEG) signals, ii) electromyographic (EMG) signals and iii) electrooculographic (EOG) signals. In most

cases the same electrodes can be used to measure different biological signals just by altering the monitored frequencies and changing the amplification level.

Electroencephalography is the recording of the human neurons electrical activity and it is the basis of the Brain Computer Interface (BCI). Generally there are two forms of BCI, invasive and non-invasive. Invasive BCI requires people to have electrodes surgically implanted onto the brain, in order to monitor its activity. In [116] [42] invasive BCI is used by a tetraplegic subject in order to control a robotic manipulator in daily living activities. When the less intrusive form of BCI is adopted, surface electrodes are put onto the user head at specific points, and electric signals of few microvolts coming from the user scalp are measured and then amplified 1000-10.0000 times. In [37] [14] non-invasive BCI is used by patients in order to control assistive robots, like exoskeletons or manipulators.

Electromyography consist of monitoring the electrical signals coming from the user muscles contraction. As for the BCI, intrusive or non-intrusive electrodes can be used to measure the user myoelectric activity. Non-invasive surface electromyography is widely used by upper-limb amputees in order to operate commercially available prosthetic devices [130]. Intrusive methods not only include surgically implantation, but also the injection of needle and wire electrodes directly into the muscle. It is mainly a research technique and it is not implemented in commercial devices yet [106]. EMG signals are also used in literature to control robotics manipulators [32], and exoskeletons [56], either to enhance users strength in military field [52] or to restore motor functionalities in rehabilitation [33] and assistive field [11]. Moreover, EMG is particularly useful for accurately detecting the level of force supplied by the user muscles, that is crucial for fine control of prosthetics [45].

Electrooculography is the process of measuring eye muscle movements, by placing electrodes on the user cheekbone. They are typically used for providing support to people with disabilities, allowing, those who cannot walk, to control a wheel chair[10], and those who cannot speak to interact with virtual keyboards [121].

Tactile devices Tactile based technology includes all the devices that require a physical interaction between the user and the machine. Several interfaces are grounded on touch technologies. The most typical is the push button, as well as joysticks that are usually adopted to control commercially available assistive robots (such as the iARM [48] and the Jaco [75]). To the tactile based technology belong also motion sensing gloves that can be a valuable option to cameras for teleoperating robotic hands [24]. Other tactile devices are the haptic interfaces, that are typically used in some surgical procedures [124].

Motion devices Motion technology includes all the inertial devices that can detect motion, as the gyroscopes and accelerometers. Typically, in order to measure position, they are

combined together in Inertial Measurement Units (IMUs) or with a magnetometer (M-IMUs), and the measured velocity, acceleration and magnetic field are processed through particular filters like complementary or Kalman filters [40]. The most typical application of these devices in HMI, is the human body tracking. Wearable magneto inertial sensors are widely used in literature to control robotic system by using a teleoperated approach [100].

Human-robot allocation of functions

Determining appropriate human-robot autonomy during robot-aided task performing is crucial for a successful accomplishment of the activity and for a better patient involvement [22]. Human-robot autonomy, is largely explained as an allocation of functions between a human and a robot and strictly depends on the type of task to be performed [41] and on the user functional and physical disability [98].

In literature the robot autonomy is referred to as the robot capability to carry out its own processes and operations and is strongly related to the frequency of the human operator intervention in the robot control. Higher robot autonomy requires less frequent user intervention; conversely, lower robot autonomy requires more frequent intervention.

The level of Human-robot autonomy measured by the amount of the user intervention in the robot control ranges from the teleoperation level in which a person is remotely controlling the robot and a constant user intervention is required, to a robot full autonomy in which no intervention of the user is required.

A user-robot shared control is typically used in rehabilitation and assistive fields. In this case the robot could have a high or low level of autonomy depending on the user disability level and on the type of task to be performed. When the robot has a low level of autonomy the user can typically control the position of the robot continuously during the task performing. This solution is best suited for patients with a low level of disability and guarantee attentive usage and fine control of the device and hence a more patient involvement without affecting the correct execution of the task.

Otherwise, when the robot has a high level of autonomy, the user can select the task to be performed by means of the user intention detection module and the robot will autonomously perform that task. Solutions based on a high level of robot autonomy are typically adopted with patient with high level of disability in which the task accomplishment is guaranteed with a less physical and cognitive demand.

Progress beyond the SoA The contribution of this thesis is to propose a user interface made of M-IMU coupled with EMG to control motion of a arm-hand robotic system.

The M-IMU has been positioned on the subject head. The head motion signals are translated into robust and quick commands for the robotic device. In order to avoid involuntary movement of the robot, the M-IMU has been combined with EMG superficial electrodes positioned on the subject arm with the aim of enabling the robot motion.

The combined use of these two interfaces allow the user to continuously control the arm-hand robotic system with a low cognitive load and a high user involvement. The proposed approach has been compared with a standard interface (consisting of the voice recognition) for continuous motion control of a robotic system. The main advantage in using the voice recognition instead of other interfaces (such as joysticks) is that it can be easily used also by subjects with severe disabilities in upper limbs.

To the best of our knowledge, since there are no studies in literature aimed to assess patients feelings related to the amount of his/her intervention in the robot control, a further contribution of this work is addressed to compare two different control strategies for robotic manipulators and exoskeletons in terms of usability and user acceptance. They are named in the following i) continuous control, that require the user to continuously interact with the device (low robot autonomy) and ii) trigger control, that require only a few actions to the user in order to start the robot movement (high robot autonomy).

To summarize, two experimental validations were carried out. They are named in the following Experimental validation 1 and Experimental validation 2. The 1^{st} experimental validation was aimed at comparing the proposed M-IMUs/EMG control interface with a standard interface consisting of the voice recognition. The experimental study has involved sixteen healthy subjects randomized in two groups who were asked to perform the drinking task by controlling the manipulator with the two interfaces. The 2^{nd} experimental validation was intended to compare the two different control modalities of the proposed M-IMUs/EMG interface, i.e. the M-IMUs/EMG continuous control and M-IMUs/EMG trigger control. Six subjects with different upper-limb impairment conditions were recruited for the study. They were asked to perform one activity of daily living, i.e. drinking, and 2 tasks belonging to the SHAP clinical test, i.e. pouring and reaching-grasping-moving-releasing a sphere, with the aid of a robotic upper-limb exoskeleton piloted by the means of both the M-IMU/EMG continuous control and M-IMU/EMG trigger control.

3.1.2 Proposed non-invasive interfaces for the control of robot manipulators and exoskeletons

The two EMG electrodes can be placed either on a pairs of antagonist muscles, i.e. biceps and triceps of left/right arm, or on the same muscle of the two arms (as it has be done in

this work), depending on the user muscle capabilities, in order to estimate the target muscles myoelectric activity and trigger the robot movements; the two M-IMUs are placed on the user's trunk and head, in order to evaluate the head orientation (i.e. Roll and Pitch). The sensor placed on the subject trunk acts as reference for the sensor positioned on the head.

Two versions of the strategy have been proposed. The former version, named in the following combined M-IMU/EMG continuous control, requires a continuous user interaction with the robotic device. It aims at facilitating a more fine control of the device and maximizing the user involvement. The latter is named combined M-IMU/EMG trigger control and aims at minimize the patient physical and cognitive load required to control the robotic device. A flux diagram of the combined M-IMU/EMG continuous control is shown in Fig. 3.1. The user can choose between two states using a cyclic selection method, by means of a double co-contraction of the left and right arm biceps. An acoustic signal notifies the user that the state changing occurred. In the first state the user can operate the robotic hand opening and closing by contracting left and right arm biceps, respectively, without moving the robot arm.

On the other hand, in the second state, when the biceps of the right arm is contracted, the user can control the end-effector movements through the head along X and Y axes. The head roll causes the robot end-effector movements along X axis and the head pitch causes the robot arm movements along Y axis. Instead, when the biceps of the left arm is contracted, the user can control the robot arm movement along Z axis and orientation about Z' axis. The head Pitch causes the robot movements along Z axis and the head Roll causes the robot end-effector rotation about Z' axis.

By means of the combined M-IMU/EMG trigger control the user may exploit: i) the head yaw motion in the negative direction to operate the movements of the robotic device which will autonomously accomplish the task and the head yaw motion in the positive direction to abort the task; ii) the contraction of the right biceps or left biceps to trigger the hand opening and the hand closing.

3.1.3 Experimental validation 1

The proposed approach has been compared with a standard interface (consisting of the voice recognition) for continuous motion control of a robotic system (composed of a robotic arm, i.e. the KUKA LWR 4+, and a robotic hand, i.e. the IH2 Azzurra). The main advantage in using the voice recognition instead of other interfaces(such as joysticks) is that it can be easily used also by subjects with severe disabilities in upper limbs. The experimental study has involved sixteen healthy subjects randomized in two groups and performing the drinking task by controlling the manipulator with the two interfaces.

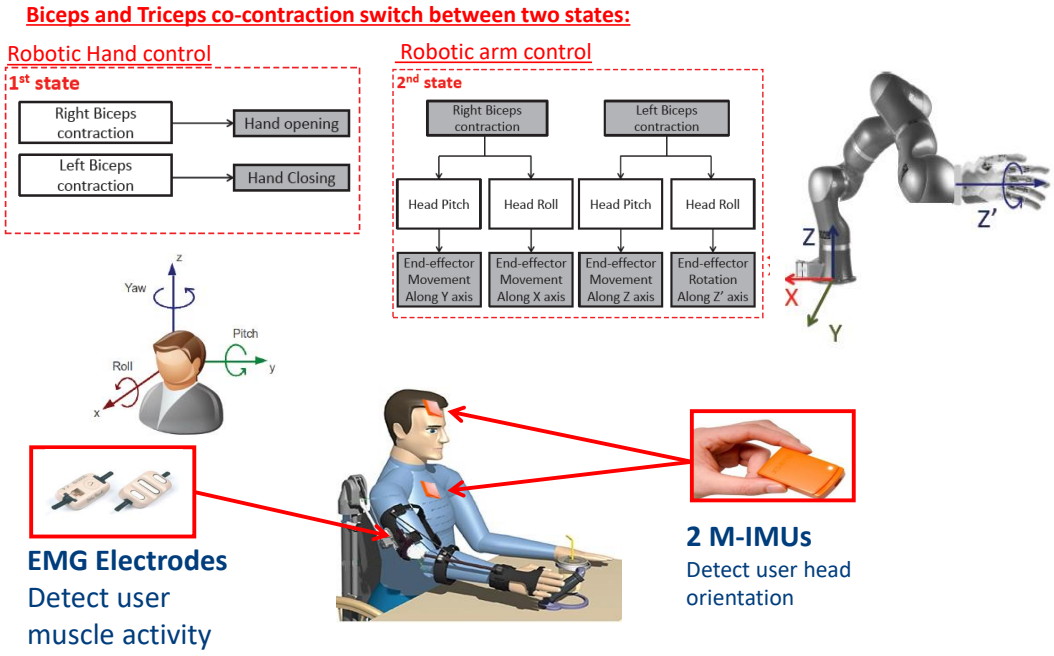

Fig. 3.1 Block scheme of the proposed control strategy for robotic manipulators and upper-limb exoskeleton

A modular architecture for managing the communication among the platform subsystems (i.e. the interface and the robotic devices) is proposed. In this work, one interface at time has been adopted by the user but, thanks to the modularity of the communication system, more than one interface could be introduced enabling the user to choose the interface that is well-suited to task execution.

Voice control

The voice control interface is based on the speech recognition software developed by Microsoft and available under the Universal Windows Platform (UWP) for Windows 10. A graphical user interface (GUI) has been developed in order to start and stop the voice acquisition. A list of possible words the user can pronounce for controlling the robotic device has been defined. In particular, the user can choose one of the actions listed in the right column of Table 3.1 and move the robot by means of the voice command reported in the left column.

The speech recognizer translates naturally spoken commands entered via a microphone into specific words using predetermined grammar. When the speech acquisition starts, the software compares the word said by the user with a dictionary available on the PC. As soon as a word is recognized, a string containing the word is generated and compared with the words in the predefined list (Table 3.1). If the words match each other, the command is

transmitted to the robot, as a state ranging from 0 to 12, through the YARP messaging system described in Sect. 3.2.5.2.

Table 3.1 Voice control interface for moving a robot

Voice Commands	States	Robot Actions
Stop	0	The robotic hand will stop moving
Up	1	The robot end-effector will move along Z axis in the positive direction until another command is delivered
Down	2	The robot end-effector will move along Z axis in the negative direction until another command is delivered
Left	3	The robot end-effector will move along X axis in the negative direction until another command is delivered
Right	4	The robot end-effector will move along X axis in the positive direction until another command is delivered
Onward	5	The robot end-effector will move along Y axis in the positive direction until another command is delivered
Backward	6	The robot end-effector will move along Y axis in the negative direction until another command is delivered
Counterclockwise	9	The robot end-effector will rotate counterclockwise about the Z' axis until another command is delivered
Clockwise	10	The robot end-effector will rotate clockwise about the Z' axis until another command is delivered
Open	11	The robotic hand will open until another command is delivered
Close	12	The robotic hand will close until another command is delivered

3.1.3.1 Experimental setup

The block scheme of the whole platform presented in this work is shown in Fig. 3.2.
As shown in Fig. 3.2, the user can control the robotic system by means of the voice or the combined M-IMU/EMG interfaces. The motion commands acquired by the user are sent, through the YARP server, to the robotic devices. All the acquired data are synchronized and saved under YARP. A work station is used to run Yarp server and perform sensor fusion.

The combined M-IMU/EMG interface used for acquiring motion command from the users is composed of two double-differential EMG electrodes (Otto Bock 13E200=50 model) with an amplification gauge ranging in between 100 and 2000 to acquire electromyographic activity of the target muscles. They have been placed on the subject's arms along the

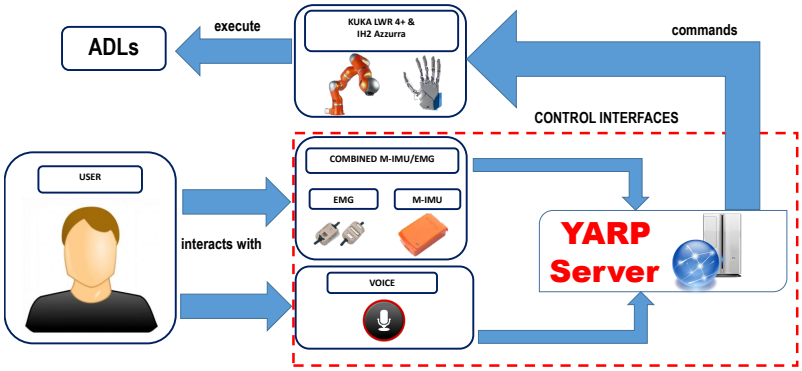

Fig. 3.2 Block scheme of the platform components outlining the information flow among the subsystems.

longitudinal mid line of the target muscles by means of elastic bands. A National Instruments (NI) USB-6003 DAQ with a 16-bit ADC has been used for analog-to-digital conversion of the EMG signal. Two wireless M-IMUs (XSens MTw) have been used to detect head movements. Each sensor has been applied onto the body of the subject by means of strap holders. The sensor positioned on the user's head gives the sensor movement with respect to the reference sensor positioned on the subject trunk. An Awinda Station has been used to check the reception at 100 Hz of synchronised wireless data from the two wirelessly connected M-IMUs.

The robotic arm is made of the Kuka Light Weight Robot 4+ [3]. It is an anthropomorphic arm with 7 active DoFs. It is equipped with position and torque sensors at joints. An UDP communication protocol is adopted for connecting a remote PC, on which runs the Fast Research Interface (FRI) Library, to the KUKA Robot Controller. The IH2 Azzurra anthropomorphic robotic hand [93], has been connected to the KUKA LWR end-effector in order to act as the hand of the robotic platform. It is a 5-finger robotic hand with a weight (640 g) and a size similar to the human ones. The hand has 11 DoFs, of which 5 active. The underactuated mechanism allows the fingers to automatically adapt to the object shape while closing.

IMU and EMG Data Fusion

The electronics integrated in the Myobock electrodes preprocess the EMG signals in order to increase the signal-to-noise ratio. In particular, a pre-amplification with a gain factor of 2000 and a high pass filter with a cut-off frequency of 20 Hz are applied to the EMG signals.
The electronic integrated in the XSens MTw elaborates the data acquired by the embedded accelerometer, gyroscope and magnetometer in order to output the sensor velocity and

orientation. Each sensor is characterized by a fixed coordinate system, named S. The sensor orientation is expressed in terms of rotation matrix and is computed between S and a earth-fixed reference coordinate system, called G. The coordinate system G is defined with X positive, when pointing to the local magnetic North, Y defined according to right handed coordinates (West) and Z positive when pointing up (as shown in Fig. 3.1). Indicating with S_1 and S_2 the fixed coordinate systems of the sensors placed on the subject trunk and head respectively, the head Roll and head Pitch, θ_1 and θ_2 are evaluated as follows

$$R_{S_1}^{S_2} = R_{S_1}^{G} R_{G}^{S_2} = \begin{bmatrix} r_{11} & r_{12} & r_{13} \\ r_{21} & r_{22} & r_{23} \\ r_{31} & r_{32} & r_{33} \end{bmatrix} \tag{1}$$

$$\theta_1 = \text{atan2}(r_{21}, r_{11}) \tag{2}$$

$$\theta_2 = \text{atan2}(-r_{31}, \sqrt{r_{32}^2 + r_{33}^2}) \tag{3}$$

The data recorded by the EMG electrodes and M-IMUs are fused to detect user motion intention. Referring to Fig. 3.1, if the 1^{st} or the 2^{nd} state is selected and the user rotates the head with an angle that exceeds a preset threshold of $0.52rad$, the muscle contration activates the robotic device motion and the robot end-effector moves and rotates according to the flux diagram in Fig. 3.1 at a preset velocity of $0.01m/s$ and $0.02rad/s$. One muscle is considered contracted when the amplitude of the EMG signals exceeds a predetermined threshold, i.e. $1V$.

3.1.3.2 Experimental protocol

Sixteen healthy subjects, 25.4 ± 3.5 years old on the average, have been recruited for this study and randomized in two groups. Eight subjects have been asked to use the voice control for performing an activity of daily living task, i.e. the drinking task, with the arm-hand robotic platform. The other eight subjects have been asked to use the combined M-IMU/EMG interface for accomplishing the same task.
Before beginning the test with the combined M-IMU/EMG interface, the M-IMUs calibration has been carried out. The participants have been seated in front of a table on which the objects have been located in a-priori known position. Before starting the data acquisition, each participant has been asked to use the interface for controlling the arm-hand robotic system to perform the drinking task 5 times, for learning the use of the interface. Then, the subjects have been asked to repeat the drinking task for 10 times. In particular, the task is composed of the following actions: (i) reaching and grasping a glass properly placed in the

the robot workspace, (ii) bringing the glass to the user's mouth, (iii) bringing and releasing the glass on the table. The starting configuration of the robot is shown in Figs. 3.3. After the trials, the subjects have been asked to evaluate the level of satisfaction by means of questionnaires and evaluation scales for evaluating the platform usability.

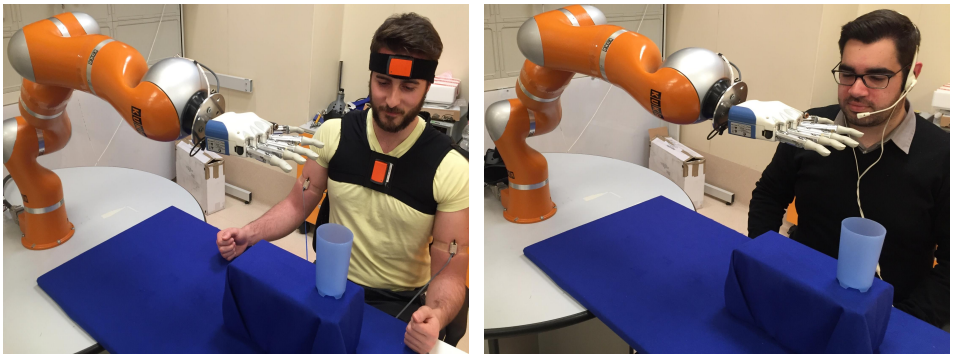

(a) (b)

Fig. 3.3 Combined M-IMU/EMG (a) and Voice control (b) for assistive robots: Experimental setup

Performance indices

The data acquired for each trial from the voice commands, the M-IMUs, the EMG sensors and the robot encoders have been segmented from the time when the velocity of the end-effector exceeded the 10% of the peak value up to the time when velocity decreased under the 10% of the peak value. The segmented signals have been processed to extract quantitative indices for describing the subject's capability of using the interfaces for controlling the arm-hand robotic system. They are listed in the following:

- **Completion time and average speed** – The completion time corresponds to the time needed for accomplishing the drinking task and is computed as the time interval from the time instant when the robot velocity grows up the 10% of the peak value to the time instant when the velocity drops to the 10% of the peak value.
- **Success rate and position error** – Success rate refers to the number of successful trials performed by a subject. The trial is considered failed when the position error, computed as the error between the final position of the robot end-effector and the a priori known object position, is higher than $0.05m$.

- **Interface delay** – The interface delay corresponds to the delay between the time when the command is sent by the user (in terms of voice or EMG/IMU activation) and the instant when the robot starts the corresponding movement.

- **Number of states** – The number of states is the number of user required actions for accomplishing the task by means of the interface.

- **Usability** – The interfaces usability has been evaluated by means of questionnaires and interviews. They are useful for studying if the users are satisfied with the interface and what features they particularly like or dislike. The subjects have been asked to fill the VAS questionnaires and answer the questions reported in Table 4.1. They are extracted from the Usefulness-Satisfaction-and-Ease-of-use-questionnaire (USE, [72]) and focus on the experience of the system usage. The last questionnaire uses a seven-point Likert rating scale. Finally, the overall workload has been estimated by means of the NASA Task Load Index.

3.1.3.3 Results and discussion

EMG, M-IMU and voice data have been recorded during the task execution. In Figs. 3.4 and 3.5, the EMG and IMU data are shown for a representative subject as an example of the performed sensor fusion. Additionally, robot motion in the task space is reported in Fig. 3.6. These data are reported from the starting time until the time when the robotic hand grasped the glass.

In Figs. 3.4–3.6, a dashed line is shown in correspondence of the state changing. The figure part delimited by two consecutive dashed lines (named (a_i in Fig. 3.4 or b_i in Fig. 3.5), indicates a single state. From these figures, one can observe that:

- when the left biceps EMG signal exceeded the threshold (part of Fig. 3.5 named $b1$) and the user's head pitch angle exceeded positive threshold (part of Fig. 3.5 named $a1$), the robot end-effector moved along the robot Z axis in the negative direction (part named $c4$);

- when the left biceps EMG signal exceeded the threshold (part named $b2$) and the user's head roll angle exceeded the negative threshold (part named $a2$), the robot end-effector rotated about Z' axis in the negative direction (part named c6);

- when the right biceps EMG signal exceeded the threshold (part named $b3$) and the user's head roll angle exceeded the positive threshold (part named $a3$), the robot end-effector moved along X axis in the positive direction (part named c1);

- when the left biceps EMG signal exceeded the threshold (part named *b*4) and the user's head pitch angle exceeded the positive threshold (part named *a*4), the robot end-effector moved along Z axis in the negative direction (part named c5);
- when the right biceps EMG signal exceeded the threshold (part named *b*5) and the user's head pitch angle exceeded the positive and negative threshold (parts named *a*5 and *a*6), the robot end-effector moved along Y axis in the positive and negative direction respectively (part named c3);
- when the right biceps EMG signal exceeded the threshold (part named *b*5) and the user's head roll angle exceeded the positive threshold (part named *a*7), the robot end-effector moved along X axis in the positive direction (part named c2);
- when both the right and left biceps EMG signal exceeded the threshold (part named *b*6) the user changed the state to the hand control and with the user's right biceps contraction (part named *b*7) the robotic hand closed and grasped the glass.

In Fig. 3.7, the states for the voice control recorded during the task execution for a representative subject are shown. Robot motion in the task space is reported in Fig 3.8. As for the combined M-IMU/EMG, these data are reported from the starting time until the time when the robotic hand grasped the glass. It is evident that:

- when the user pronounced the word "Right", state 4 was selected (part of Fig. 3.7 named *d*1) and the robot end-effector moved along X axis in the positive direction (part of Fig. 3.8 named *e*1);
- when the user said the word "Clockwise", state 10 was selected (part named *d*2) and the robot end-effector rotated about Z axis clockwise (part named *e*3);
- when the user said the word "Down", state 2 was selected (part named *d*3) and the robot end-effector moved along Z in the negative direction (part named *e*2);
- when the user said the word "Close", state 12 was selected (part named *d*4) and the robotic hand closed and grasped the glass.

Mean value and Standard Deviation (SD) of the above mentioned performance indices evaluated on the ten trials for each subject and control strategy are reported in Table 3.2

The interface delay is significantly higher for the voice control than for the M-IMU/EMG control. In fact, the mean value $\pm$ SD for the voice recognizer delay is 1.6 ± 0.8 and for the M-IMU/EMG delay is 0.7 ± 0.9. This is due to the limits of the developed speech

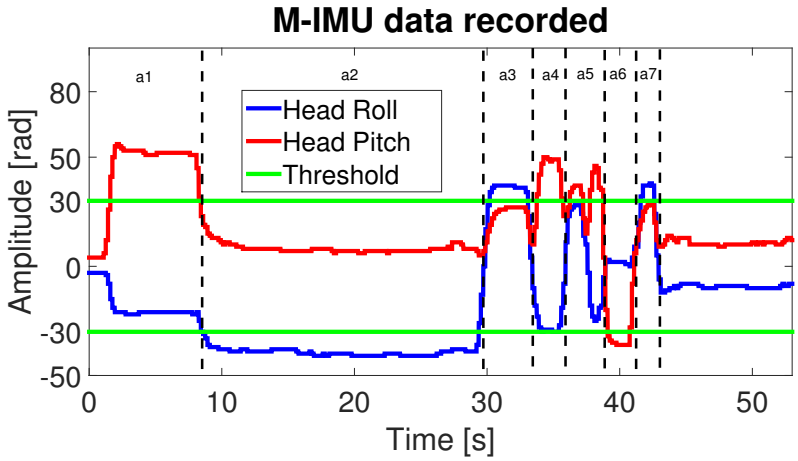

Fig. 3.4 M-IMU data recorded for a representative subject during the execution of the task with the Combined M-IMU/EMG interface.

recognizer system that has to look for the words in a dictionary. This also influences the position error; when the robot motion is controlled by means of the M-IMU/EMG, it is lower (0.03 ± 0.03) than the error measured when the robot motion is controlled by means of the voice (0.18 ± 0.37). In fact, the delay between the voice command and the robot movement implies the difficulty to perform fine movements, and then position the robot end-effector with a high level of accuracy. Therefore, being the user able to accurately control the robot motion, she/he tends to make the robot perform a high number of movements in order to minimize the position error. Consequently, it is evident a higher success rate for the users that control the robot by the M-IMU/EMG (88 ± 47) than for the subjects using the voice (72 ± 21).

Table 3.2 Performance results

Interface	Success Rate [%]	Execution Time [s]	Number of States	Error [m]	Delay EMG [s]	Delay M-IMU [s]	Delay Voice Recognizer [s]
Combined M-IMU/EMG	88 ± 47	128 ± 47	43 ± 10	0.03 ± 0.03	0.4 ± 0.4	0.7 ± 0.9	–
Voice control	72 ± 21	129 ± 37	22 ± 8	0.18 ± 0.37	–	–	1.6 ± 0.8

Performance indices value (given by using a seven-point Likert rating scale) are also reflected in the answers the subjects provided to the USE questionnaire (Table 4.1). The mean and standard deviation (SD) of the questionnaire factors are presented. Furthermore, the subjects have been asked to point out their major concern about the difficulties in using the interface for controlling the robotic platform. The subjects referred that the main problem they met while using the vocal command was related to the delay between the vocal command and the robot motion; on the other hand, for the combined M-IMU/EMG interface they referred

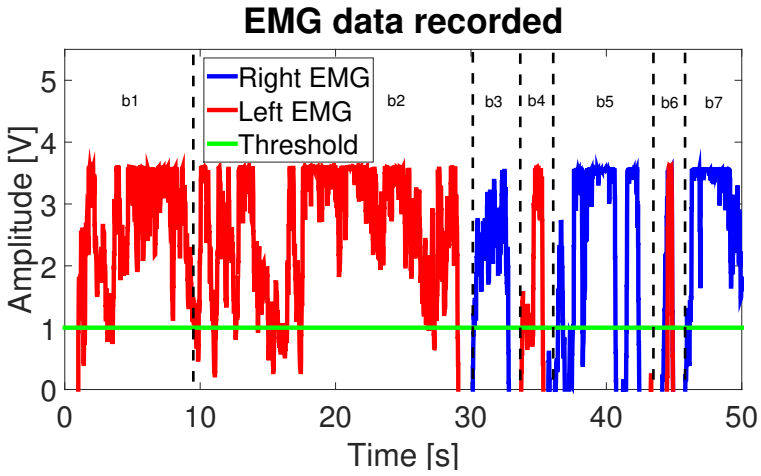

Fig. 3.5 EMG data recorded for a representative subject during the execution of the task with the Combined M-IMU/EMG interface.

that the threshold for the IMU activation was too high. All the subjects were able to improve their performance in the drinking task after a short period of training, thus suggesting that the successful use of the interfaces is rather intuitive. This aspect is also confirmed by the answer to the question, reported in Table 4.1, about how essential was the training for properly using the interface.

The overall satisfaction in the use of the interfaces has been evaluated by means of the VAS device satisfaction. The mean and standard deviation obtained for the voice recognizer (i.e. 6.8 ± 0.8) and for the M-IMU/EMG interface (i.e. 7.9 ± 1.2) confirm the results obtained for the performance indices. The overall workload computed with the NASA TLX questionnaire for the subjects that used the M-IMU/EMG interface (i.e. 50) was comparable to the one of the voice recognizer (i.e. 47).

3.1.4 Experimental validation 2

The 2^{nd} experimental validation was aimed to carry out a comparative analysis between the M-IMU/EMG continuous control and M-IMU/EMG trigger control presented in Sect. 3.1.2, in terms of patient's acceptability and effects on the task completion.

3.1.4.1 Experimental setup and protocol

Six subjects with different upper-limb impairment conditions were recruited for the study. They were 37.5 ± 12.11 years old and had a Barthel index of 8.16 ± 6.79. Three of them suffered from limb-girdle muscular dystrophy, two of them by spinal muscular atrophy and one was a post-stroke patient. They were asked to perform one activity of daily living, i.e.

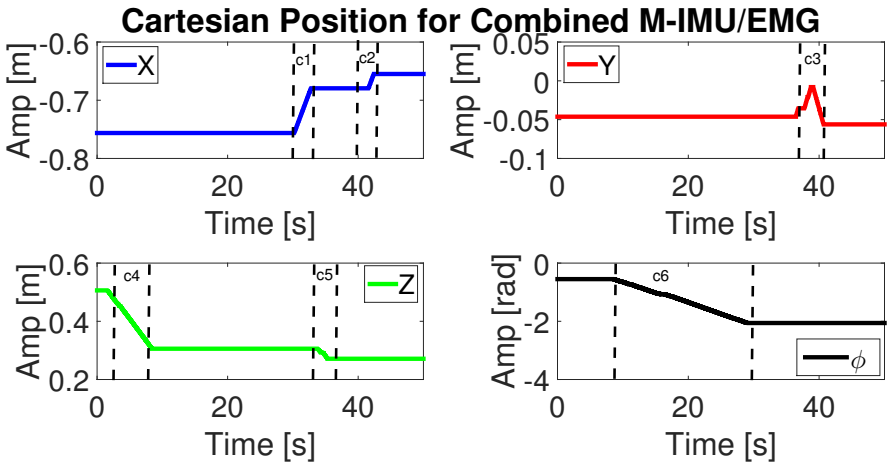

Fig. 3.6 Robot position recorded for a representative subject during the execution of the task with the Combined M-IMU/EMG interface. ϕ is the end-effector rotation about z'-axis.

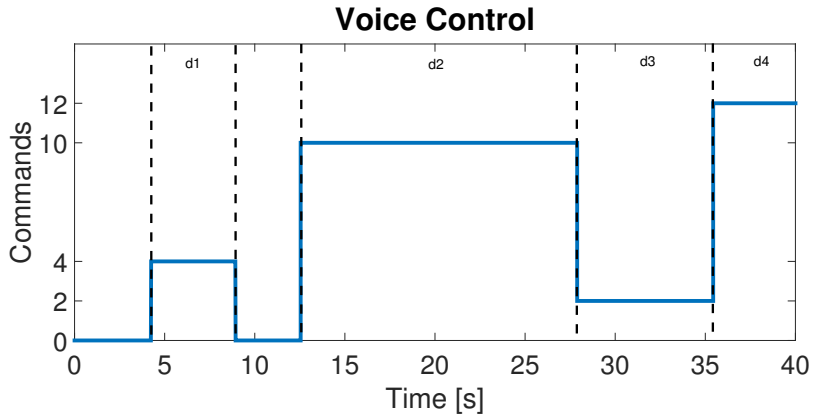

Fig. 3.7 Voice states recorded for a representative subject during the execution of the task with the Voice control interface.

drinking, and 2 tasks belonging to the SHAP clinical test, i.e. pouring and reaching-grasping-moving-releasing a sphere, with the aid of a robotic upper-limb exoskeleton composed of a 4-DoF shoulder-elbow exoskeleton and a 5-DoF wrist-hand exoskeleton (see Sect. 3.2.4 for more details about the experimental setup). Three trials per task were performed by each subject with the aid of the robotic exoskeletons piloted by the patients by means of both the M-IMU/EMG continuous control and M-IMU/EMG trigger control.

For the trials with the M-IMU/EMG trigger control, drinking, pouring and reaching-grasping-moving a sphere tasks have been performed according to the scheme presented in Fig. 3.9

The following sequence of states has been implemented by means of a Finite State Machine (FSM):

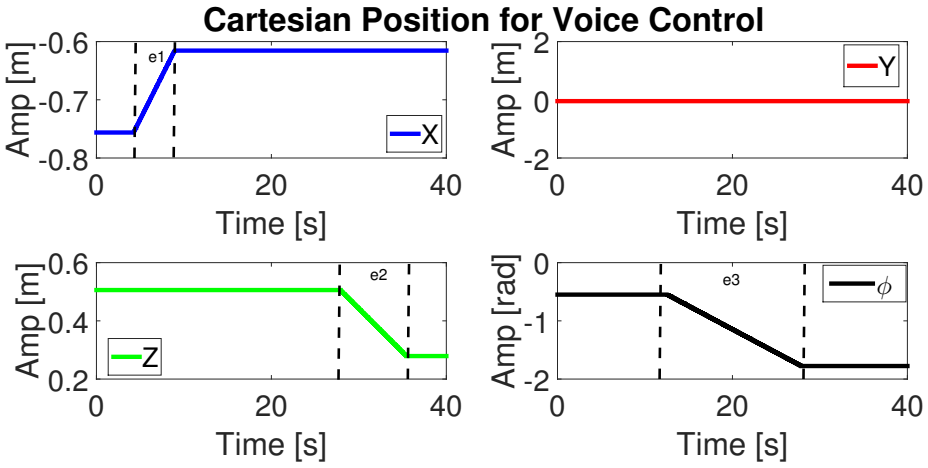

Fig. 3.8 Robot position recorded for a representative subject during the execution of the task with the Voice control interface. ϕ is the end-effector rotation about z'-axis.

- From the resting position, the user can select the object he/she wants to grasp;
- The movement of the arm exoskeleton is triggered by the user interface;
- The Hand Trigger is used to command the closing of the hand exoskeleton.
- Once the hand is closed, the exoskeleton automatically starts to move toward the "Target 2 Position" with "Angle T2" arm orientation.
- After the completion of the movement, another Hand Trigger is required to open the hand and bring the exoskeleton back to the initial position.

For the M-IMU/EMG continuous control, the user has been requested to perform drinking, pouring and reaching-grasping-moving a sphere tasks, without any restriction on the sequence of actions to be executed. A predefined maximum time of 5 minute has been chosen to perform the task, after which the trial has been considered unsuccessful.

The user could control the movement of the arm and wrist exoskeleton in the Cartesian space, by continuously moving the end-effector along planar direction within the workspace of the robot. By combining the activation of the EMG signals (contraction of the biceps and contraction of the triceps) with the head movements detected by the M-IMUs, different planar movements of the end-effector have been allowed, grouped in two subsets according to the muscle which has been activated. The co-contraction of the two muscles allowed to switch between the hand and the arm exoskeleton control.

In the continuous control of the arm exoskeleton, the following combination have been implemented:
Biceps contraction combined with:

Table 3.3 Questionnaire

Question	Answer for Combined IMU/EMG	Answer for Answer for Voice Control
The interface is intuitive and easy to use	6.2 ± 0.7	6 ± 0.2
The training was essential for properly using the interface	6 ± 0.8	6.8 ± 0.1
I felt confident using the system	6.5 ± 0.2	6.7 ± 0.2
The system was easy to use	6.1 ± 0.3	6 ± 0.5
I imagine that most people can quickly learn how to use this system	6.1 ± 0.5	5.5 ± 0.7
My whole concern about the interface	High threshold value for the imu activation	High voice recognition delay

- Neck extension: the End Effector (EE) moves up in the frontal plane (cranial direction)
- Neck flexion: the EE moves down in the frontal plane (caudal direction)
- Neck left lateral bending: the EE moves to the left in the horizontal plane (medial direction)
- Neck right lateral bending: the EE moves to the right in the horizontal plane (lateral direction)

Triceps contraction combined with:

- Neck extension: the EE moves backward in the sagittal plane (posterior direction)
- Neck flexion: the EE moves forward in the sagittal plane (anterior direction)
- Neck left lateral bending: wrist pronation
- Neck right lateral bending: wrist supination

In the control of the hand exoskeleton, the opening and closing of the hand have been triggered by the biceps contraction and triceps contraction, respectively. The switching from the hand control to the arm control has been allowed only after the opening/closing movement has been completed. A visual interface (Fig. 3.10) has been used to provide the user with a feedback about the device he/she was controlling (i.e. arm or hand exoskeleton), the option available upon the activation of a specific muscle and the time remaining for the trial.

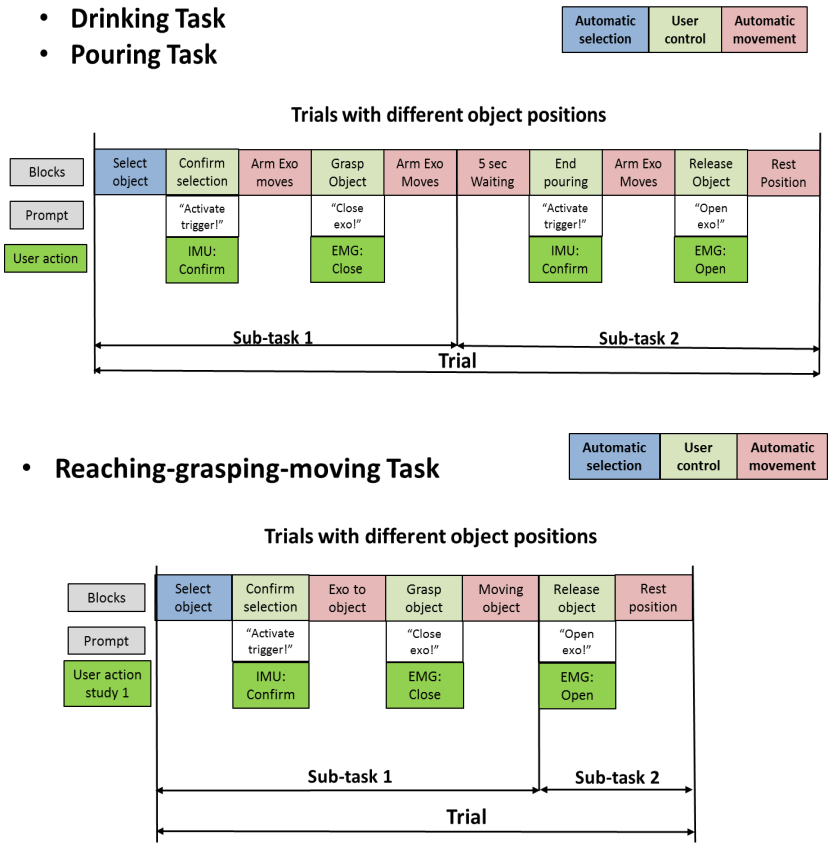

Fig. 3.9 Study design of the M-IMU/EMG trigger control for drinking and pouring tasks (up) and reaching-grasping-moving tasks (down).

None of the subjects was able to sustain a prolonged contraction of the selected muscles (in particular in the trials with the M-IMU/EMG continuous control), thus the EMG electrodes have been pressed as ON-OFF switches with the finger. One of the subject was not able to properly wear the exoskeleton, thus only the trials with the continuous control were performed, using the arm exoskeleton as an external manipulator. Another subject performed the trials with the continuous control at the beginning and was not able to complete the protocol with the M-IMU/EMG trigger control trials, because of weariness. For similar reasons, the first subject, which started with the M-IMU/EMG trigger control, was not able to complete the protocol with the continuous control.

3.1.4.2 Results and discussion

The NASA TLX test was submitted to the patients after using the M-IMU/EMG trigger control and the M-IMU/EMG continuous control. The analysis of the obtained data let us

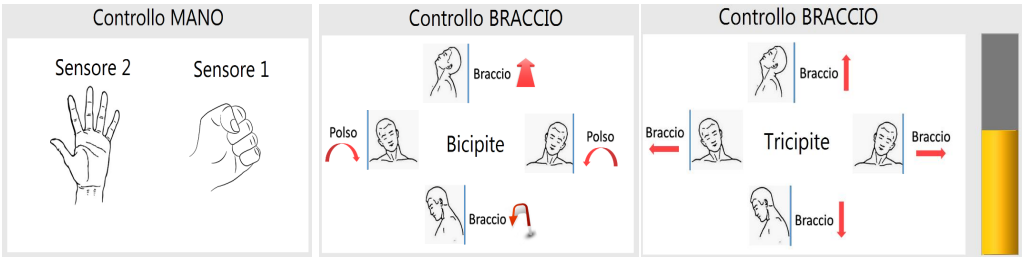

Fig. 3.10 Frame of the visual interface for the continuous control.

evaluate if the control strategy influences the subjective perception of the task workload. In the following the M-IMU/EMG trigger control will be named "Condition1", and the M-IMU/EMG continuous control will be named "Condition2", since they can be considered as two workload conditions. Four of the six patients involved in the study are taken into account in the following analysis since they were able to perform both the control conditions. In order to evaluate the significance in the difference between the two conditions, the Mann-Whitney test has been used. Statistical significance has been set at a p-value<0.05. In Tab. 3.4, results of the non-parametric statistical test are listed. As supposed, statistically significant differences have been found for the "Temporal demand" and the "Effort". For the other scales of the NASA TLX test, no statistically significant differences have been found between the two conditions in the subjective evaluation.

The two control modalities have been compared in terms of success rate in the task execution. Four subjects (number 1, 2, 3, 5) completed the protocol with the trigger-based trial; five subjects (number 2, 3, 4, 5, 6) completed the protocol with the continuous-based trials.

Tab. 3.5 reports the results in terms of success rate (percentage of successful trial over the total number of trials) for each subject in the two conditions.

With the exception of Subject 5, the M-IMU/EMG trigger control had higher success rate in the subjects which performed the trials with both control modalities. Indeed, the activation of the interfaces have been easier in the M-IMU/EMG trigger control, where just one head movement has been required to trigger the movement of the exoskeleton.

The two conditions performance has been evaluated also in terms of success rate (i.e. number of times that the activity has been correctly carried out). When the M-IMU/EMG trigger interface was adopted a success rate ranging from 70% to 100% was achieved;

	Trigger		Continuous	
	Success rate (Success/Total)	Task type	Success rate (Success/Total)	Task type
S1	100 % (16/16)	Drinking (4) Pouring (4) R-G-M (8)	-	
S2	100 % (16/16)	Drinking (4) Pouring (4) R-G-M (8)	60 % (3/5)	Drinking (2) Pouring (2) R-G-M (1)
S3	90 % (9/10)	Drinking (3) Pouring (4) R-G-M (3)	66.7 % (4/6)	Drinking (3) R-G-M (3)
S4	-		50 % (3/6)	Drinking (3) R-G-M (3)
S5	72,7 % (8/11)	Drinking (4) Pouring (4) R-G-M (3)	100 % (6/6)	Drinking (3) R-G-M (3)
S6	-		100 % (6/6)	Drinking (3) R-G-M (3)

Table 3.4 Results of Mann–Whitney test for the NASA-TLX test.

whereas when the M-IMU/EMG continuous control was adopted, the success rate ranged between 50% and 100%.

The obtained results demonstrated a high patient involvement in using a M-IMU/EMG continuous control, but better performance, in terms of success rate, has been achieved with the trigger-based control.

3.2 Motion planning of robot manipulators and exoskeletons

3.2.1 Introduction

For the last few decades, part of the research activity in robotics has been focusing on the human-robot interaction, since the modern robotics is increasingly orientating towards scenarios in which robots start operating in human-inhabited environments [81]. Developing motion planning strategies, that allow the robot moving like a human and permit untrained users to easily program and safely use such a service device, plays therefore a paramount role in this context [70] [38].

A typical strategy for determining the desired trajectory to be tracked by the robot in complex tasks, such as the Activities of Daily Living (ADLs), is to replicate human movements [5]. Joint trajectories from unimpaired volunteers, caregivers or therapists

Evaluation Parameter	Rank sum	z-value	p-value
Mental Demand	15.5	-0.6193	0.5357
Physical Demand	16	-0.4383	0.6612
Temporal Demand	13.5	-1.1907	0.0234*
Performance	17	-0.1443	0.8852
Effort	14	-1.0226	0.0307*
Frustation	16	-0.4383	0.6612

Table 3.5 Results of Mann–Whitney test for the NASA-TLX test.

can be pre-recorded and later executed by the robotic system throughout specific mapping methods, i.e. spline decomposition [53], or else optimization of ad hoc developed objective functions [94]. However, these methods are successful in structured environments, since they cannot manage variability in the environment and external perturbations.

For ADLs in unstructured environment, a Cartesian motion planner can be conveniently adopted [76], and a purposely developed mathematical model of human motor behavior should be formulated in order to plan the desired trajectories in a way similar to humans. This is the case, for example, of the minimum jerk criterion [30] or the minimum torque model [118] for point-to-point reaching tasks.

For the exoskeletons, the approach based on Cartesian motion planning requires that inverse kinematics (IK) [58] is applied for computing joint motion, with the consequent increase of the computational burden. Moreover, the traditional IK algorithm with inverse Jacobian allows exploiting the available DoFs of the robot kinematic chain to achieve the desired end-effector pose; however, it does not guarantee that anthropomorphic criteria in the whole human-robot workspace are satisfied, especially in non-redundant structures. Alternative methods that account for anthropomorphic configurations in the joint space, are based on the computation of the swivel angle. It can be estimated by means of geometric methods [79] or analytical methods based on the augmented Jacobian [87]; however, in the case of non-redundant exoskeletons (as most of the commercially available ones [76]), the computation of the swivel angle causes the reduction of the number of Cartesian DoFs to be controlled, since the swivel angle is computed in lieu of one of the controlled Cartesian

coordinates; as a consequence, this entails a reduction of the success rate in the fulfilment of the ADLs.

A new approach to movement planning and imitation learning is represented by Learning by Demonstration (LbD), where the human subject is observed during the task execution and the robotic systems replicate the learned movement. LbD approaches, compared to a minimum jerk trajectory planner, have the possibility to easily replicate human-like movements and more complex tasks. Moreover, compared to a simple replicator of a recorded trajectory, or to a spline-based fitting method, they offer the advantage to be adaptable to the environment variability and modify the initial and the final points of the demonstrated trajectory by keeping the same movement shape. LbD seems to be very suitable for easily planning robot movements since it does not require an operator with technical expertise to re-plan new movements for the robot [15]. Moreover, LbD significantly improves robot behavior predictability and hence user safety, as it is well-known in literature that a human-like motion of the robot can be more easily interpreted by humans [25]. Indeed, if the robot moves in a human like-manner, the human subject can conveniently predict the robot motion and accordingly adjust his/her activity to avoid possible injuries.

Learning by demonstration based on Dynamic Movement Primitives

Three main features need to be taken into account while programming an anthropomorphic robot by demonstration: (i) generalization capability, (ii) ability to solve the correspondence problem and (iii) robustness against perturbation [90]. The generalization capability is the robot ability to adapt its behaviour to changes of the target position and it is required if one does not want to show to the robot every single movement it is expected to perform. The correspondence problem is the difference between the kinematics of the teacher and of the robot, and arises when there is a possible mismatch of link lengths and joints between the robot and the demonstrator (i.e. the human subject). Finally, the robustness against perturbation is the robot ability to on-line adapt the planned trajectory to the environment change and is essential to manage, for instance, the sudden presence of an obstacle along the planned path.

A Learning by Demonstration approach that addresses these three issues is the one based on Dynamic Movement Primitives (DMPs), i.e. a set of nonlinear differential equations with a well-defined landscape attractor [49]. In fact, Learning by Demonstration based on DMPs naturally addresses the generalization problem since DMPs are formulated in a way that convergence to different target positions is guaranteed [49]. Moreover, it deals with the correspondence problem by recording human movements in the task space, computing DMPs and then translating them in the resulting robot joint motion using Inverse Kinematics

(IK) [49]. Finally, Learning by Demonstration based on DMPs ensures robustness against external perturbation, since a differential equation has the advantage to automatically correct the dynamics of the system according to the perturbation, e.g. the presence of an obstacle [49].

Existing techniques of imitation learning require usually multiple, sometimes many, demonstrations of the same task in order to make the robot generalize learned movements to different and unseen situations [4]. Nevertheless, providing the robot with many demonstrations is not very user-friendly. LbD based on DMPs requires only one, or a few demonstrations at most, of the same task and is able to generalize to different situations [49][65][63]. The attractor landscape allows replicating the recorded trajectory by means of a weighted sum of equally spaced Gaussian Kernels. A generic modelling approach to learn the landscape attractor is proposed in [105] and consists of extracting the weight parameters (DMP parameters) from demonstrated movements, in a single shot, by means of linear regression algorithms.

DMP singularity issues DMPs can be basically used to plan the robot motion by demonstration either in the joint or in the task space. Usually, a set of independent variables, namely the joint angles or the Cartesian coordinates, are used to encode the robot motion by means of the DMP parameters. Hence, one DMP is computed for each of these variables. If the variables used to encode the robot motion exhibit some properties and are therefore linearly dependent, one will expect that those properties remain unchanged when the robot motion is planned throughout DMPs. However, this requirement is not met when DMPs are directly applied on linearly dependent variables. Thus, when planning the robot motion in the Operational space, a minimal representation of the end-effector orientation, e.g. independent variables like Euler angles, needs to be adopted with the consequent occurrence of singularity issues [112].

One way to solve this issue is to reduce the end-effector orientation Range of Motion (RoM). Nevertheless, working in a limited range is quite restricting especially for the motion planning of complex tasks, like the Activity of Daily living, that require a wide RoM to be accomplished [74]. Another effective solution that is typically used in literature to address singularity issues is to work with a redundant representation of the orientation, e.g. by means of Rotation matrices or Unit Quaternions [27].

Rotation matrices give a redundant description of frame orientation as they are characterized by nine elements which are not independent; these elements are related by six constraints that are due to the orthogonality conditions between the rotation matrix columns [85]. Rotation matrices basically constitute a Lie group, that is referred to as SO(3), with an associated Lie algebra, which is the tangent space around the identity element of the group [16].

Another non minimal representation of the orientation can be obtained by resorting to four parameters, i.e. the Unit Quaternion. These parameters are constrained by the condition that the sum of their square is 1 and are, therefore, linear dependent [120]. Also the Unit Quaternions form a Lie group, called S^3, and they thus inherit all the properties which this group is endowed with. Nevertheless, DMPs equation cannot be directly used when a redundant representation for the orientation is adopted, e.g. Rotation Matrices or Quaternions, since the variables used to encode and reproduce the robot motion by means of DMPs have to be linearly independent [49].

DMP obstacle avoidance By adding a coupling term in the Cartesian DMP equations one can avoid collisions between obstacle and robot end-effector. In [44] an acceleration term in the DMPs formulation was added in order to avoid collision with a moving obstacle. Other approaches in literature, combine DMPs and Potential fields in order to handle multiple obstacles avoidance. In [119] an impedance factor, calculated using a potential field, was added to the goal state of the DMPs in order to avoid collision with not point-like objects.

In [88] a dynamic potential field that depends on the relative velocity between end-effector and obstacle is used in order to have smoother movements when avoiding obstacle. All of these methods are basically grounded on predefined obstacle avoidance control policy, and cannot be taught by a demonstrator to avoid obstacle in a way similar to human. Conversely, methods based on learnt coupling terms as the advantage to allow a human subject teaching a robot his/her own desired policy of avoiding a collision with different objects. In [28] a 2-D dynamical model to describe human behaviours of steering towards a goal point while avoiding a collision with an obstacle is proposed. This model has been used in [90] as repulsive force term in the DMP equation and has been extended to the 3-D in [97].

Obstacle avoidance in the configuration space is always managed by using the kinematic redundancy of the robot. In redundant robots, the extra Degree of Freedom (DoF), is typically exploited by means of IK algorithms in order to avoid collisions between robot links and obstacles [88]. This method ensures high accuracy of the motion reconstruction in the task space, but does not guarantee that the robot kinematic chain performs the movement in a way similar to the human demonstrator, e.g. guaranteeing anthropomorphic criteria in the joint space for instance. Moreover, when these methods are adopted, the robot cannot learn by a human demonstrator how to accommodate the joint space motion to be close to the human one or to avoid obstacles, since this method doesn't resort to a DMP-based approach for the joint space motion computation.

An approach that combines Joint and Cartesian DMPs could be a suitable solution to allow a human subject teach a robot how to perform a task in a way similar to humans, both

in the Cartesian and Joint space. Moreover, by providing the Cartesian and Joint DMPs with coupling terms that are learnt by demonstration, the robot can even be additionally taught by the human demonstrator to avoid obstacle.

Progress beyond the SoA The contribution of this thesis is to resort to the LbD method based on DMP and proposed in [88] for improving motion planning strategies in rehabilitation and assistive robotics. The overall idea is to develop a motion planning system that stores in a database a set of distinctive features of the trajectories recorded during demonstration. Subsequently, depending on the type of task and the target position, the system selects the proper set of features from the database and builds the trajectory to suitably accomplish the task. The proposed motion planning system is also able to manage modification in the robot initial and target pose as well as complex trajectories. Four variations of LbD method presented in [88] are proposed.

- The 1^{st} variation is aimed to improve the accuracy of the trajectory reconstruction and to optimize the size of the database to be stored, thus achieving significant savings in terms of computational time to access the database. Due to the several amount of ADLs to be learned, the database size could reach high dimensions in daily living scenarios [102]. To this purpose, 1) an optimized kernel allocation depending on the trajectory complexity has been proposed. This complexity is mainly increased by critical points, such as minimum, maximum or inflection points, that are typical in complex trajectories such as the ones performed in ADLs. 2) The number of kernel is not a priori defined but it is properly found by means of a recursive method. In particular, one can notice from [88] that the points of the trajectory worst approximated by LbD algorithm are the above mentioned critical points. In [88], in order to reduce the error in the trajectory reconstruction, an increase of the kernel functions number and, thus, of the DMP parameters number, is required. This could cause a significant extension of the memory size required to record the database in a scenario in which the amount of tasks to be learned by the robot could be high, requiring consequently a long processing time to access the database. Therefore, an optimization of the number of DMP parameters required to ensure a reconstruction error less than a pre-set threshold is applied in this work. The optimization has been achieved by increasing the spatial distribution of the gaussian kernel in correspondence of the critical points of the trajectory. It will achieve significant savings in terms of size of the dataset to be recorded and of processing time to access the database.
- The 2^{nd} variation is mainly addressed to extend the LbD approach in [49] for the control of upper-limb exoskeletons and to significantly improve it by introducing a

Neural Network (NN), that learns the motion features and the robot inverse kinematics. The proposed method offers the following three main advantages with respect to the available techniques used in literature to plan the motion of upper-limb exoskeletons (i.e. motion planning in the Cartesian space and inverse kinematics): i) it does not require the formulation of mathematical models of human motor behavior in order to accomplish the task in a way similar to humans; ii) it allows performing the task also in unstructured environments (where a variability can be caused, for example, by the object position changes and subject different anthropometries); iii) it guarantees the task accomplishment in the feasible workspace by preserving anthropomorphic configurations of the assisted human arm.

- The 3^{rd} variation to the original DMP formulation of [49], is based on the combined use of recorded motion both in joint and Cartesian spaces, that (i) allows to re-map the human joint and Cartesian motion on the robot kinematic chain, (ii) avoids collision between robot links and obstacles preserving the robot kinematic chain motion similar to that of the human demonstrator. This solution is best suited for anthropomorphic robots.

- The 4^{th} variation consists of applying DMPs to a non-minimal representation of the orientation, thus avoiding singularity issues when programming the robot motion by demonstration. The proposed approach resort to the Lie theory as proposed in [123] and integrate in the DMP equations two important operations related to the Lie algebra, namely the Exponential and Logarithmic map, that convert any element of the Lie group into an element of the tangent space and viceversa. Hence, by means of this approach, one can adopt the DMP equations directly in the tangent space of the Lie group with the main advantages of preserving all the properties exhibited by the elements of this group, e.g. orthogonality conditions between the columns for the Rotation matrix or the property to have a unitary norm for the Unit Quaternions. However, differently from [123], the approach proposed in this thesis is based on a dynamic parameterization of the element of the tangent space that allow to avoid discontinuity in the logarithmic map and hence singularity issues. Indeed, when the argument of the logarithmic map, i.e. an element of the tangent space, has a norm close to π, the logarithmic map switches from positive to negative values thus hindering the adoption of DMPs. Therefore, the contribution of this work is to show how to choose different parameterizations for the element of the tangent space in order to avoid singularity issues.

Four experimental validations were carried out in order to assess the proposed motion planner performance. They are named in the following Experimental validation 1, 2, 3, and 4. The first experimental validation was aimed to test the 1^{st} variation applied do the DMP equations. Eight healthy subjects were recruited for the study. They were asked to perform three activities of daily living i.e. drinking, pouring and eating with the aid of a robotic manipulator attached to their wrist. The second experimental validation was aimed to test the 2^{nd} variation applied do the DMP equations. Four patients with Limb girdle muscular dystrophys were involved in the experimental validation. The were asked to to perform one activity of daily living, i.e. the drinking task and two activities belonging to the SHAP clinical test, i.e. the pouring and reaching-grasping-moving-releasing a sphere, with the aid of an upper-limb exoskeleton. The third experimental validation was aimed to test the 3^{rd} variation applied do the DMP equations. The offline database was built during the third experimental validation on 8 healthy subjects performing 9 reaching and pouring tasks. The proposed approach was then experimentally tested on an anthropomorphic robot arm and a comparative analysis with a literature method based on Cartesian DMPs and IK was performed. The fourth experimental validation was aimed to test the 4^{th} variation applied do the DMP equations. The proposed motion planning was used to teach the Tiago robot how to fulfill an Activity of Daily living (ADL), i.e. the pouring task, and the obtained results were compared to the one achieved by using the original formulation of the DMPs [49] [123].

3.2.2 The proposed DMP-based motion planning

In Fig. 3.11, a block scheme of the proposed motion planning is shown. It is grounded on a LbD approach based on DMPs [49].
Trajectories performed by a demonstrator are firstly recorded in the task space during the execution of Activities of Daily Living (Motion recording). The demonstrator could be a human subject or the robot itself moved by an operator throughout a hands-on approach. Subsequently, distinctive features (called DMP parameters) are extracted using the Locally Weighted Regression algorithm. Hence, a dataset of DMP parameters is built (Off-line dataset building).
Afterwards, when a human subject wants the robot to perform one of the recorded Activities of Daily Living, an online extraction of the trajectory from the dataset is performed (DMP parameters selection). It consists of a lookup table which, depending on the task type and object position, selects the proper set of DMP parameters from the database for computing the reference trajectory that best fit the desired task (DMP computation). This trajectory is then given in input to a Low Level Control (LLC) that makes the robot perform the desired task.

In the following, theoretical details about the modules of DMP computation and DMP parameters extraction are provided.

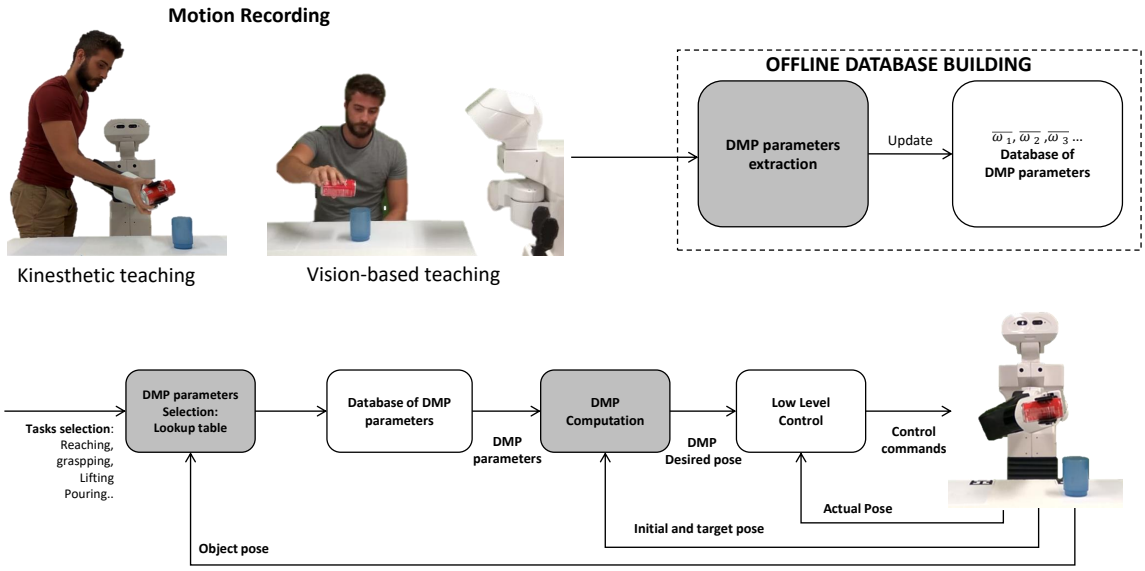

Fig. 3.11 Block scheme of the proposed motion planning for rehabilitation and assistive robotics

DMP computation

A DMP is a non-linear second order system with a landscape attractor that accounts for the desired kinematic state of the robot, i.e. position, velocity and acceleration. The attractor landscape allows replicating the recorded trajectory by means of a weighted sum of equally spaced Gaussian Kernels. A theoretical formulation for the DMPs is given as follows

$$\tau \ddot{y} = \alpha_y \left(\beta_y \left(g - y \right) - \dot{y} \right) + f_y \tag{3.1}$$

τ is a time constant, α_y and β_y are positive constants, y_0 and g are the initial and final point of the trajectory, respectively, and f is a forcing term that implements the landscape attractor of the system. The solution of (3.25), i.e. y, provides the trajectory named Dynamical Movement Primitive (DMP) for each robot DoF. The forcing term is expressed as

$$f_y\left(x\right) = \frac{\sum_{i=1}^{N} \Psi_i\left(x\right) \psi_i}{\sum_{i=1}^{N} \Psi_i\left(x\right)} x \left(g - y_0 \right) \tag{3.2}$$

In (3.54), $\Psi_i(x)$ are fixed basic functions written as Gaussian functions as

$$\Psi_i(x) = \exp\left(-\frac{1}{2\sigma^2}(x-c_i)^2\right) \tag{3.3}$$

where σ_i, c_i, N represent width, centres and number of Gaussian functions, ψ_i are the weight parameters (i.e. the DMP parameters) used to fit the recorded trajectory, and x is a state variable introduced to delete the time dependency of the system. Indeed, it is worth noticing that time dependency of equation (3.25) is expressed as

$$\tau\dot{x} = -\alpha_x x \tag{3.4}$$

that relates time and state x of the whole system.

DMP parameters extraction

A locally weighted regression (LWR) algorithm [105] is adopted to learn DMP parameters ψ_i in (3.54). Data y_d, $\dot{y}_d$ and $\ddot{y}_d$, i.e. position, velocity and acceleration, from the recorded trajectories (joint angles or Cartesian positions) are inserted in the forcing term of (3.54) as follows

$$f_{yd} = \tau\ddot{y}_d - \alpha_y(\beta_y(g-y_d) - \dot{y}_d) \tag{3.5}$$

hence, a function approximation problem is formulated in order to find ψ_i parameters that make f_{yt} as closed as possible to f_y. For each kernel function $\Psi_i(t)$, LWR looks for the corresponding ψ_i that minimises the locally weighted quadratic error through the following cost function

$$J_i = \sum_{t=1}^{P} \Psi_i(t)(f_t(t) - \psi_i \varepsilon(t))^2 \tag{3.6}$$

$$\varepsilon(t) = x(g-y_0) \tag{3.7}$$

3.2.2.1 1^{st} variation to the DMP original formulation

In [49] the range of variation of state x and centres c_i is [0,1] and c_i is a monotonic linear function of x (bottom left in Fig. 3.12); hence, the Gaussian kernels are equally distributed over x. In the approach proposed in this work, the spatial distribution of the Gaussian kernels is varied in order to increase the kernel number in the critical points, by keeping constant the total number of kernel functions for a given trajectory, and consequently reduce the error between the human recorded trajectory and the robot learned one. To this purpose, c_i and σ_i

are defined as follows

$$c(x) = \frac{\int_0^x V_c(z)\,dz}{||\int_0^1 V_c(z)\,dz||} \tag{3.8}$$

$$V_c(z) = 1 - \alpha_z \sum_{k=1}^{p} exp\left(-\beta_z\,(z - z_k)\right) \tag{3.9}$$

$$\sigma(x) = \gamma_z \frac{V_c(x)}{N} + \delta_z \tag{3.10}$$

$$c_i = c(\frac{i}{N}) \tag{3.11}$$

$$\sigma_i = \sigma(\frac{i}{N}) \tag{3.12}$$

where α_z, β_z, γ_z and δ_z are positive constants, P is the number of critical points of the recorded trajectory and z_k is the normalised time instant of these critical points. In Fig. 3.12 an example of c and σ function for both the different modality to allocate the Gaussian Kernels is provided.

3.2.2.2 2^{nd} variation to the DMP original formulation

The 2^{nd} variation of LbD method used in [49] is shown in Fig. 3.13. It is best suited for the motion planning of upper-limb exoskeletons. In particular, in this work, differently from [49], a combination of DMP and supervised learning is adopted with the aim of avoiding motion planning in the Cartesian space and inverse kinematics. The proposed motion planning consists of two main stages, named off-line neural network training and DMP computation. In the off-line neural network training, the trajectories executed by a healthy human subject, e.g. the therapist or the caregiver, are recorded by means of motion tracking devices such as magneto inertial sensors or the robot itself when backdriven, and distinctive features, named DMP parameters, are subsequently extracted using a LWR algorithm ("Motion recording and DMP parameters extraction" block in Fig. 3.13). Hence, a neural network is trained through the Levenberg-Marquardt (LM) supervised learning algorithm in order to associate DMP parameters and robot joint target position to context factors taken in input (i.e. object position and task to be performed).
In the DMP computation, the patient can perform an ADL task with the assistance of the exoskeleton. Depending on the task and object position, the trained neural network provides the proper set of DMP parameters and robot joint target positions for computing the set of DMPs that best fit the desired task ("DMP computation" block).

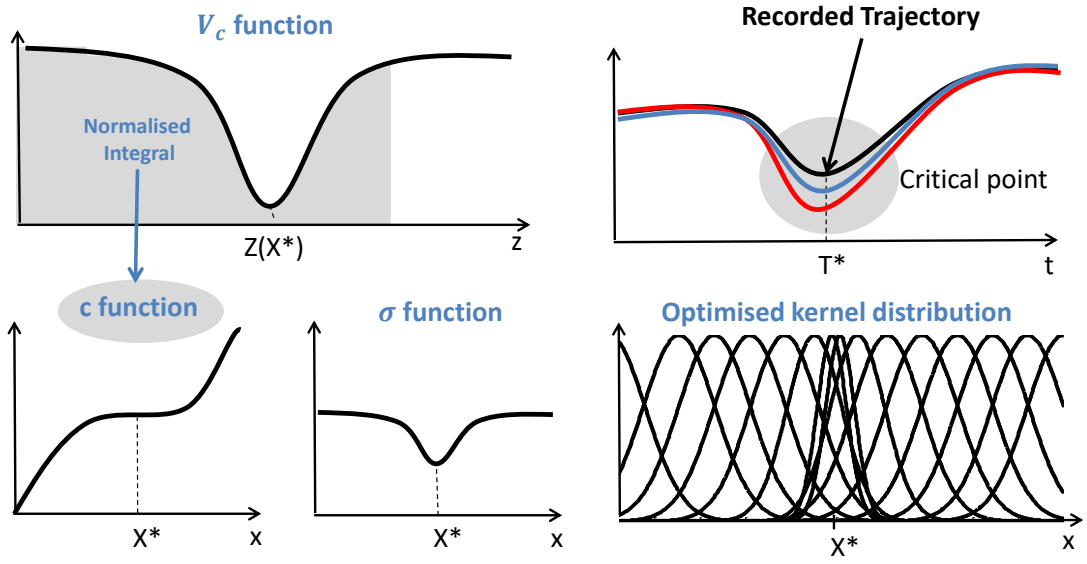

Fig. 3.12 c and σ function in the two different modality to allocate the Gaussian Kernels. The trajectories computed with equally spaced and optimised kernel distribution are outlined in red and blue, respectively. X* and T* are the state and time corresponding to the critical point.

Off-line neural network training A Levenberg-Marquardt algorithm (LM) has been adopted for the off-line neural network training [71]. Given a parameter vector $p \in \Re^n$ and a measurement vector $x \in \Re^m$, the LM algorithm finds the functional relation (f) that maps the parameter vector p into an estimated measurement $\hat{x}$ ($\hat{x} = f(p)$). A linear approximation of f in the neighborhood of p is provided by a Taylor series expansion

$$f(p+\delta_p) = f(p) + J\delta_p + o(p) \tag{3.13}$$

Neglecting the higher order terms $o(p)$, Eq. (3.25) could be approximated as,

$$f(p+\delta_p) \approx f(p) + J\delta_p \tag{3.14}$$

where J is the Jacobian matrix $\frac{\delta f(P)}{\delta P}$.

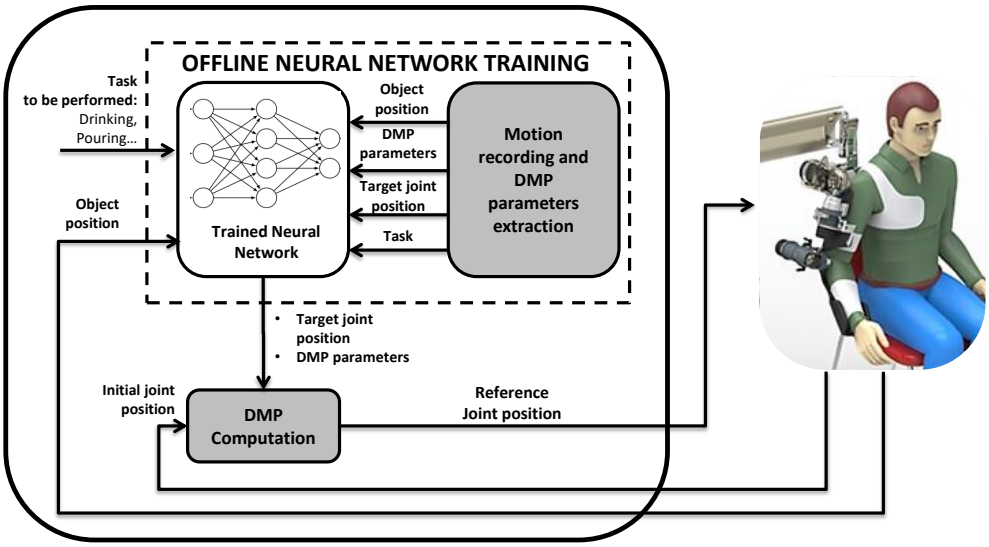

Fig. 3.13 Block scheme of the proposed motion planning for upper-limb exoskeletons

At each step of the iterative process, LM looks for the δ_p that minimizes the error defined as $\|x - f(p+\delta_p)\| = \|x - f(p) + J\delta_p\| = \|\varepsilon - J\delta_p\|$. The error is minimized when $J\delta_p - \varepsilon$ is orthogonal to the column space of J, namely when the following condition holds

$$J^T(J\delta_p - \varepsilon_p) = 0 \tag{3.15}$$

$$J^T J\delta_p = J^T \varepsilon_p. \tag{3.16}$$

In the LM method Eq. (3.16), called *normal equation*, is written as

$$N\delta_p = J^T \varepsilon_p \tag{3.17}$$

$$N = \mu + J^T J \tag{3.18}$$

where $J^T J$ and μ are called damping and damping term, respectively. One iteration of LM algorithm consists of finding an acceptable value of the damping term that reduce the error ε_p. In other words, if δ_p computed from Eq. (3.55), leads to a reduction of the error ε_p, the damping term is decreased and the following iteration is processed; otherwise, the damping term is increased and Eq. (3.55) is solved again. The LM algorithm stops running when, at least, (i) $J^T \varepsilon_p$ of Eq. (3.55) is lower than a preset threshold ε_1 or (ii) δ_p is lower than a threshold ε_2 or (iii) a maximum number of iteration N_{MAX} is reached. For the sake of brevity

the complete LM algorithm is not shown; further theoretical details about the implemented method could be found in [71].

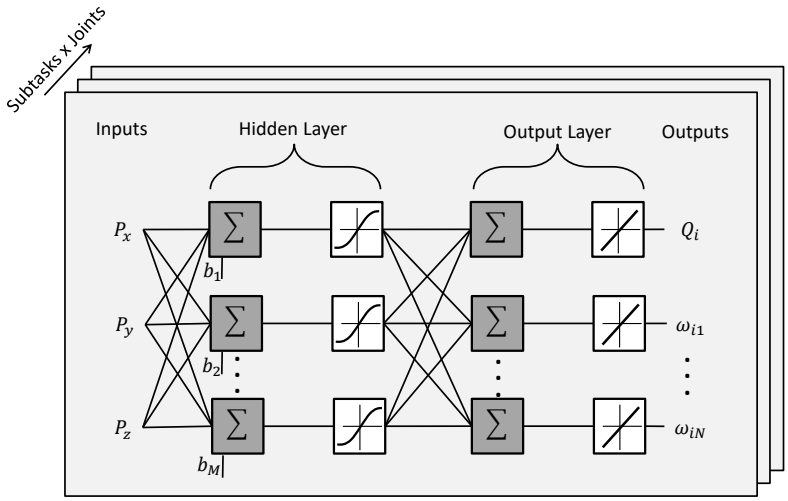

Fig. 3.14 Structure of the adopted neural network

The structure of the adopted neural network is reported in Fig. 3.14. A two layer feed-forward network with M sigmoid hidden neurons and $N+1$ linear output neurons is used for each joint and for each task the user wants to perform. The inputs of each network are the Cartesian target positions to be reached, P_x, P_y and P_z (e.g. object position); on the other hand, the outputs of each network are the DMP parameters, ω_1, $\omega_2 ... \omega_N$, and the target joint angles, Q_i (N is the number of DMP parameters computed for the i-th joint).

Adapting NN outputs to different subject anthropometries In order to adapt the proposed method to different human bodies, a recursive method that adjusts the NN outputs for distinct subject anthropometries was used. Its functioning principle is shown in Fig. 3.15.

In the block scheme, P_d is the Cartesian target position to be reached, Q is the output configuration of the robot joints, subject 1 is the person involved in the NN training phase while subject 2 is the assisted person, who wants to perform an ADL thanks to the exoskeleton assistance. It is worth noting that, with the aforementioned exoskeletons and the described tasks, two loops of the recursive algorithm are suitable to obtain an acceptable error in reaching the target position (less than 10 mm).

3.2.2.3 3^{rd} variation to the DMP original formulation

DMPs in [49] are typically used to plan the robot motion by demonstration either in the joint or in the task space. In this work we propose a new DMPs formulation, based on

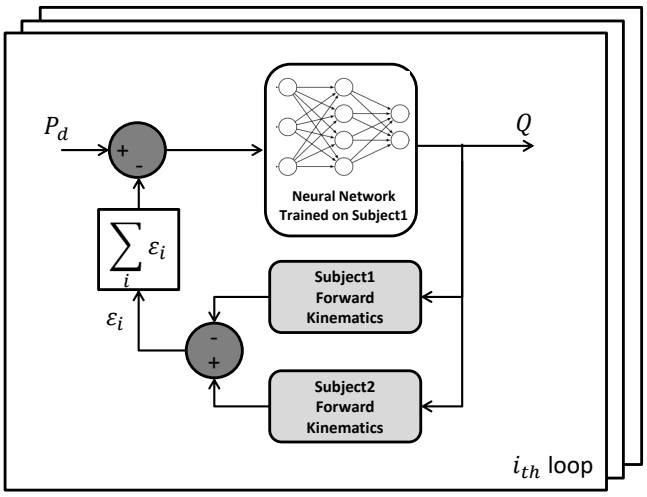

Fig. 3.15 Block scheme of the recursive method used to adjust the NN outputs for different subject anthropometries

the combined use of recorded motion both in joint and Cartesian spaces that can be used with anthropomorphic robots and that (i) allows to re-map the human joint and Cartesian motion on the robot kinematic chain, (ii) avoids collision between robot links and obstacles preserving the robot kinematic chain motion similar to that of the human demonstrator. It is named Hybrid Joint/Cartesian DMPs and is shown in the block scheme of Fig. 3.16.

As for a typical LbD approach, human motion trajectories are firstly recorded, both in the joint and task spaces, during the execution of Activities of Daily Living (Human motion recording). They are performed by a human demonstrator and distinctive features (called DMP parameters) are subsequently extracted using a Locally Weighted Regression algorithm. Hence, a dataset of Cartesian and Joint DMP parameters is built (Off-line dataset building). Afterwards, when a human subject wants the robot to perform one of the recorded Activities of Daily Living , an online extraction of the trajectory from the dataset is performed (DMP parameters selection). It consists of a lookup table which, depending on the task type and object position, selects the proper set of DMP parameters from the database for computing the one that best fits the desired task (DMP computation). Cartesian and joint DMPs are then combined by means of a multi-priority coupling equation. By exploiting the robot redundancy, this coupling equation is intended to compute the most appropriate reference joint position that ensures a low error in the task space, as first priority, and that is as close as possible to the computed joint DMPs, as second priority. Hence, this reference joint

position is given in input to a Low Level Control (LLC) in the joint space that makes the robot perform the desired task.
In the following, theoretical modifications about the modules of DMP computation and DMP parameters extraction are provided.

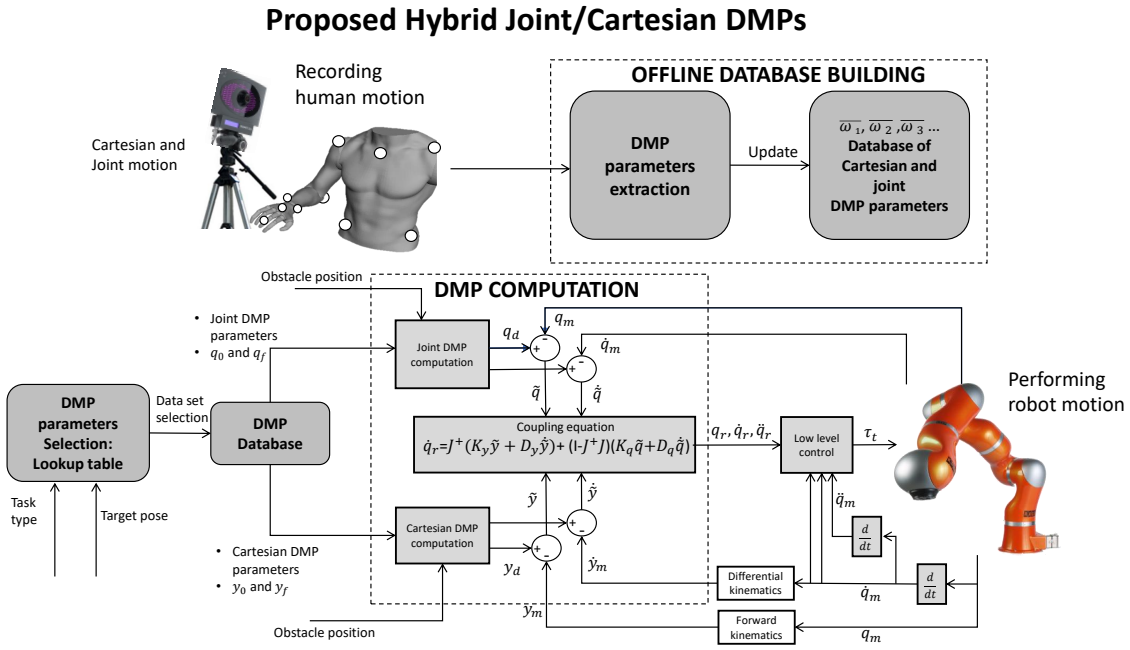

Fig. 3.16 Block scheme of the proposed motion planning for anthropomorphic robots

DMP computation As shown in Fig. 3.16, one DMP is computed for each robot DoF both in the joint and in the task space. A theoretical formulation for the Cartesian DMPs is given as follows

$$Cartesian \quad DMPs: \quad \tau_y \ddot{\mathbf{y}} = \alpha_y \left(\beta_y \left(\mathbf{g_y} - \mathbf{y}\right) - \dot{\mathbf{y}}\right) + \mathbf{f_y} + \mathbf{C_y} \tag{3.19}$$

where τ_y is a time constant, α_y and β_y are positive constants, $\mathbf{y_0}$ and $\mathbf{g_y}$ are the initial and final point of the Cartesian trajectory, respectively, $\mathbf{f_y}$ is a forcing term that implements the landscape attractor of the system and $\mathbf{C_y}$ is a coupling term that accounts for the end-effector obstacle avoidance. The solution of (3.19), i.e. $\mathbf{y}$, provides a vector of 6 Cartesian trajectories named Cartesian DMPs.

The forcing term $\mathbf{f_y}$ is expressed as

$$\mathbf{f_y}\left(x\right) = \frac{\sum_{i=1}^{N_y} \Psi_i\left(x\right) \boldsymbol{\omega_{iy}}^T}{\sum_{i=1}^{N_y} \Psi_i\left(x\right)} x \left(\mathbf{g_y} - \mathbf{y_0}\right) \tag{3.20}$$

In (3.20), $\Psi_i(x)$ are fixed basic functions written as Gaussian functions as

$$\Psi_i(x) = exp\left(-\frac{1}{2\sigma_i^2}(x-c_i)^2\right) \tag{3.21}$$

where σ_i, c_i, N_y represent width, centres and number of Gaussian functions, ω_{iy} are the weight parameters (i.e. the DMP parameters) used to fit the Cartesian trajectory, and x is a state variable introduced to delete the time dependency of the system. Indeed, it is worth noticing that time dependency of (3.19) is expressed as

$$\tau\dot{x} = -\alpha_x x \tag{3.22}$$

that relates time and state x of the whole system. The state variable x as well as centres c_i range in between 0 and 1.

As mentioned above, an optimized spatial allocation of the Gaussian kernels is adopted, depending on the complexity of the recorded trajectory. In order to make the robot end-effector avoid the obstacles, a coupling term C_y in the Cartesian DMPs equation needs to be added. Given $\mathbf{y}^* = [y_1 \quad y_2 \quad y_3]$ and $\dot{\mathbf{y}}^* = [\dot{y}_1 \quad \dot{y}_2 \quad \dot{y}_3]$, the suitable coupling term C_y that makes the end-effector avoid an obstacle placed in a position $\mathbf{o} = [o_1 \quad o_2 \quad o_3]$, is defined as $\mathbf{C_y} = [C_{y1}^* \quad C_{y2}^* \quad C_{y3}^* \quad 0 \quad 0 \quad 0]$, where

$$\mathbf{C_y^*} = \gamma \mathbf{R}\dot{\mathbf{y}}^* \theta exp(-\beta\theta) \tag{3.23}$$

and

$$\theta = arccos\left(\frac{(\mathbf{o}-\mathbf{y}^*)^T\dot{\mathbf{y}}^*}{\|\mathbf{o}-\mathbf{y}^*\|\|\dot{\mathbf{y}}^*\|}\right) \tag{3.24}$$

θ is the angle between the velocity vector $\dot{\mathbf{y}}^*$ and the difference vector $(\mathbf{o}-\mathbf{y}^*)$ between the obstacle and the current position. The vector $\mathbf{r}$ is perpendicular to the plane spanned by $\dot{\mathbf{y}}^*$ and $(\mathbf{o}-\mathbf{y}^*)$, and serves to define a rotation matrix $\mathbf{R}$, which causes a rotation of 90 degrees about $\mathbf{r}$ [49]. Intuitively, the coupling term adds a movement perpendicular to the current motion direction as a function of the distance vector to the obstacle [44].

Conversely, the joint DMPs are defined as

$$Joint \quad DMPs: \quad \tau_q\ddot{\mathbf{q}} = \alpha_q\left(\beta_q(\mathbf{g_q}-\mathbf{q}) - \dot{\mathbf{q}}\right) + \mathbf{f_q} + \mathbf{C_q} \tag{3.25}$$

where τ_q is a time constant, α_q and β_q are positive constants, $\mathbf{g_q}$ is the final point of the joint trajectory, $\mathbf{f_q}$ is a forcing term that implements the landscape attractor of the system and $\mathbf{C_q}$ is a coupling term that accounts for the robot kinematic chain obstacle avoidance. In order

to make the joint DMPs converge to a solution, g_q, that is compatible with the Cartesian target position g_y and is as close as possible to the recorded joint position g_{q_0}, the joint target position g_q was defined as follow

$$\dot{\mathbf{g}}_\mathbf{q} = \mathbf{J}^{+}\mathbf{K}_{\mathbf{g_y}}(\mathbf{g_y} - k(\mathbf{g_q})) + (\mathbf{I} - \mathbf{J}^{+}\mathbf{J})\mathbf{K}_{\mathbf{g_q}}(\mathbf{g_{q_0}} - \mathbf{g_q}) \tag{3.26}$$

where $\mathbf{K}_{\mathbf{g_y}}$ and $\mathbf{K}_{\mathbf{g_q}}$ are positive diagonal matrix, $k(\mathbf{g_q})$ is the Forward Kinematics computed on $\mathbf{g_q}$, $\mathbf{J}^{+}$ is the right Jacobian pseudo-inverse and $\mathbf{I} - \mathbf{J}^{+}\mathbf{J}$ is the null projector of the Jacobian.

The forcing term $\mathbf{f_q}$ is expressed as

$$\mathbf{f_q}(x) = \frac{\sum_{i=1}^{N_q} \Psi_i(x)\, \boldsymbol{\omega}_{\mathbf{iq}}{}^{T}}{\sum_{i=1}^{N_q} \Psi_i(x)} x(\mathbf{g_q} - \mathbf{q_0}) \tag{3.27}$$

where $\mathbf{q_0}$ is initial point of the joint trajectory, σ_i, c_i, N_q represent width , centres and number of Gaussian functions, respectively, ω_{iq} are the weight parameters (i.e. the DMP parameters) used to fit the joint trajectory, and x is a state variable introduced in (3.22). The coupling term C_q is introduced in the joint DMPs equation in order to make the robot kinematic chain avoid the obstacle. The coupling term $\mathbf{C_q}$ is defined as

$$\mathbf{C}_q = \sum_{k=1}^{j} \mathbf{K}\mathbf{d_k} \tag{3.28}$$

where $\mathbf{K}$ is a positive diagonal matrix,

$$\mathbf{d_k} = \begin{bmatrix} \frac{\partial}{\partial q_1}\|\mathbf{y_j^*} - \mathbf{o}\| \\ \vdots \\ \frac{\partial}{\partial q_k}\|\mathbf{y_j^*} - \mathbf{o}\| \\ 0 \\ \vdots \\ 0 \end{bmatrix} \tag{3.29}$$

and $y_j^* = [y_{j1} \quad y_{j2} \quad y_{j3}]$ is the Cartesian position of the j-th robot joint. The Cartesian and Joint DMPs are combined through the following coupling equation

$$\dot{\mathbf{q}}_\mathbf{r} = \mathbf{J}^{+}(\mathbf{K_y}\tilde{\mathbf{y}} + \mathbf{D_y}\dot{\tilde{\mathbf{y}}}) + (\mathbf{I} - \mathbf{J}^{+}\mathbf{J})(\mathbf{K_q}\tilde{\mathbf{q}} + \mathbf{D_q}\dot{\tilde{\mathbf{q}}}) \tag{3.30}$$

where $\mathbf{K_y}$, $\mathbf{D_y}$, $\mathbf{K_q}$ and $\mathbf{D_q}$ are positive diagonal matrix, $\tilde{\mathbf{y}}$ is the error between the Cartesian DMP ($\mathbf{y}$) and the Forward kinematics ($\mathbf{y_m}$) computed on the measured joint position ($\mathbf{q_m}$), $\dot{\tilde{\mathbf{y}}}$ is the error between the Cartesian DMP velocity ($\dot{\mathbf{y}}$) and the Differential Kinematics ($\dot{\mathbf{y}}_\mathbf{m}$) computed on the derivative of the measured joint position ($\dot{\mathbf{q}}_\mathbf{m}$), $\tilde{\mathbf{q}}$ is the error between the Joint DMP ($\mathbf{q}$) and the measured joint position ($\mathbf{q_m}$) and $\dot{\tilde{\mathbf{q}}}$ is the error between the Joint DMP velocity ($\dot{\mathbf{q}}$) and the derivative of the measured joint position ($\dot{\mathbf{q}}_\mathbf{m}$). It is worth noticing that by means of (3.46) the convergence to the Cartesian DMP ($\mathbf{y}$) is guarantee with high priority. Then the robot redundancy is exploited, by means of the null projector $\mathbf{I}-\mathbf{J}^{+}\mathbf{J}$, to make the robot joints position be close to the joint DMP ($\dot{\mathbf{q}}$), with lower priority.

DMP parameters extraction A locally weighted regression (LWR) algorithm [49] is adopted to learn DMP parameters ω_{iy} in (3.20) and ω_{iq} in (3.54). Data $\mathbf{y_d}$, $\dot{\mathbf{y}}_\mathbf{d}$ and $\ddot{\mathbf{y}}_\mathbf{d}$, i.e. position, velocity and acceleration, from the recorded Cartesian trajectories are inserted in the forcing term of (3.20) as follows

$$\mathbf{f_{ty}} = \tau^2 \ddot{\mathbf{y}}_\mathbf{d} - \alpha_y \left(\beta_y \left(\mathbf{g} - \mathbf{y_d}\right) - \tau \dot{\mathbf{y}}_\mathbf{d}\right) \tag{3.31}$$

hence, a function approximation problem is formulated in order to find $\omega_\mathbf{iy}$ parameters that make $\mathbf{f_{ty}}$ as close as possible to $\mathbf{f_y}$. For each kernel function $\Psi_i(t)$, LWR looks for the corresponding $\omega_\mathbf{iy}$ that minimizes the locally weighted quadratic error through the following cost function

$$\mathbf{J_i} = \sum_{t=1}^{P} \Psi_i(t) \left(\mathbf{f_{ty}}(t) - \omega_\mathbf{iy}{}^T \varepsilon(t)\right)^2, \tag{3.32}$$

where

$$\varepsilon(t) = x\left(\mathbf{g_y} - \mathbf{y_0}\right) \tag{3.33}$$

Likewise, data $\mathbf{q_d}$, $\dot{\mathbf{q}}_\mathbf{d}$ and $\ddot{\mathbf{q}}_\mathbf{d}$, i.e. position, velocity and acceleration, from the recorded joint trajectories are inserted in the forcing term of (3.54), and by means of a function approximation problem $\omega_\mathbf{iq}$ is found, as well.

3.2.2.4 4^{th} variation to the DMP original formulation

The 4^{th} variation to the DMP equations proposed in this work makes DMPs to be efficiently applied to a non-minimal representation of the orientation, thus avoiding singularity issues when programming the robot motion by demonstration. The proposed approach resorts to the Lie theory as proposed in [123] and integrates in the DMP equations two important operations related to the Lie algebra, namely the Exponential and Logarithmic map, that converts any element of the Lie group into an element of the tangent space and viceversa.

Hence, by means of this approach, one can adopt the DMP equations directly in the tangent space of the Lie group with the main advantages of preserving all the properties exhibited by the elements of this group, e.g. orthogonality conditions between the columns for the Rotation matrix or the property to have a unitary norm for the Unit Quaternions.

However, differently from [123], the approach proposed in this work is based on a dynamic parameterization of the element of the tangent space that allows to avoid discontinuity in the logarithmic map and hence singularity issues. Indeed, when the argument of the logarithmic map, i.e. an element of the tangent space, has a norm close to π, the logarithmic map switches from positive to negative values thus hindering the adoption of DMPs.

Therefore, contribution of this work is to show how to choose different parameterizations for the element of the tangent space in order to avoid singularity issues.

Concepts on Lie groups In the following, theoretical details of Lie groups as well as mathematical conventions and notations are provided [16]. Nevertheless, this section does not give a rigorous introduction to Lie groups as it does attempt only to provide the reader with the necessary information useful to employ Lie groups in Robotics. A Lie group is a topological group that is also a smooth manifold. An N-dimensional manifold M is a space where every point p $\in$ M is endowed with local Euclidean structure. In other words, it means that, in an infinitely small vicinity of a point p the space looks "flat". Associated with every Lie group is a Lie algebra, which is a vector space also called tangent space and denoted as T_xM, that has a dimensionality of D (identical to that of the manifold) in non-singular points. Informally, a tangent space in p can be visualized as the vector space of the derivatives of all possible smooth curves that pass through p. Associated to a Lie group M and its Lie algebra m there are two important functions:

- The exponential map, which maps elements from the algebra m to the manifold M:

$$\exp : m \rightarrow M \tag{3.34}$$

- The logarithm map, which maps elements from the manifold M to the algebra m:

$$\log : M \rightarrow m \tag{3.35}$$

Lie algebra of SO(3) The group SO(3), also called special orthogonal group, is the group of 3×3 rotation matrices and has an associated Lie algebra so(3), whose base are three 3×3

skew symmetric matrices, each corresponding to infinitesimal rotations along each axis

$$G_1 = \begin{bmatrix} 0 & 0 & 0 \\ 0 & 0 & -1 \\ 0 & 1 & 0 \end{bmatrix}, G_2 = \begin{bmatrix} 0 & 0 & 1 \\ 0 & 0 & 0 \\ -1 & 0 & 0 \end{bmatrix}, G_3 = \begin{bmatrix} 0 & -1 & 0 \\ 1 & 0 & 0 \\ 0 & 0 & 0 \end{bmatrix} \tag{3.36}$$

An element of so(3) could be therefore expressed as a linear combination of the generators. Let $\phi \in \mathbb{R}^3$ be a 3-vector of coefficients such that $\omega = \frac{\mathbf{d}\phi}{\mathbf{dt}}$ accounts for the robot end-effector angular velocity. A generic element of so(3) is expressed as

$$[\phi]_\times = \phi_1 G_1 + \phi_2 G_2 + \phi_3 G_3 \tag{3.37}$$

where $[\phi]_\times \in so(3)$ is the skew symmetric matrix of the 3-vector ϕ. The exponential map that transform one element from SO(3) to an element of so(3) is simply the matrix exponential over a linear combination of the generators

$$\exp([\phi]_\times) = \exp \begin{pmatrix} 0 & -\phi_3 & \phi_2 \\ \phi_3 & 0 & -\phi_1 \\ -\phi_2 & \phi_1 & 0 \end{pmatrix} \tag{3.38}$$

$$\exp([\phi]_\times) = \mathbf{I_3} + \frac{sin(\|\phi\|)}{\|\phi\|}[\phi]_\times + \frac{1 - cos(\|\phi\|)}{\|\phi\|^2}[\phi]_\times^2 \tag{3.39}$$

where (3.39) is referred to as Rodrigues' formula. Conversely, the logarithmic map, that transform one element from so(3) to an element of SO(3), is the logarithm of the 3×3 rotation matrices $\mathbf{R} \in SO(3)$, and is given by the well-known Rodrigues rotation formula

$$\log(\mathbf{R}) = \frac{\theta}{2sin(\theta)(\mathbf{R} - \mathbf{R}^T)} \tag{3.40}$$

$$cos(\theta) = \frac{tr(\mathbf{R}) - 1}{2} \tag{3.41}$$

$$\phi = [\log(\mathbf{R})]_\triangle \tag{3.42}$$

where $tr(.)$ is the trace of a matrix and $[.]_\triangle$ is the inverse operation of the skew-symmetric matrix operator $[.]_\times$. Lie algebra of S^3 The S^3 group, is the group of Unit quaternions. A Unit Quaternion, $Q = (q_0, \tilde{q})$, is composed of a real part, $q_0 \in \mathbb{R}$, and an imaginary part, $\tilde{q} \in \mathbb{R}^3$, which meet $q_0^2 + \|\tilde{q}\|^2 = 1$. Also for the S^3 group, it is possible to define an associated Lie algebra, i.e. the tangent space, with two operations that map any element of S^3 into an

element of the tangent space and viceversa. They are defined as

$$\exp(\phi) = (q_0, \tilde{q}) = \left(cos(\|\phi\|/2), sin(\|\phi\|/2) \frac{\phi}{\|\phi\|} \right) \tag{3.43}$$

$$\log(Q) = 2\ atan2(\|\tilde{q}\|, q_0) \frac{\tilde{q}}{q_0} \tag{3.44}$$

Lie theory applied to DMPs DMPs are typically used to plan the robot motion by demonstration either in the joint or in the task space. One important feature to be addressed when planning the robot motion by means of DMPs, is to encode/decode the robot motion using a set of independent variables, e.g. the joint angles or the Cartesian coordinates. Indeed, if the used variables are related by some properties or constraints and are therefore linearly dependent, it is not guaranteed that those properties or constraints remain unchanged when the robot motion is planned throughout DMPs. As a consequence, this implies that a minimal representation of the end-effector orientation, e.g. independent variables like Euler angles, needs to be adopted when planning the robot motion in the Operational space. However, by using a minimal representation of the end-effector orientation, one has to face the main drawback of singularity issues. This problem could be addressed by reducing the robot RoM; but sometimes it is not the best solution, especially for the motion planning of complex activities, that require a wide RoM to be fulfilled. Therefore, a DMP formulation that could be adopted on a non minimal representation of the orientation, like Rotation Matrix or Unit Quaternion, is introduced in the following. The formulation is based on a dynamic parameterization of the element of the tangent space that allow to avoid discontinuity in the logarithmic map. It is one the contributions of this work and aims at addressing singularity issues and preserving, at the same time, all the properties exhibited by the variables used to plan the end-effector orientation by demonstration, e.g. orthogonality conditions between the columns for the Rotation matrix or the property to have a unitary norm for the Unit Quaternions. *Orientation decoding A DMP formulation that could be applied either to the Rotation Matrix or to the Unit Quaternion is defined as

$$\tau \dot{\omega} = \alpha_\omega \left(\beta_\omega \ \log \left(\Phi_t \Phi^{-1} \right) - \omega \right) + f_\omega \tag{3.45}$$

where τ is a time constant, α_ω and β_ω are positive constants, Φ_t is the target orientation, expressed as Rotation Matrix or Unit Quaternion, Φ, ω and $\dot{\omega}$ are the orientation, angular velocity and angular acceleration, respectively, and f_ω is the forcing term that implements

the landscape attractor of the system that is expressed as

$$f_\omega(x) = \frac{\sum_{i=1}^{N} \Psi_i(x)\, \psi_i}{\sum_{i=1}^{N} \Psi_i(x)} x \log\left(\Phi_t \Phi_0^{-1}\right) \tag{3.46}$$

where Φ_0 is the end-effector initial orientation, x is the state variable of the system, defined in (3.56), and $\log(.)$ is the logarithmic function that map an element, Φ, of the Lie group, e.g. $SO(3)$ or S^3, to an element belonging to the tangent space of that group, ϕ. This logarithmic map is defined in (3.40)-(3.42) for the Rotation Matrix and in (3.44) for the Unit Quaternion. The solution of (3.45), i.e. Φ, provides the orientation trajectory expressed by means of Rotation Matrices or Unit Quaternions that can be found as

$$\Phi(t) = \exp\left(\int_{t_0}^{t} \omega(s)\, ds + \frac{1}{2}\iint_{t_0}^{t} \dot{\omega}(s)\, ds^2\right) \tag{3.47}$$

where t_0 is the initial time, $\exp(.)$ is the exponential function that map an element of the tangent space, i.e. ϕ, to an element of the Lie group $SO(3)$ or S^3, i.e. Φ. This exponential map is defined in (3.39) for the Rotation Matrix and in (3.43) for the Unit Quaternion. Orientation encoding In order to learn the DMP parameters ψ_i of (3.46), a LWR algorithm [105] is adopted . Therefore, data Φ_d, ω_d and $\dot{\omega}_d$, i.e. recorded orientation, angular velocity and angular acceleration are inserted in the forcing term of (3.46) as follows

$$f_{\omega d} = \tau \dot{\omega}_d - \alpha_\omega\left(\beta_\omega \log\left(\Phi_t \Phi_d^{-1}\right) - \omega_d\right) \tag{3.48}$$

As for the position DMPs, a function approximation problem is formulated in order to find ψ_i parameters that make f_ω as close as possible to $f_{\omega d}$. The cost function to be minimized is defined as

$$J_i = \sum_{t=1}^{P} \Psi_i(t)\left(f_\omega(t) - \psi_i \varepsilon_\omega(t)\right)^2 \tag{3.49}$$

$$\varepsilon_\omega(t) = x \log\left(\Phi\, \Phi_0^{-1}\right) \tag{3.50}$$

Addressing orientation singularities The main drawback of the DMP formulation based on the Lie theory and proposed in (3.45) - (3.48) is that the output of the logarithmic map has a gap of 2π when the norm of its argument is close to π. Hence, in order to avoid orientation singularities a dynamic parameterization needs to be introduced in in (3.45) - (3.48) as follows

$$\tau \dot{\omega} = \alpha_\omega\left(\beta_\omega\, v_k\, \log\left(\Phi_t \Phi^{-1}\right) - \omega\right) + f_\omega \tag{3.51}$$

$$f_{\omega d} = \tau \dot{\omega}_d - \alpha_\omega\left(\beta_\omega\, v_k\, \log\left(\Phi_t \Phi_d^{-1}\right) - \omega_d\right) \tag{3.52}$$

$$v_k = v_{k-1}\frac{1-2k\pi}{\|v_{k-1}\phi\|} \quad k = 1...n \tag{3.53}$$

where $\phi \in \mathbb{R}^3$ is a 3-vector of coefficients such that $\omega = \frac{\mathbf{d}\phi}{\mathbf{dt}}$. Let us explain the rationale behind (3.51), (3.52) and (3.53) with a practical example. Suppose the robot end-effector is required to perform a rotation of 4π about the X, Y, and Z axis. The output of the logarithmic map in (3.48) as well as its norm, will be the one shown in Figs. 3.17 - 3.20. One can notice from these figures that ϕ is discontinuous when $\|\phi\|$ reaches π or 0. Therefore when LWR is adopted on these variables, the DMP parameters cannot be properly computed. Hence, (3.53) needs to be adopted in order to avoid this discontinuity. In Figs. 3.17 - 3.20, the output of the logarithmic map in (3.52) as well as its norm, is shown for different values of k in (3.53). It is worth underlining that all the parameterizations chosen for ϕ account for the same rotation in SO_3.In order to have a continuous function for ϕ on which LWR could be properly adopted, different values for k in (3.53) should be set. Simply, from Figs. 3.17 - 3.20, is evident that when $\|\phi\|$ reaches $(k+1)\pi$ and $\frac{d}{dt}\|\phi\| > 0$ k has to be increased; conversely, when $\|\phi\|$ reaches $(k)\pi$ and $\frac{d}{dt}\|\phi\| < 0$ k has to be decreased.

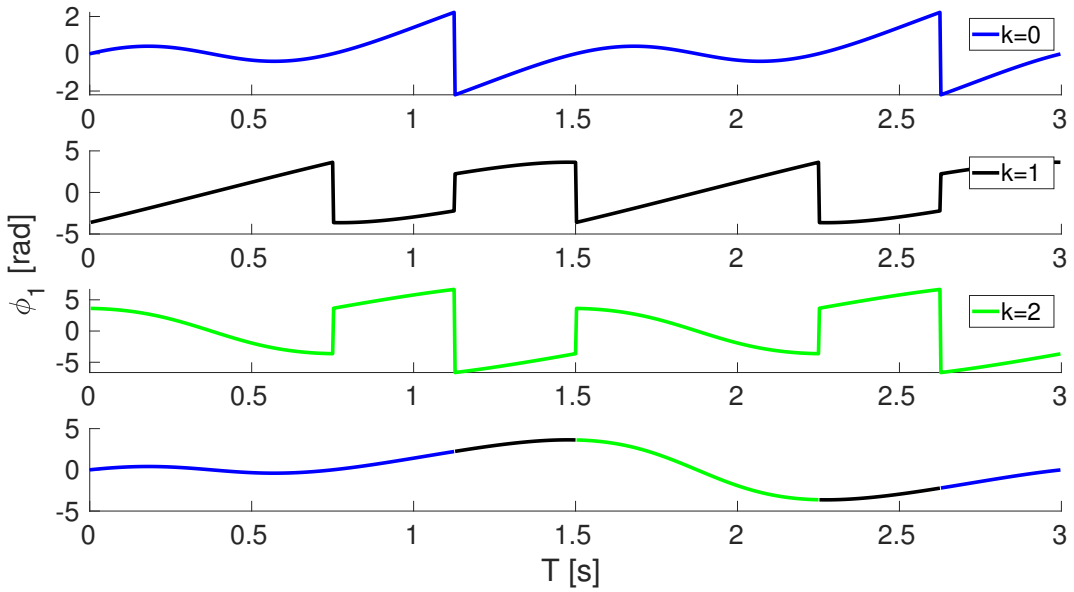

Fig. 3.17 Grafical illustration of ϕ_1 for three different values of the dynamic parameterization factor (k=0,1,2)

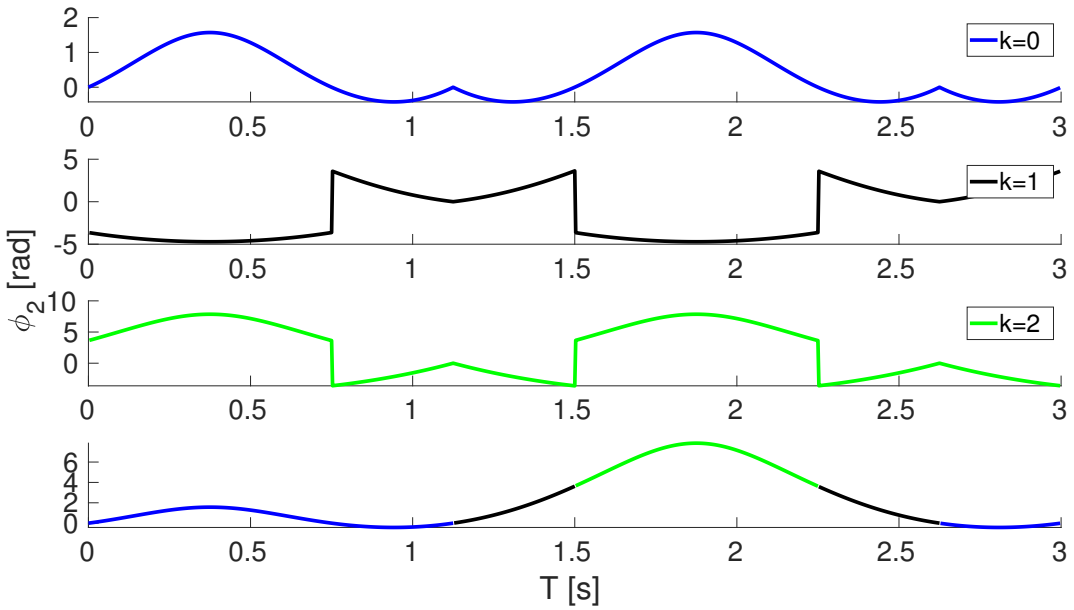

Fig. 3.18 Grafical illustration of ϕ_2 for three different values of the dynamic parameterization factor (k=0,1,2)

3.2.3 Experimental validation 1

The approach proposed in Sect.3.2.2.1 has been implemented and tested on the anthropomorphic robotic arm Kuka LWR 4+, and compared with the algorithm in [49] in order to assess its accuracy. Additionally, given the experimental scenario of robotic assistance during ADL execution, the generalization level of the proposed system is verified over 3 ADLs (i.e. drinking, eating and pouring), by evaluating the success rate of the task execution.

3.2.3.1 Experimental setup and protocol

The experimental setup used to validate the approach proposed in Sect.3.2.2.1 is shown in Fig. 3.42 . The KUKA-LWR 4+ is a 7 DoFs anthropomorphic robotic arm with position and torque sensors at joints. The communication between the robot and a remote PC is guaranteed by the Fast Research Interface (FRI) Library, which runs on a remote PC connected to the KUKA Robot Controller via a UDP communication protocol. Eight healthy subjects volunteered to participate in the experimental validation. They have been asked to perform three ADLs (i.e. drinking, eating and pouring), with the wrist attached to the robot end-effector by means of a purposely developed flange. Each ADL has been divided into a number of subtasks listed in the following:

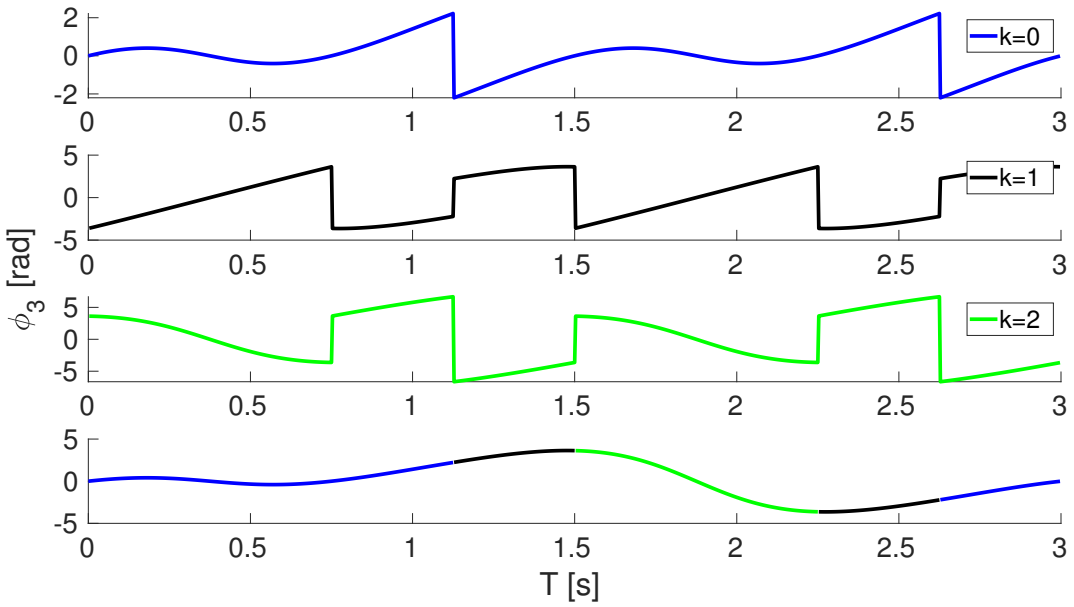

Fig. 3.19 Grafical illustration of ϕ_3 for three different values of the dynamic parameterization factor (k=0,1,2)

- The drinking task has been divided into 4 subtasks: reach the glass, reach the mouth, reach the table for releasing the glass, go back to the rest position;
- The eating task has been divided into 5 subtasks: reach the cutlery, reach the dish, take the food and reach the mouth, reach the table for releasing the cutlery, go back to the rest position;
- The pouring task has been divided into 4 subtasks: reach the bottle, pour the water, release the bottle, go back to the rest position.

The experimental validation consisted of two different sessions, described below. Each session could be divided into two phases: a) DMP parameters extraction and b) DMP computation.

1^{st} experimental session

The first experimental session aimed at comparing the proposed version of DMP computation module in Eqs. (3.8)– (3.41) with respect to the original formulation in [49]. The main difference is in the allocation of Gaussian kernels and the main findings are related to the trajectory reconstruction error, the reproduction accuracy of the user's personal motion style and the required memory allocation for the database of DMP parameters.

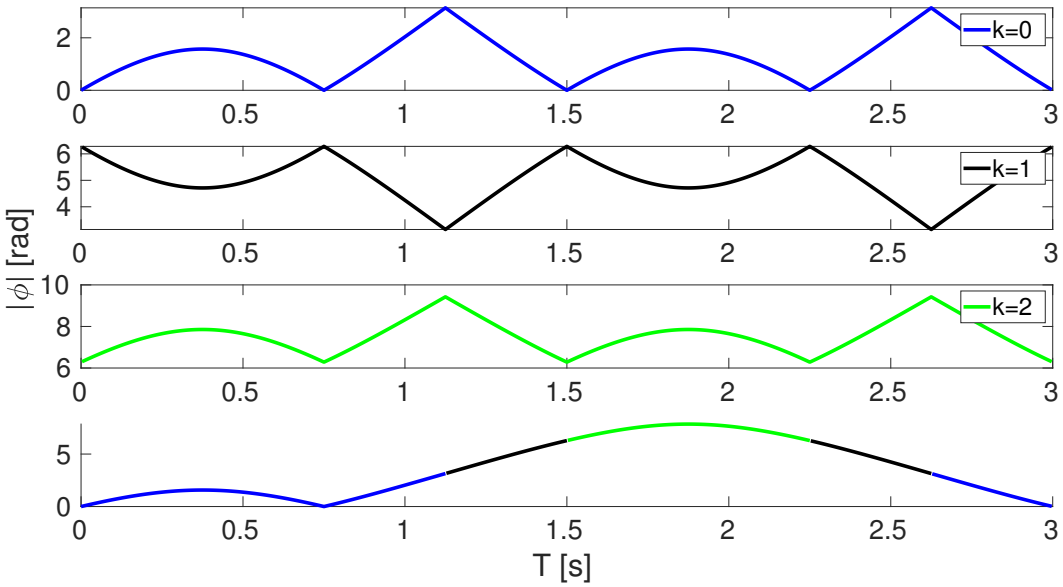

Fig. 3.20 Grafical illustration of $\|\phi\|$ for three different values of the dynamic parameterization factor (k=0,1,2)

DMP parameters extraction In the 1^{st} phase, the robotic arm worked in a passive mode: the subject's arm actively guided the robot arm by the wrist, and robot sensors have been used to record joint trajectories. Cartesian trajectories have been subsequently computed via forward kinematics. Each task has been repeated five times. The subject was seated in front of a table where the objects were placed in a priori known position. Each trial started from the same initial configuration in which the shoulder was abducted of 0^o in the frontal plane and flexed with an angle of 0^o in the sagittal plane, the elbow was flexed with an angle of 90^o in the sagittal plane and the wrist was in a neutral position with 0^o for flexion/extension, 0^o for radio-ulnar deviation and 0^o for prono/supination. Subsequently, DMP parameters has been extracted from the 7 joint trajectories and the 6 cartesian position for each task and trial.

DMP computation In the second phase the robot arm worked in an active mode. Firstly, DMPs have been computed in the joint space. The subject arm has not been attached to the robot end-effector and DMPs have been replicated by means of a PID position control with the purpose of measuring performance of the two algorithms in the case of highest level of robot accuracy ($0.002rad$). Subsequently, DMPs have been computed in the Cartesian space. The subject arm has been attached to the robot and has been passively guided in the execution of the 3 ADLs with an impedance control with high gains (for the position variables gains

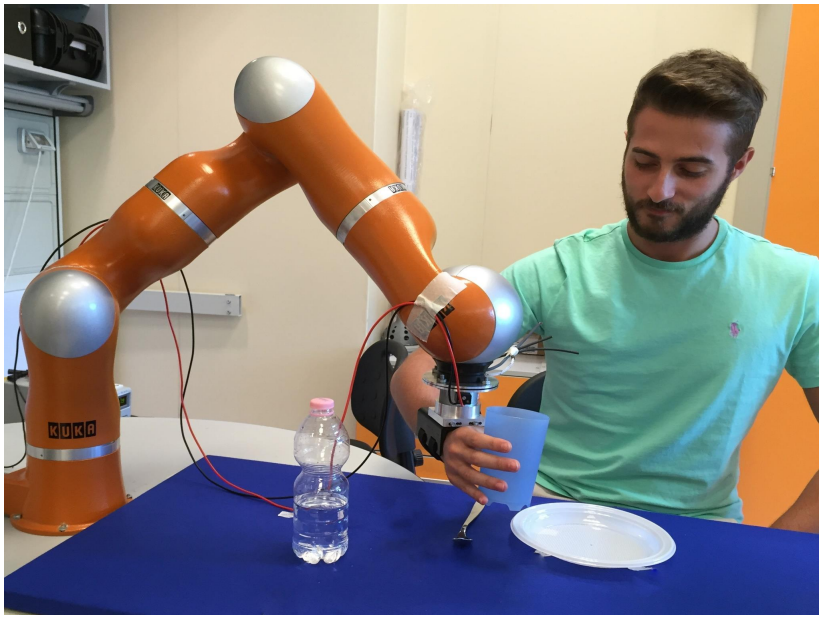

Fig. 3.21 Experimental setup.

were set to $2000 N/m$ for stiffness and $0.7 Ns/m$ for damping; for the orientation variables the gains were set to $2000 Nm/rad$ for stiffness and $0.7 Nms/rad$ for damping). This setting makes the robot provide the patient with a high level of assistance. The two algorithms have been compared in terms of reconstruction error between the recorded and the DMP trajectory, given the same number of Gaussian kernels, and number of DMP parameters for ensuring a trajectory reconstruction error lower than a preset threshold (5% of $\|g - y_0\|$, where y_0 and g are the initial and final point of the trajectory). This threshold corresponds to a reconstruction error of $0.02m$ calculated on a maximum Cartesian motion of $0.4m$ (see Fig. 3.43) and of $0.08rad$ calculated on a maximum orientation angle of $1.57rad$. This value is especially significant during the execution of activities of daily living that require high motion accuracy. Take, for example, opening/closing a drawer, a window, a door, a jar and other activities that require to strictly track motion for a successful result.

Additionally, measures of the algorithm capability to accurately reproduce the user's personal motion style and of the memory allocation required to record DMP parameters in a database have been carried out.

2^{st} experimental session

The 2^{nd} experimental session aimed to demonstrate the algorithm capability to generalize with respect to the object position changes. To this purpose, the target objects used in the ADLs (i.e. glass for drinking, bottle for pouring and plate for eating) have been placed in 24

different positions of the human-robot workspace, with respect to initial recording position (i.e. the point of coordinates $[X_3, Y_3]$ in Fig. 3.43. The glass to be filled during pouring task and the fork to be used during eating task have not been moved from the initial position, i.e. $[-0.04, -0.41]m$ and $[-0.6, -0.34]m$, respectively, in the robot reference frame.

DMP parameters extraction The first phase of the 2^{nd} session is similar to the one of the 1^{st} session. The subject's arm actively moved the robot by the wrist during the execution of the 3 ADLs. The task has been repeated for 5 times. Joint angles have been recorded by the sensors embedded in the robotic arm and Cartesian trajectories have been computed via forward kinematics. Subsequently, DMP parameters have been extracted from the mean of 5 trials computed on the 6 Cartesian positions for each sub-task.

DMP computation In the 2^{nd} phase, DMPs have been computed in the Cartesian space (6 DMPs for each sub-task and object position). The subject's wrist has been assisted by the robotic arm to perform the previously described ADLs with an impedance control with high gains, thus achieving a high level of assistance. For the position variables gains were set to $2000 N/m$ for stiffness and $0.7 Ns/m$ for damping; for the orientation variables the gains were taken as $2000 Nm/rad$ for stiffness and $0.7 Nms/rad$ for damping. The algorithm capability to generalize with respect to the change in the object position has been measured through the task execution success rate.

Data analysis Recorded joint trajectories and Cartesian positions have been processed with a digital 1^{st} order Low Pass Filter with a cut-off frequency of 20 Hz and subsequently segmented. For segmentation, the time instants when the velocity grows up or decreases to the 10% of the peak value have been considered.

For the 1^{st} experimental session a set of DMP parameters has been extracted with a preset number of 30 Gaussian Kernels, on the 5 trials of each sub-task per subject. DMP computation for the 7 joints and 6 Cartesian positions is then applied with the two versions of spatial allocation of the Gaussian kernels. They have been compared, on real hardware, in terms of Normalised Displacement Error (NDE) expressed as

$$NDE = \frac{DE}{\|g - y_0\|} 100 \tag{3.54}$$

where DE is the displacement error between recorded trajectories and the learned ones in output from the algorithms. It is worth noticing that the amplitude of the displacement error depends on the trajectory Range of Motion (RoM). Subsequently, a recursive algorithm has been performed in order to find the proper number of DMP parameters required to ensure a

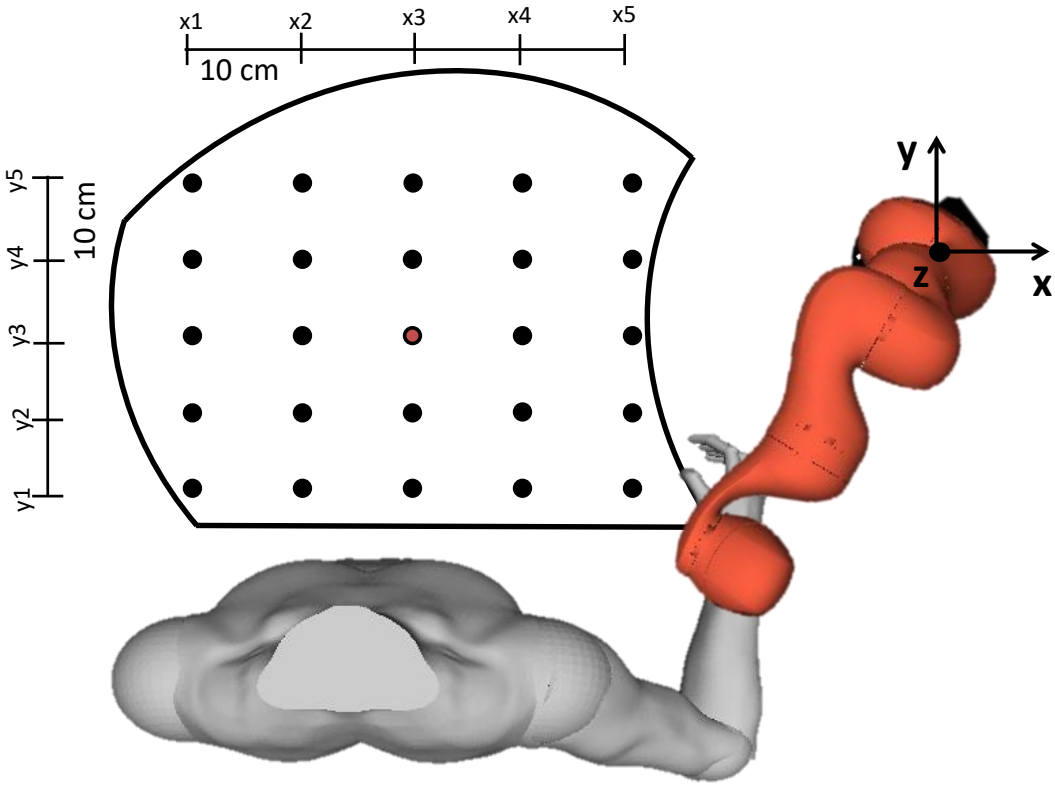

Fig. 3.22 Human-robot workspace (delimited by the black line). The positions in which the objects are moved in the considered workspace with respect to a initial recording position (red dot) are outlined with black dots.

threshold NDE of 5% on all the trajectories adopting the two versions of spatial allocation of the Gaussian kernels and two proper databases, one for each version, have been built.

Database Memory Size (MS) has been expressed as

$$MS = \sum_{i=1}^{T} \sum_{j=1}^{7} 4N_{ij}, \quad [byte] \tag{3.55}$$

where T is the total number of sub-tasks and N_{ij} is the number of parameters required for fitting the ij-th trajectory. In equation (3.55) we suppose to store floating point of 4 bytes.

In order to compute the time required to scroll the two databases, and thus the time to select the queue set of parameters in the stored databases, a time index has been introduced. It refers to the computational complexity needed to perform a linear search in the two databases.

It is expressed as

$$T_{ind} = \frac{o(N_a)}{o(N_b)} \tag{3.56}$$

where T_{ind} is the proportional factor between the time required to scroll the two databases and N_a and N_b are the number of parameters stored in them. $o(.)$ symbolically express the asymptotic behavior of N_a and N_b. Algorithm capability to accurately reproduce the user's personal motion style is measured through a motion style index expressed as

$$MSI = \sqrt{\frac{1}{N}\sum_{J=0}^{N}\left(a_{ij}^{r} - a_{ij}^{c}\right)^{2}} \tag{3.57}$$

where N is the number of time instants, a_{ij}^{r} is the acceleration of the i-th recorded Cartesian position at the j-th time instant and a_{ij}^{c} is the acceleration of the i-th Cartesian position computed at the j-th time instant by means of the DMP algorithm.

In the 2^{nd} experimental session, mean value and Standard Deviation (SD) of the segmented Cartesian trajectories have been computed on the 5 trials of each sub-task per subject, and a set of DMP parameters has been extracted by adopting the proposed algorithm in order to build a database. The recorded parameters have been used to compute the Cartesian DMPs by means of the DMP computation algorithm, for each sub-task and for different initial and final positions. Given the high robot repeatability, i.e. ± 0.05 *mm*, the tasks have been executed one time per object position. System generalization capabilities have been evaluated in terms of the success rate of the task execution.

Mean value and SD of the all previously described indices have been computed on the eight subjects. Hence, a statistical analysis based on Wilcoxon paired-sample test has been performed. Since this analysis has been carried out on multiple comparisons, the significant factor has been corrected with Bonferroni method. Therefore, it has been reported for $p - value < 0.05/n_c$, where n_c is the number of multiple comparisons.

3.2.3.2 Results and discussion

1^{st} **session experimental results** Figs. 3.23a and 3.24a report two representative joint trajectories of one subtask (i.e. reaching the cutlery). In particular, the trajectories of joints 3 and 5 executed by a representative subject are reported, but similar trajectories are executed for the other joints and by the other subjects. These figures show how well the optimized kernel distribution and equally spaced kernels perform the recorded trajectory approximation in two types of critical points, i.e. inflection (Fig. 3.23a) and minimum (Fig. 3.24a) points. Figs. 3.23b and 3.24b report, for joint 3 and 5 respectively, the error of the recorded trajectory approximation, when the optimized kernel distribution and equally

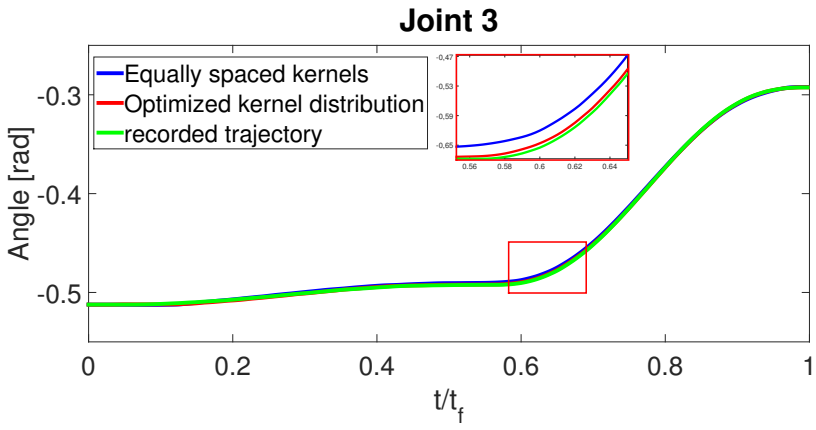

(a)

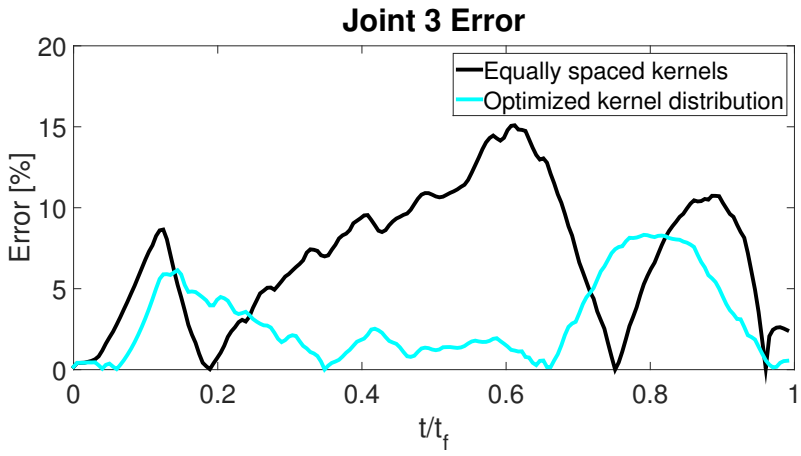

(b)

Fig. 3.23 Joint 3: (a) trajectory and (b) reconstruction error computed for a representative subject.

spaced kernels are adopted. This error is normalized with respect to the recorded trajectory RoM. The time is normalized, as well, with respect to the time needed to complete the movement (t_f). From Figs. 3.23b and 3.24b it is evident that a better approximation of the recorded trajectory is achieved in the critical points when the kernel distribution is optimized. Furthermore, in Tabs. 3.12 and 3.14 the NDE of the joint angles and Cartesian positions, with mean value and SD is reported. It has been computed on each task and subject for both the versions of kernel distribution.

On one hand, it could be noticed that the optimized kernel distribution provides an average improvement of the NDE for the 7 joint angles of 15%, 13% and 14% for task 1, 2 and 3, respectively. This corresponds to an average improvement of 0.10 *rad*, 0.091 *rad* and

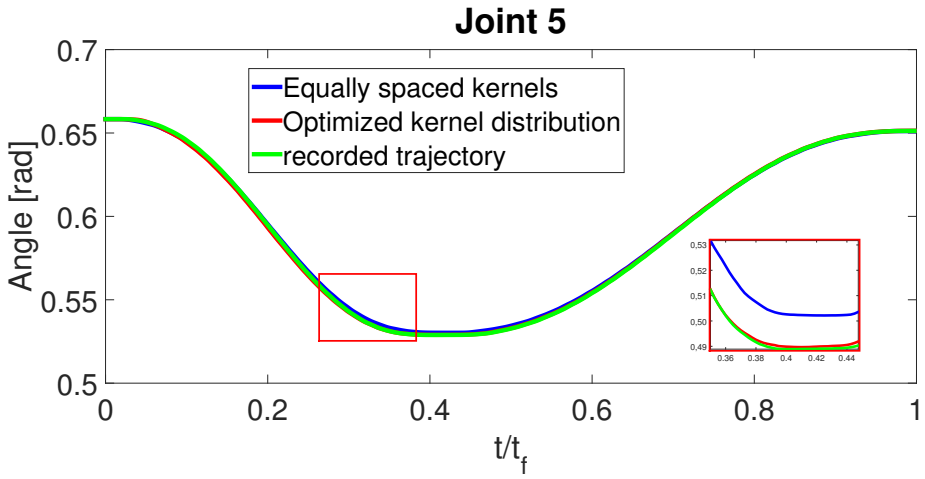

(a)

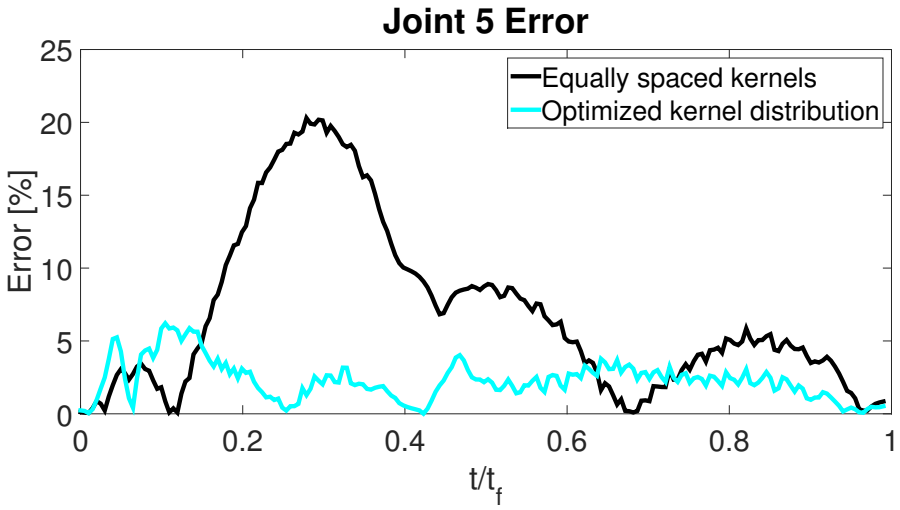

(b)

Fig. 3.24 Joint 5: (a) trajectory and (b) reconstruction error computed for a representative subject.

0.098 *rad*, respectively, if computed on the average motion of the performed joint trajectories, i.e. $\|g - y_0\|$.

On the other hand, for task 1, 2 and 3, an average improvement of the NDE in the 3 Cartesian positions of 17%, 14% and 12% is observed; while for the 4 quaternion parameters an average improvement of 17%, 18% and 16% is observed for each task. These values correspond to a Cartesian position error of 0.034 *m*, 0.028 *m* and 0.024 *m* and to an orientation error (expressed in unit quaternion) of 0.020, 0.021 and 0.019 for task 1, 2 and 3, respectively, if computed on the average motion of the performed trajectories, i.e. $\|g - y_0\|$. It is worth noticing that such an error reduction is especially substantial for the execution of activities of daily living that require high motion accuracy along the trajectory, such as opening/closing a drawer, a window, a door, a jar and other tasks that require to strictly track a motion. Indeed, an error of a few centimeters (about 0.02 m) and a few degrees (about 0.012 in quaternion representation and about 4.5^o in Euler Angles representation) could compromise their accomplishment. The benefit due to the improvement of position and orientation NDE can further grow if the approach is extended to the control of robotic devices for hand rehabilitation and assistance, which could require significantly higher motion accuracy.

The statistical analysis performed with a Wilcoxon paired-sample test over eight subjects and 5 trials, for each task, showed significant differences in the joint space ($p - value < 0.016$ over the 7 joint angles in Tab. 3.12 for each task), and in the Cartesian space ($p - value < 0.0083$ over the 3 Cartesian coordinates for task 1 and 2 and over the 4 quaternion parameters in Tab. 3.14 for each task).

Additionally, in Tab. 3.13 the mean value and SD of the number of DMPs (N_G) required to reach a NDE lower than 5% are reported, for all the Cartesian positions. They are computed over the eight subjects, for each task, for the both versions of Gaussian distribution. Significant differences between the two different modalities of allocation of Gaussian kernels have been achieved. Again, the statistical analysis was performed through the Wilcoxon paired-sample test over eight subjects and 3 Cartesian position for each task, and over eight subjects and 4 quaternion parameters for each task.

Two databases (named database1 and database2) have been built for the optimized kernel distribution and the equally spaced kernels, respectively. The mean value and SD of the memory size occupied by the two databases have been computed over the eight subjects. Database1 has a size of 4.5 ± 0.7 *MB*, while database2 has a size of 7.3 ± 0.9 *MB*. Hence, 2.8 ± 0.9 *MB* have been saved with the optimized kernel distribution. Moreover, considerations about the computational saving could be extracted by replacing in Eq. 3.56 the values in Tab. 3.13. A time index (T_{ind}) equal to 0.61 has been obtained, indicating that the time to scroll database2 is about 61% of the time to scroll database1.

Table 3.6 Joint NDE % obtained in session I

Equally spaced kernels[1]							
Task	Joint 1	Joint 2	Joint 3	Joint 4	Joint 5	Joint 6	Joint 7
1	15 ± 6	20 ± 4	25 ± 5	19 ± 3	15 ± 6	21 ± 6	22 ± 3
2	12 ± 4	19 ± 10	16 ± 4	18 ± 2	16 ± 4	25 ± 5	18 ± 4
3	16 ± 5	21 ± 6	17 ± 3	14 ± 5	23 ± 3	18 ± 10	19 ± 11
Optimized kernel distribution[1]							
Task	Joint 1	Joint 2	Joint 3	Joint 4	Joint 5	Joint 6	Joint 7
1	4 ± 3	7 ± 2	6 ± 3	5 ± 2	5 ± 5	6 ± 4	7 ± 3
2	6 ± 4	4 ± 6	7 ± 3	3 ± 1	4 ± 3	7 ± 4	3 ± 2
3	3 ± 1	2 ± 2	7 ± 2	4 ± 3	8 ± 3	4 ± 5	5 ± 4

Time and memory savings are directly proportional to the number of stored parameters. Hence, saving could significantly increase if the number of tasks grows. For instance, in a home scenario there could be hundreds of possible tasks involving interaction with the environment [102]; thus, a memory saving of hundreds of MB, with a correspondent time saving of some seconds, can be achieved. In a rehabilitation scenario where the amount of patients treated per year is significantly higher, the above mentioned savings could be notably increased.

Finally, in Tab. 3.9 the mean value and SD of the motion style index, calculated over the eight subjects for the two versions of spatial allocation of the Gaussian kernels, are reported. Accuracy increase is achieved in the user's personal motion style reproduction when the optimised kernel distribution is adopted. The motion style index is reduced by about 2 cm/s^2, 8 cm/s^2 and 7 cm/s^2 on average of the 3 Cartesian axes and is reduced of about 6 $10^{-3}/s^2$, 9 $10^{-3}/s^2$ and 10 $10^{-3}/s^2$ on average of the 4 quaternion parameters, for task 1, 2 and 3, respectively. It is interesting to note that the improvements achieved in terms of user motion style reproduction are statistically significant, as verified with the Wilcoxon paired-sample test on 5 trials and eight subjects, applied both to the 3 Cartesian axes and to the 4 quaternion parameters for each task ($p - value < 0.0083$).

2^{nd} **session experimental results** X and Y Cartesian trajectories, executed by the robotic arm in assisting a representative subject to perform drinking and eating task, are shown in Figs. 3.25 and 3.26. The other Cartesian coordinates are not shown, being Z and orientation coordinates not varied when the objects are placed in the 24 different positions of Fig. 3.43.

Table 3.7 Cartesian NDE % obtained in session I

Equally spaced kernels[2]							
Task	X	Y	Z	Q_0	Q_1	Q_2	Q_3
1	22 ± 6	25 ± 6	23 ± 6	24 ± 8	19 ± 7	25 ± 9	21 ± 6
2	24 ± 5	21 ± 5	20 ± 7	25 ± 5	22 ± 6	23 ± 6	27 ± 8
3	19 ± 7	18 ± 7	18 ± 5	20 ± 5	24 ± 3	21 ± 5	26 ± 9
Optimized kernel distribution[2]							
Task	X	Y	Z	Q_0	Q_1	Q_2	Q_3
1	7 ± 6	7 ± 5	3 ± 4	7 ± 5	5 ± 5	4 ± 3	5 ± 2
2	9 ± 8	5 ± 6	9 ± 7	8 ± 4	6 ± 2	4 ± 5	7 ± 4
3	6 ± 9	4 ± 6	8 ± 5	13 ± 2	3 ± 4	3 ± 4	8 ± 3

Table 3.8 Number of kernels (N_G) obtained in session I

Equally spaced kernels[2]							
Task	X	Y	Z	Q_0	Q_1	Q_2	Q_3
1	208 ± 14	255 ± 21	220 ± 24	250 ± 21	145 ± 16	220 ± 15	242 ± 20
2	237 ± 16	188 ± 22	170 ± 12	360 ± 23	340 ± 18	203 ± 14	156 ± 15
3	210 ± 17	350 ± 18	230 ± 18	270 ± 16	254 ± 19	313 ± 21	201 ± 18
Optimized kernel distribution[2]							
Task	X	Y	Z	Q_0	Q_1	Q_2	Q_3
1	92 ± 10	91 ± 16	55 ± 14	100 ± 8	65 ± 15	71 ± 10	66 ± 11
2	124 ± 11	70 ± 15	123 ± 11	115 ± 7	90 ± 16	82 ± 13	98 ± 9
3	130 ± 12	95 ± 11	170 ± 17	95 ± 14	85 ± 13	63 ± 14	72 ± 15

Table 3.9 Motion style index (MSI) obtained in session I

Equally spaced kernels[2]							
Task	X^3	Y^3	Z^3	${Q_0}^4$	${Q_1}^4$	${Q_2}^4$	${Q_3}^4$
1	7 ± 0.6	6 ± 0.5	0.7 ± 0.6	9 ± 0.9	8 ± 2	7 ± 3	9 ± 4
2	6 ± 1	9 ± 0.6	13 ± 0.5	11 ± 1	10 ± 0.7	12 ± 3	13 ± 3
3	8 ± 0.9	7 ± 0.8	11 ± 0.7	8 ± 3	12 ± 4	13 ± 1	11 ± 4
Optimized kernel distribution[2]							
Task	X^3	Y^3	Z^3	${Q_0}^4$	${Q_1}^4$	${Q_2}^4$	${Q_3}^4$
1	3 ± 0.1	2 ± 0.2	0.3 ± 0.3	3 ± 0.3	1 ± 0.3	2.3 ± 0.3	1.2 ± 0.2
2	1 ± 0.1	0.9 ± 0.1	0.5 ± 0.1	2 ± 0.2	0.7 ± 0.2	1.2 ± 0.2	2.3 ± 0.1
3	2 ± 0.3	0.8 ± 0.2	0.7 ± 0.2	4 ± 0.4	0.5 ± 0.4	0.5 ± 0.3	0.8 ± 0.5

Furthermore, also pouring task is not shown being very similar to the drinking task in terms of X and Y Cartesian trajectories. In Fig. 3.25 and 3.26 the red trajectory refers to the recorded one (in this case objects are in $[X_3, Y_3]$ position). It could be noticed from these figures that the different target positions of the object, i.e. $[X_1, Y_1], [X_1, Y_2] \ldots [X_4, Y_5], [X_5, Y_5]$ of Fig. 3.43, are reached with a movement shape similar to the recorded one in all the tasks. Similar results have been achieved over the other subjects. In summary, a success rate of 100% for all the tasks has been achieved on the eight subjects.

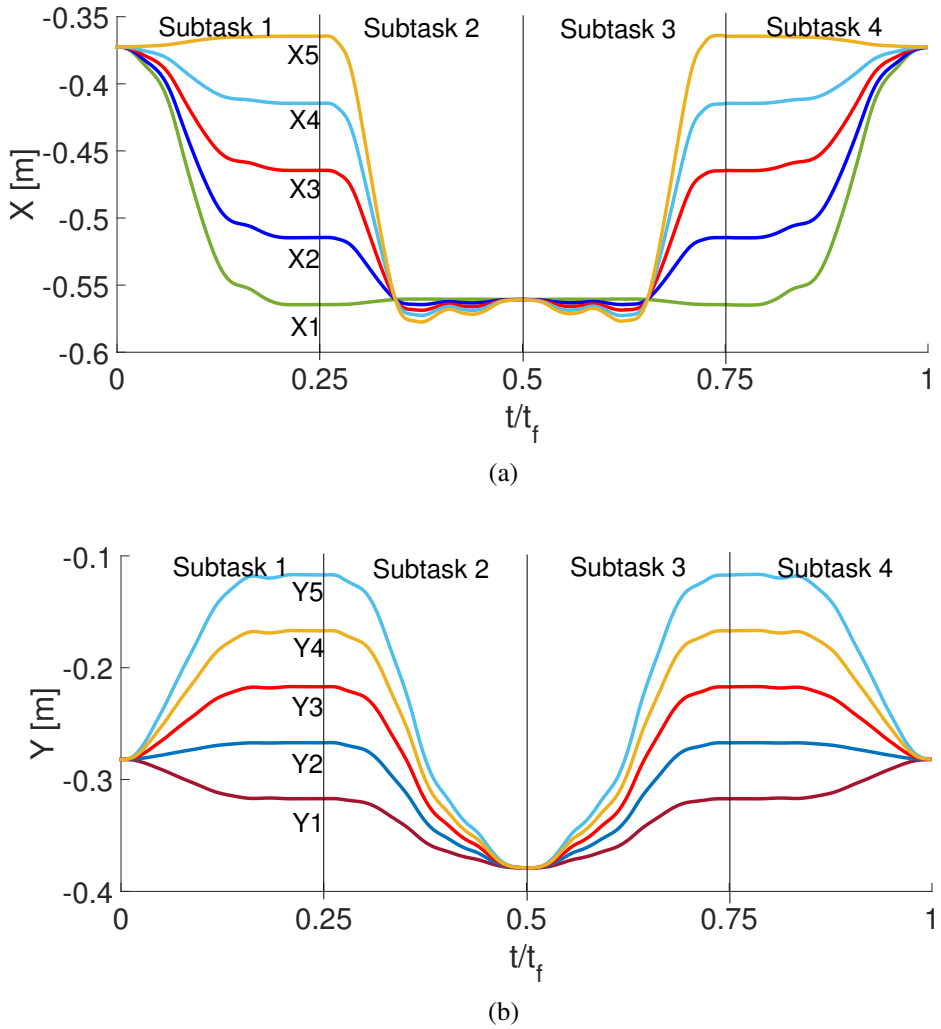

Fig. 3.25 Cartesian coordinate trajectories executed by the robotic arm during the drinking task with 24 glass different positions. (a) X coordinate, (b) Y coordinate. The recorded trajectory is outlined in red.

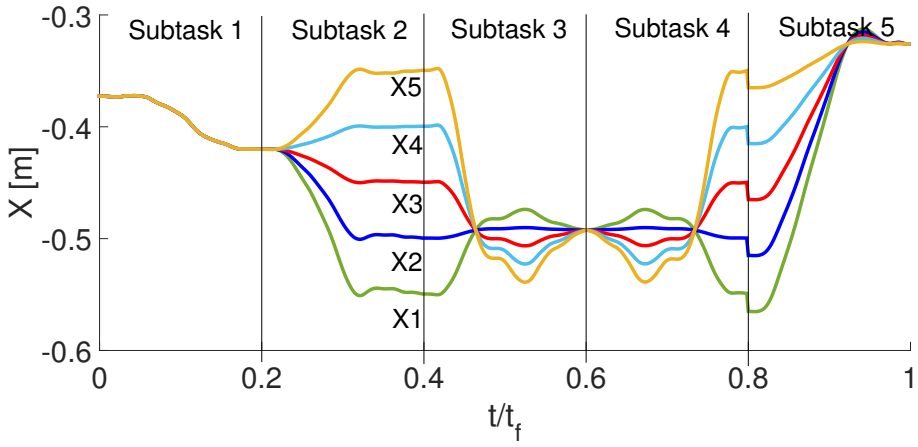

(a)

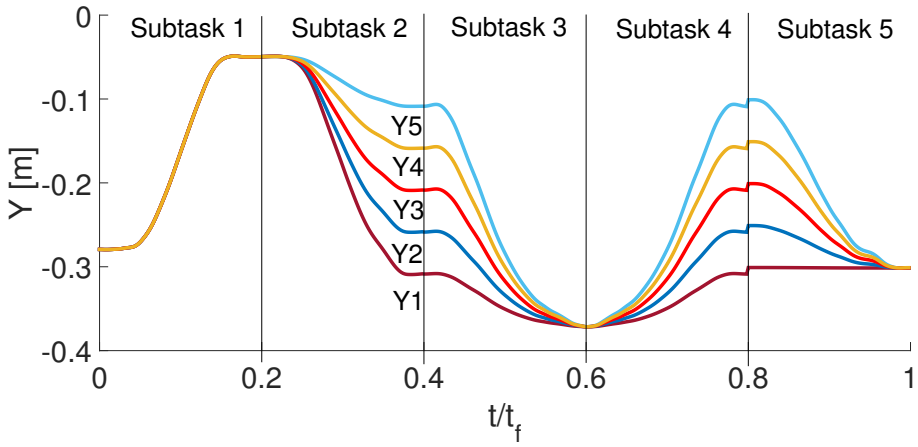

(b)

Fig. 3.26 Cartesian coordinate trajectories executed by the robotic arm during the eating task with 24 plate different positions. (a) X coordinate, (b) Y coordinate. The recorded trajectory is outlined in red.

3.2.4 Experimental validation 2

The motion planner proposed in Sect.3.2.2.2 was tested on an upper-limb exoskeleton during ADLs tasks. The exoskeleton was made of a 4-DoF shoulder-elbow exoskeleton (i.e. NeuroExos Shoulder-Elbow Module (NESM) [21]) for reaching movements, and a 5-DoF wrist-hand exoskeleton responsible for the grasping phase. The system was experimentally validated on four patients with Limb Girdle Muscular Dystrophy (LGMDs). They were asked

[1]These results was achieved piloting the robot with a PID control
[2]These results was achieved piloting the robot with an impedance control
[3]The units of these values are $[cm/s^2]$
[4]The units of these values are $[10^{-3}/s^2]$

to perform one ADL (i.e. the drinking task) and two activities belonging to the Southampton Hand Assessment Procedure (SHAP) clinical test (i.e. pouring and lifting a light sphere, consisting in reach-grasp-move-release a spherical object). The position of the object to be grasped was acquired by means of an external camera (Optitrack).

A comparative analysis with the traditional approach based on path planning and IK for upper-limb exoskeletons was carried out. Moreover, the data acquired during the experimental session were used to assess the generalization capability of the proposed motion planning system with respect to the different anthropometry of the patients and the different object positions. Performance of the proposed motion planning system were measured through a set of performance indicators, consisting of success rate, distance from target position, distance from the physiological behaviour and computational burden.

Exoskeletons

The upper-limb exoskeleton used to validate the proposed motion planning system is shown in Fig. 3.27. It consists of the NESM 4-DoF exoskeleton and a 5-DoF Wrist-hand exoskeleton, described in the following.

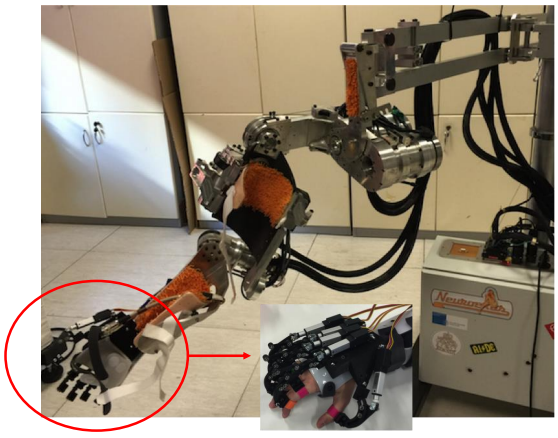

Fig. 3.27 NESM upper-limb exoskeleton with the wrist-hand exoskeleton

NESM NESM is an upper-limb exoskeleton consisting of four active DoFs addressing the shoulder abduction/adduction (sA/A), flexion/extension (sF/E) and internal/external rotation (sI/E), as well as the elbow flexion/extension (eF/E) movements [21]. Additional passive degrees of freedom and size regulations are included within the kinematic chain to improve the safety and wearability of the device: this system automatically compensates

for joint misalignments of the elbow and shoulder complex and allows users with different anthropometries wearing the device.

Each actuation unit has a series-elastic actuator (SEA), comprising a DC motor and reduction gear in series with a custom spring. Two absolute encoders placed at both sides of the spring allow sensing the joint torque by measuring the spring deformation and, at the same time, the encoder mounted more proximally to the human joint provides the joint angular value. By virtue of the SEA architecture, both position and torque control strategies have been implemented.

The sA/A and sF/E actuation units are identical and are able to withstand peak torques up to $60Nm$. Similarly, the sI/E and eF/E actuation units can deliver up to $30Nm$ of peak torques. These features make the exoskeleton suitable to assist users having highly reduced or null residual motion capabilities of their upper arm. Notably, in this study the position control modality is employed to perform completely passive mobilization of the user's arm.

Each joint can move within the following range of motion (the zero configuration is with the arm parallel to the trunk): 0 to $-90deg$ for sA/A and sF/E, -75 to $25deg$ for sI/E and 0 to $120deg$ for eF/E.

Wrist-hand exoskeleton The wrist-hand exoskeleton is composed of two modules, the hand and the wrist, that can be used separately or in combination. The wrist exoskeleton guarantees the activation of the prono/supination movements. It consists of a DC motor with a reduction stage, which drives a geared ring guide. The guide is attached to an orthosis that aligns the forearm with the guide axis. Joint limits are mechanically provided, but, if necessary they can be reduced via software for increasing the safety in the human-robot interaction.

The hand exoskeleton has 4 active DoFs: F/E of the index finger Metacarpophalangeal (MCP) joint, F/E of the middle finger MCP joint, F/E of the ring and little finger MCP joints and F/E of the thumb MCP joint. A linkage mechanism between the MCP and the Proximalinterphalangeal (PIP) joint is adopted on each finger and is driven by a linear actuator, for moving both PIP and MCP joints. A unique linear actuator is used for driving the PIP and MCP joints of both the third and the fourth fingers. The thumb A/A is fixed in a suitable position.

The wrist exoskeleton can be easily connected to the shoulder-elbow exoskeleton. In fact, by simply removing the forearm cuff from the NESM, the cuff integrated to the wrist exoskeleton can be attached to the output frame of the elbow actuation unit. The resulting device is a full-arm robotic exoskeleton.

Low Level Control (LLC)

The control system used to operate the NESM implements two control strategies: joint position and joint torque control modes. When controlled in position, each actuation unit drives the joint position along a reference value or trajectory. The controller is based on a proportional-integral-derivative (PID) regulator, which operates on the difference between the reference joint angle and the measured one. The output is a current commanded to the driver of the SEA actuation unit to provide the torque necessary to achieve the movement with null steady-state error.

In the torque control mode, each motor is controlled to provide a certain amount of torque. The closed-loop torque controller output is dependent on the difference between the desired joint torque and the measured one and it is built on a PID regulator as well. When a reference torque of $0Nm$ is commanded on each joint, the device can be used in transparent mode, allowing the user to freely move the arm. Conversely, the wrist module and the hand exoskeleton could be controlled only in position; the controller used to operate these devices is based on a PID regulator, which operates on the difference between the reference joint angle and the measured one.

Traditional path planning and IK

A simple path planning, based on a third-order polynomial function, was implemented in order to generate Cartesian trajectories with null velocity at the beginning and at the end of the movement. It can be written as

$$z = -2\frac{z_f - z_i}{D^3}t^3 + 3\frac{z_f - z_i}{D^2}t^2 + z_i \tag{3.58}$$

where z is the desired exoskeleton Cartesian pose, z_f and z_i are the final and initial desired Cartesian pose, respectively, and D is the motion duration.

Hence, two IK methods were adopted to generate the reference joint position for the exoskeleton. They are IK based on the computation of the swivel angle (named in the following *IK with swivel angle*) and IK with the inverse Jacobian (named in the following *IK Inverse Jacobian*).

IK with swivel angle The IK algorithm with swivel angle was ad-hoc developed for a 4-DoF spherical-revolute (S-R) manipulator (i.e. the shoulder-elbow exoskeleton), based on geometrical considerations. An additional constraint was imposed to calculate the analytical solution for the last revolute DoF of the upper-limb exoskeleton (i.e. the wrist prono-

supination). For the sake of clarity, the Denavit-Hartenberg model and parameters of the upper-limb exoskeleton are reported in Fig. 3.28.

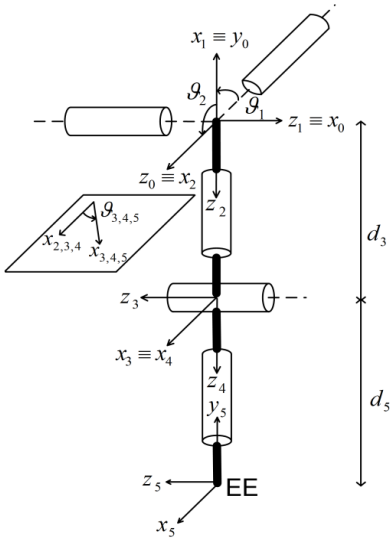

ϑ	d	a	α
$\vartheta_1 + \pi/2$	0	0	$\pi/2$
$\vartheta_2 + \pi/2$	0	0	$-\pi/2$
ϑ_3	d_3	0	$-\pi/2$
ϑ_4	0	0	$\pi/2$
ϑ_5	d_5	0	$-\pi/2$

Fig. 3.28 NEMS reference frames positioning according to the Denavit-Hartenberg (D-H) convention

The IK algorithm for the shoulder-elbow exoskeleton manages three Cartesian coordinates and one orientation coordinate and consists of the following steps:

- Being the target position known (vector $\vec{p}$), the solution for the elbow angle is derived geometrically:

$$q_4 = \pi - acos\left(\frac{d_3^2 + d_5^2 - |\vec{p}|^2}{2d_3d_5}\right) \tag{3.59}$$

- The orientation coordinate is a free parameter, (γ), introduced for guaranteeing anthropomorphic criteria and is defined as the angle, on the frontal plane ($x_0 - y_0$ in Fig. 3.28), between the plane containing the upper arm and forearm and the frontal plane. Once γ is chosen, two possible configurations of the elbow (i.e. left or right) allow the arm lying in the chosen plane: the solution with the four angles in the physiological range is selected.

- Then, the shoulder joint angles can be derived from forward kinematics:

$$q_1 = atan\left(\frac{y_{o_3}}{x_{o_3}}\right) \tag{3.60}$$

$$q_2 = acos\left(\frac{z_{o_3}}{d_3}\right) \tag{3.61}$$

$$q_3 = -\arccos\left(\frac{z_{ee} - d_3\cos q_2 - d_5\cos q_2\cos q_4}{d_5\sin q_4\sin q_2}\right) \tag{3.62}$$

- The wrist prono-supination angle is calculated, by imposing a constraint on the hand orientation. For the addressed tasks (i.e. drinking, pouring, reaching-grasping-moving-releasing of the sphere), two configurations were considered:

  1) Palm of the hand pointing downward (for pouring and sphere reaching-moving):

$$q_5 = \arctan\left(\frac{\cos q_4(\cos q_1\sin q_3 + \cos q_2\cos q_3\sin q_1) + \sin q_1\sin q_2\sin q_4}{\cos q_2\sin\vartheta_1\sin q_3 - \cos q_1\cos q_3}\right) \tag{3.63}$$

  2) Palm of the hand pointing left (for drinking):

$$q_5 = \arctan\left(\frac{\cos q_1\cos q_3 - \cos q_2\sin q_1\sin q_3}{\cos q_4(\cos q_1\sin q_3 + \cos q_2\cos qa_3\sin q_1) + \sin q_1\sin q_2\sin q_4}\right) \tag{3.64}$$

IK with Inverse Jacobian The IK algorithm with inverse Jacobian is well-described by the following equation [113],

$$\dot{q} = J_A^{-1}(q)(\dot{x}_d + Ke) \tag{3.65}$$

where J_A^{-1} is the analytical inverse Jacobian computed on the kinematic chain of Fig. 3.28, q and $\dot{q}$, are the joint angle and its derivative, respectively, $\dot{x}_d$ is the desired velocity in the Cartesian space, K is a positive definite matrix (usually diagonal) and e is the *operational space error* defined as $e = x_d - x_e$. The desired joint configuration q is obtained by numerically integrating Eq. 3.65 through the Euler method.

3.2.4.1 Experimental setup

The experimental platform for the validation of the proposed motion planning system based on LbD is shown in Fig. 3.29.

A user graphical interface is used to show the action to perform to the subject. The control system architecture consisted in a finite-state machine, which divides the main task (i.e. drinking, pouring and reach-grasp-move-release a sphere) into several elementary actions (corresponding to the subtasks listed in Tab. 3.10) that the different devices can accomplish (e.g. waiting for the trigger, reaching the glass, grasping, etc.). Each subtask is triggered by the user by means of the combined M-IMU/EMG interfaces, letting him/her to control the

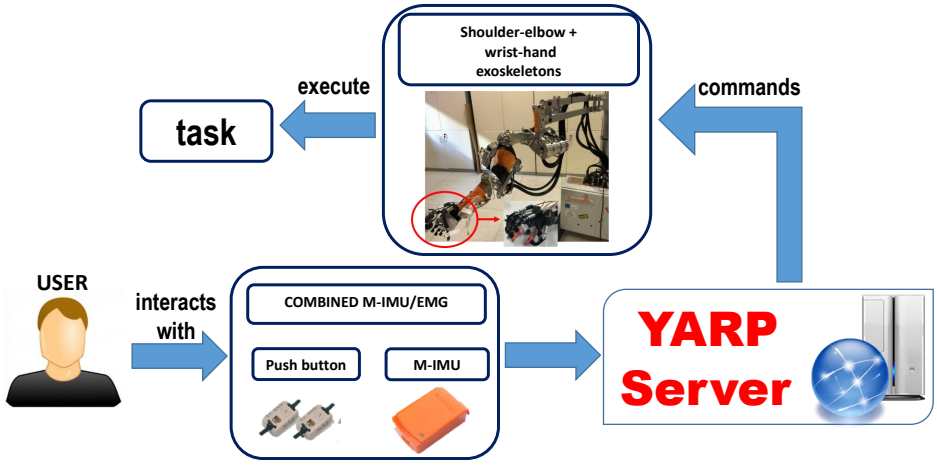

Fig. 3.29 Block scheme of the platform

exoskeletons. An abort function was also implemented in the state machine to safely abort the execution of the task at any time.

The communication within the subsystems composing the platform is managed by the Yet Another Robotic Platform (YARP) messaging system. The motion commands acquired by the user are sent, through the YARP server, to the exoskeletons. All the acquired data are synchronized and saved under YARP.

The platform components are shown in Fig. 3.30 and are detailed in the following.

User interface The interface adopted to detect the user movement intention is based on the combined use of 2 push-buttons and 2 M-IMUs [64].

The 2 push-buttons were placed on a table in order to be activated by the index and the thumb fingers and to be used as a switch. Moreover, the two M-IMUs (XSens MTw) were placed on the user trunk and head in order to detect his/her neck motion. An Awinda Station was used to record at 100 Hz of synchronised wireless data from the two M-IMUs.

By means of the developed interface the user may exploit: i) the head yaw motion in the negative direction to operate the upper-limb exoskeleton movements and the head yaw motion in the positive direction to abort the task; ii) the index finger and thumb residual motion to trigger the hand opening and the hand closing.

3.2.4.2 Experimental protocol

Off-line neural network training The developed neural network was trained off-line on a healthy volunteer subject (with upper arm length $L_{UpperArm} = 0.33m$ and forearm length

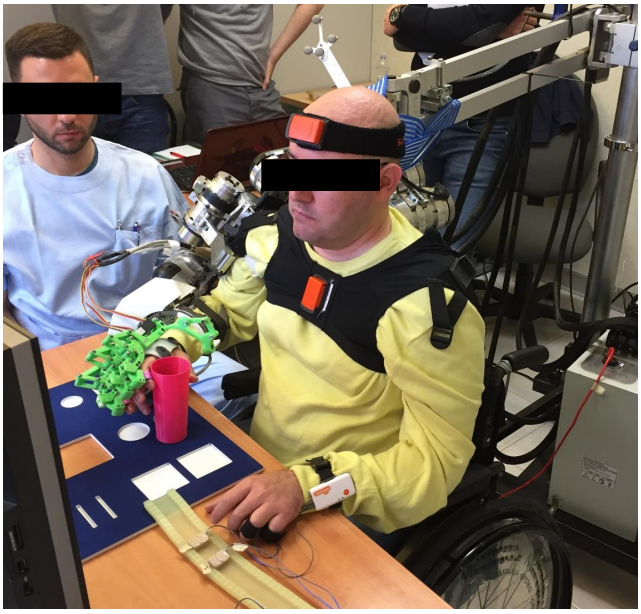

Fig. 3.30 A representative subject performing the task (the subject signed an informed consent document to authorize publication of this picture)

$L_{forearm} = 0.3m$). He was asked to perform the drinking task, with 41 different glass positions (Fig. 3.43a), and two activities belonging to the SHAP clinical test, i.e. pouring (for 15 different positions of the glass and the bottle as in Fig. 3.43b) and reach-grasp-move-release a sphere (for 25 different positions of the sphere as in Fig. 3.43c). Each task was performed 5 times per each object position and arm motion was recorded. The shoulder motion, i.e. the sA/A, sF/E, sI/E and eF/E movements was recorded through the NESM used in transparent mode; conversely the wrist Prono-Supination wP/S was recorded by means of two M-IMUs placed on the subject forearm and hand.

About 70% of the recorded data was used to train the neural network; the remaining 30% was used to validate and test the neural network in order to avoid over-fitting issues.

DMP computation and control The experimental session was aimed to measure performance of the proposed motion planning system, compare with the traditional approach based on inverse kinematics described in Sect 3.2.4 and assess generalization capability. The system was tested during the fulfillment of the same ADLs used for training, i.e. drinking, the pouring and reach-grasp-move-release a sphere. In the following they are named task 1, 2 and 3, respectively. Additionally, each task is divided into a number of subtasks listed in Tab. 3.10.

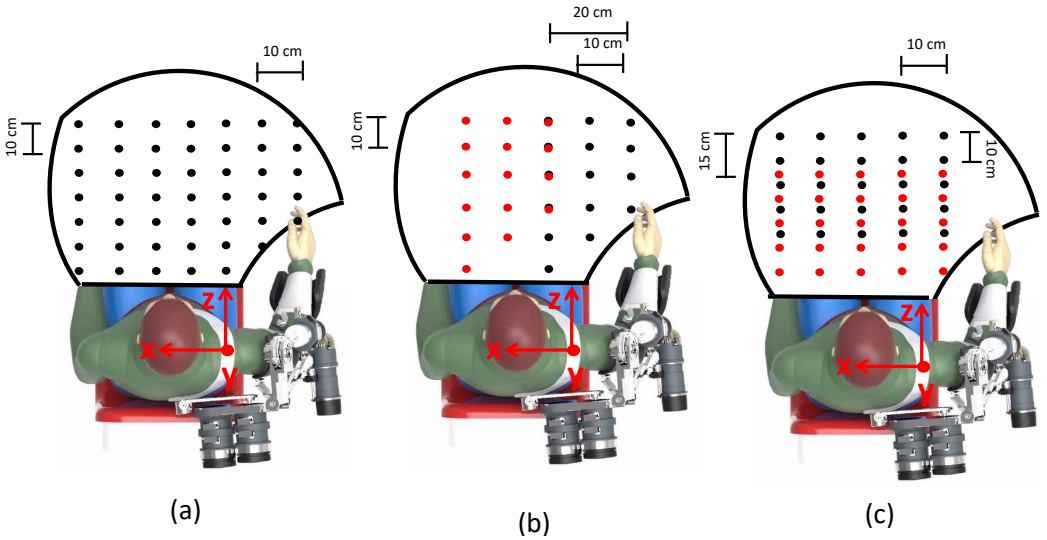

Fig. 3.31 The workspace reached during the assistive tasks is delimited by the black line. Object positions during training are indicated by black dots (the glass in the drinking task in (a), the bottle in the pouring task in (b) and the initial position of the sphere in the SHAP task in (c)). Conversely, the glass positions during the pouring task and the sphere final positions in the SHAP task are indicated by red dots in (b) and (c), respectively.

The validation was performed in simulation and in the real setting with patients. Simulation tests allowed evaluating system performance in the whole human-robot workspace (238, 75 and 125 object positions were considered for task 1, 2 and 3, respectively). On the other hand, in the real setting system performance was assessed on four patients with Limb Girdle Muscular Dystrophy (LGMDs). They, aged 38.5 on average (Standard Deviation 14.6), volunteered to participate in this study. The experimental protocol was approved by the local Ethical committee (Comitato Etico Università Campus Biomedico di Roma, reference number: 01/17 PAR ComEt CBM), by the Italian Ministry of Health (Registro - classif. DGDMF/I.5.i.m.2/2016/1096) and complied with the Declaration of Helsinki. The subjects were asked to perform three repetitions of the three tasks thanks to the assistance of the 4-DoF upper-limb and 5-DoF wrist-hand exoskeletons (3 object positions for each task were considered in this case).

Comparative Analysis (CA) with inverse kinematics methods The CA was aimed to measure performance of the proposed motion planning based on LbD during the control of the exoskeleton and compare the results with the traditional approaches based on path planning and inverse kinematics described in Sect. 3.2.4. The comparative analysis (CA) was carried out in simulation on a subject modeled with 30 cm upper arm and forearm lengths, and with 238, 75 and 125 different object positions.

Table 3.10 Tasks description

Task 1: Drinking	
subtask 1-1	reach the glass
subtask 1-2	reach the mouth
subtask 1-3	reach the table for releasing the glass
subtask 1-4	go back to the rest position
Task 2: Pouring	
subtask 2-1	reach the bottle
subtask 2-2	pour the water into the glass
subtask 2-3	reach the table for releasing the bottle
subtask 2-4	go back to the rest position
Task 3: SHAP sphere	
subtask 3-1	reach the sphere
subtask 3-2	move the sphere to another position on the table
subtask 3-3	go back to the rest position

Generalization Capability Assessment (GCA) The GCA was aimed to evaluate the generalization level of the proposed motion planning with respect to the different anthropometries of the patients and the different object positions. Firstly, it was tested in simulation environment (GCA–sim) for 238, 75 and 125 object positions (for task 1, 2 and 3 respectively) per 25 different subject anthropometries, i.e. the combination of the following upper arm and forearm lengths: $L_{UpperArm} = 30cm, 32cm, 34cm, 36cm, 38cm$ and $L_{forearm} = 30cm, 32cm, 34cm, 36cm, 38cm$. Subsequently, the proposed motion planning was tested on the four patients (GCA–real), with $L_{UpperArm} = 33cm$ and $L_{forearm} = 30cm, 30cm, 35cm, 37cm$, for 3 object positions per task.

System performance was measured through three quantitative indicators reported below.

Performance indices The proposed performance indicators are: i) $Position\ Err1$, $Orientation\ Err1$, $Position\ Err2$, $Orientation\ Err2$, ii) PhJL iii) Success Rate and iv) mean cycle time. They are aimed at evaluating i) distance from target position, ii) distance from anthropomorphic configurations, taking into account the physiological joint limits, iii) the success rate of the task execution and iv) the computational burden.

Distance from target position

The error was measured during subtasks 1-1, 2-1, 3-1 and 3-2 (in Tab. 3.10) as

$$Position\ Err = \frac{1}{2}\sqrt{(x_t - x)^2 + (y_t - y)^2 + (z_t - z)^2} \tag{3.66}$$

$$Orientation\ Err = \|\alpha_t - \alpha\| \tag{3.67}$$

where x_t, y_t and z_t are the coordinates of the target position and x, y and z are the coordinates of the actual position reached by the robot end-effector; α_t is the desired angle α that needs to be 0 for a successful task fulfillment; α is illustrated in Fig. 3.32 and is defined for subtask 1-1 and 2-1 as

$$\alpha_1 = acos(\frac{X_{ee}^T Y_0}{\|X_{ee}\|\|Y_0\|}) \tag{3.68}$$

Conversely, for subtask 3-1 and 3-2 α is defined as

$$\alpha_2 = acos(\frac{Z_{ee}^T Y_0}{\|Z_{ee}\|\|Y_0\|}) \tag{3.69}$$

where Y_0, X_{ee} and Z_{ee} are defined in the base reference frame [X_B,Y_B,Z_B] as $Y_0 = [0,1,0]$, $X_{ee} = T_B^{ee}[1,0,0,1]$ and $Z_{ee} = T_B^{ee}[0,0,1,1]$ (T_B^{ee} is the base/end-effector transformation matrix).

For subtask 2-2 the position and orientation error are expressed as

$$Position\ Err_{2-2} = \frac{1}{2}\sqrt{(x_{bottle} - x_{glass})^2 + (z_{bottle} - z_{glass})^2} \tag{3.70}$$

$$Orientation\ Err_{2-2} = \|\beta_t - \beta\| \tag{3.71}$$

$$\begin{bmatrix} x_{bottle} \\ y_{bottle} \\ z_{bottle} \\ 1 \end{bmatrix} = T_B^{ee} T_{ee}^{bottle} \begin{bmatrix} 0 \\ 0 \\ 0 \\ 1 \end{bmatrix} \tag{3.72}$$

$$\beta = \frac{\pi}{2} - acos(\frac{X_{ee}^T Y_0}{\|X_{ee}\|\|Y_0\|}) \tag{3.73}$$

where x_{bottle}, z_{bottle}, x_{glass} and z_{glass} are expressed in the [X_B,Y_B,Z_B] reference frame (see Fig. 3.32), T_{ee}^{bottle} is the end-effector/bottle-tip transformation matrix during the whole subtask 2-2 (i.e. when the hand exoskeleton is grasping the bottle) and β_t is the desired β that needs to range from 0 to $\frac{\pi}{3}$ in order to successfully accomplish the pouring task. Thus, defining $\beta_t = 0$, an acceptable value of the orientation error, for a successful task fulfillment, ranges from 0 to $\frac{\pi}{3}$.

Distance from the physiological joint limits The distance from the physiological joint limits is measured to assess the level of anthropomorphism of the reached configuration

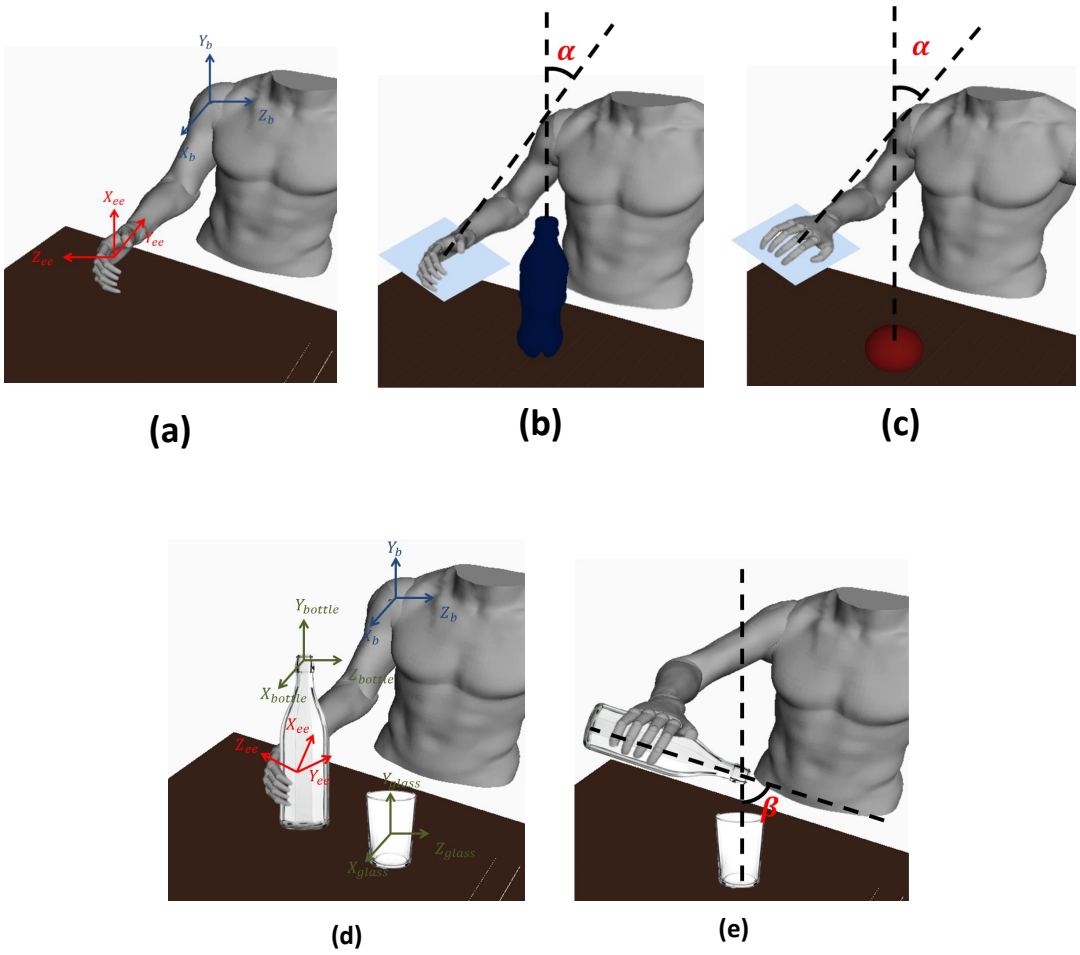

Fig. 3.32 (a) a graphical representation of the end-effector and the base reference frame is shown; (b) the α angle for task 1-1, 2-1 is shown; (c) the α angle for task 3 is shown; (d) The base reference frame and bottle, end-effector and glass reference frames are shown; (e) the β angle for task 2-2 is shown.

during motion. It is expressed as

$$PhJL = \left\| \frac{2(q_i - \bar{q}_i)}{q_{iM} - q_{im}} \right\| \tag{3.74}$$

where q_i is the actual position of the i-th joint, q_{iM} and q_{im} are the upper and lower physiological limit of the i-th joint and $\bar{q}_i$ is the mean value between q_{iM} and q_{im}. An acceptable value of $PhJL$ for the considered tasks ranges in between 0 and 1 .

*Success rate of the task execution The success rate of the task execution is evaluated as

$$Success\ rate = \frac{N_{succ}}{N_{tot}} \cdot 100 \tag{3.75}$$

where N_{succ} is the number of trials successfully accomplished and N_{tot} is number of all the performed trials. Trials of tasks 1 and 3 are considered successfully accomplished if all the following conditions are satisfied:

- $Position\ Err \leq 15mm$,
- $Orientation\ Err \leq \frac{\pi}{12} rad$,
- $0 \leq PhJL \leq 1$.

Conversely, trials of Task 2 are considered successfully accomplished if all the following conditions are satisfied:

- $Position\ Err_{2-1} \leq 15mm$,
- $Orientation\ Err_{2-1} \leq \frac{\pi}{12} rad$,
- $Position\ Err_{2-2} \leq 30mm$ (i.e. the glass radius),
- $0 \leq Orientation\ Err_{2-2} \leq \frac{\pi}{3} rad$,
- $0 \leq PhJL \leq 1$.

The aforementioned ranges were experimentally retrieved. Computational burden The computational burden of the three compared methods is evaluated through the mean cycle time; it is the time required to complete one cycle of the algorithm that computes the desired joint trajectory starting from the object position and the task type. The computational time of the 3 methods was evaluated under the same hardware conditions (Processor: Intel(R) Core(TM)2 Duo CPU 3.00GHz) and development environment (MATLAB R2014b).

Statistical analysis For motion planner comparative analysis, mean value and SD of the computed performance indices were calculated for each task on the different object positions and subject anthropometries. For the generalization tests, mean value and SD of the computed performance indices were also calculated for all the subjects and the number of repetitions of each task. A statistical analysis based on Wilcoxon paired-sample test was performed for the comparative analysis between the proposed motion planning system and the traditional motion planner based on inverse kinematics. The analysis was carried out on multiple comparisons with Bonferroni correction; hence, significance was achieved for $p - value < 0.05/n_c$, where n_c is the number of multiple comparisons.

3.2.4.3 Results and discussion

The results of the comparative analysis are reported in Fig. 3.33. In particular, mean value and standard deviation of the position error, orientation error and PhJL computed on the 238, 75 and 125 object positions (for task 1, 2 and 3 respectively) are reported.

One can observe that the DMP based control always exceeded the other two algorithms based on inverse kinematics in terms of success rate. The DMP based control always achieved 100% while the IK inverse Jacobian reached 71.4% and the IK swivel angle reached 84.7%. The differences are statistically significant with $p-value < 0.0083$ (for the DMP based control compared to IK inverse Jacobian $p-value = 0.0031$ and for DMP based control compared to IK swivel angle $p-value = 0.0045$).

On the other hand, as expected, the DMP based control suffers from a position error higher than the one achieved with the other two algorithms (this difference is statistically significant with $p-value = 0.0012$ for the DMP based control compared to IK inverse Jacobian and $p-value = 0.0008$ for DMP based control compared to IK swivel angle), for all the subtasks except for subtask 2-2.

Indeed, about the position error of the subtask 2-2, the results achieved with the DMP based control are comparable to the one achieved with IK inverse Jacobian ($p-value = 0.09$), but are better than the one achieved with IK swivel angle ($p-value = 0.0033$).

Conversely, the orientation error achieved for each task with the DMP based control is comparable to the one achieved with IK with swivel angle ($p-value = 0.12$). The difference is statistically significant between the orientation error achieved by the DMP based control and the one achieved with IK inverse Jacobian, which is lower ($p-value = 0.0028$).

Moreover, the results clearly show that the DMP based control and IK with swivel angle ensure a more anthropomorphic configuration than IK inverse Jacobian, measured through *PhJL*. The differences are statistically significant, with $p-value = 0.0024$ for the comparison between DMP based control and IK inverse Jacobian and $p-value = 0.0019$ for the comparison between IK swivel angle and IK inverse Jacobian.

Finally, considerations about the computational burden of the three methods have been made; a mean cycle time of 0.4 ms, 7.2 ms, and 0.1 ms for the DMP based control, IK inverse Jacobian and IK with swivel angle, respectively, have been estimated. As expected, IK inverse Jacobian has a higher computational burden compared the other two methods, since it is an iterative method. Conversely, it is interesting to note that the proposed DMP based method, once trained, has a relatively low computational burden (comparable to the geometrical approach based on the swivel angle) since the DMP resolution is not computationally heavy.

The experimental results of the GCA are shown in Tab. 3.12. Mean value and standard deviation of position error, orientation error and PhJL are reported. They were computed

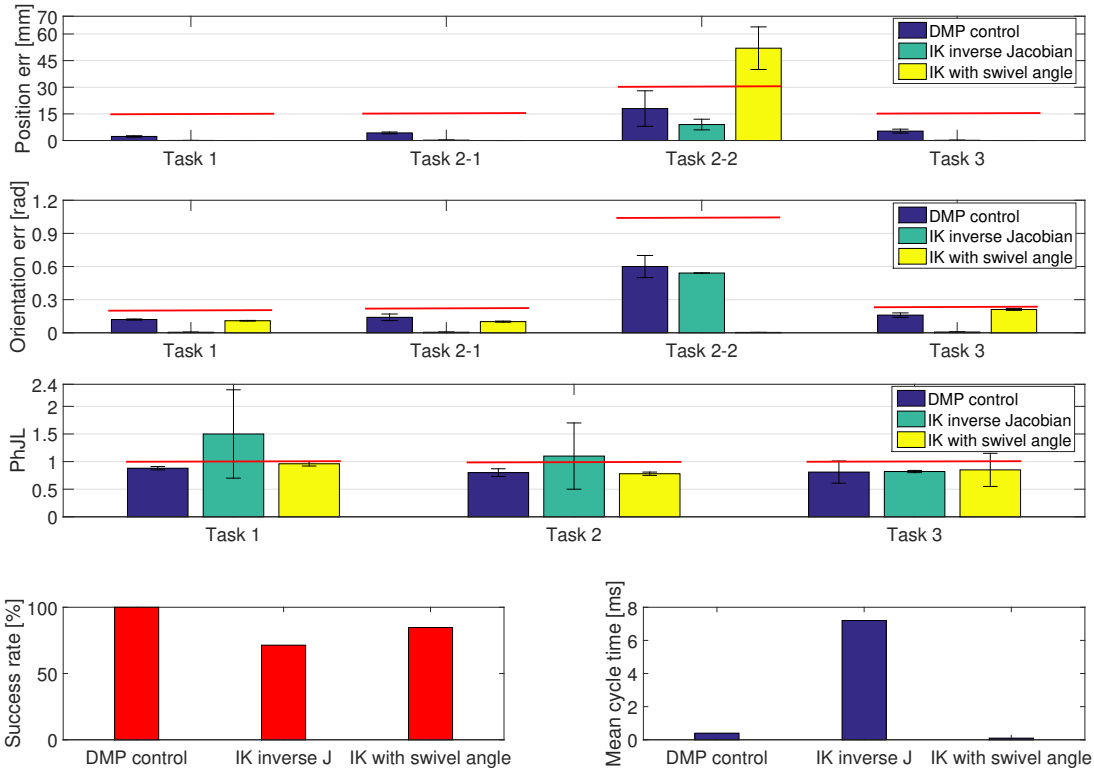

Fig. 3.33 Experimental results obtained for CA. The red lines denote the range within which the task is considered successfully accomplished.

Table 3.11 Experimental results obtained for GCA

		GCA–sim	GCA–real
Task 1	Position Err [mm]	2.7 ± 0.4	3.9 ± 0.5
	Orientation Err [rad]	0.14 ± 0.01	0.164 ± 0.008
	PhJL	0.51 ± 0.03	0.64 ± 0.04
Task 2-1	Position Err1 [mm]	3.2 ± 0.9	4.0 ± 3.1
	Orientation Err1 [rad]	0.10 ± 0.07	0.116 ± 0.05
Task 2-2	Position Err2 [mm]	19 ± 6	21 ± 5
	Orientation Err2 [rad]	0.57 ± 0.07	0.5 ± 0.1
Task 2	PhJL	0.56 ± 0.04	0.64 ± 0.05
Task 3	Position Err [mm]	7.3 ± 1.2	9.5 ± 1.9
	Orientation Err [rad]	0.157 ± 0.02	0.14 ± 0.02
	PhJL	0.6 ± 0.4	0.5 ± 0.36
	Success rate [%]	100	100

for GCA–sim on 238, 75 and 125 object positions (for task 1, 2 and 3, respectively) and 25 different subject anthropometries. Instead, for GCA–real they were calculated on the four subjects and 3 object positions for each task. It is interesting to note that performance achieved in the real setting are very close to the simulation results; moreover, the proposed motion planning based on DMP has a high generalization level with respect to the different object positions and subject anthropometries, since the success rate achieved for the 3 task is 100%.

The comparative analysis (Fig. 3.33) showed that the IK inverse Jacobian has better performance than the DMP based control in terms of position and orientation error, but it does not guarantee physiological configuration and always the success of the operation in the whole human-robot workspace. Conversely, the IK with swivel angle reached better results than DMP based control in terms of position and orientation error for tasks requiring the control of only one orientation parameter (e.g. tasks 1, 2-1 and 3). Instead, it increased in more complex tasks that required the control of more than one orientation parameter (task 2-2).

Nevertheless, it is worth pointing out that the position error obtained with the DMP based control (even though higher than the traditional approaches) is fully compatible with the considered application domain which does not require very high accuracy. In fact, it is shown in the literature that accuracy of human movements during the execution of ADLs is around 1-2 cm [78]. The achieved position error is moreover well balanced by the very

high success rate and the guarantee of an anthropomorphic configuration (which also entail system reliability and safety during the task fulfilment).

Furthermore, the high generalization level of the proposed approach ensures higher robustness to the environmental changes than the two other traditional methods, especially the one based on the computation of the swivel angle, which needs to be a priori specified. A geometrical approach for inverting kinematics (see Sect.3.2.4) has the clear advantage of a low computational burden, but it is not guaranteed that it can be easily applied on all the kinematic chains. Conversely, the proposed DMP based method offers the advantage of being applicable to any kinematic chain, thanks to the offline training, and has a good computational time (which is comparable with the IK swivel angle and significantly lower than the IK algorithm with inverse Jacobian).

3.2.5 Experimental validation 3

The 3^{rd} variation to the DMP equations, presented in 3.2.2.3 and named in the following Hybrid Joint/Cartesian DMPs, was experimentally validated on the robotic arm Kuka Light Weight Robot 4+. It learnt from a human demonstrator how to perform point-to-point reaching tasks in presence of obstacles. A comparative analysis between the proposed approach and the current method used in literature to program a robot by demonstration, i.e. based on the computation of Cartesian DMPs and IK [88] was performed. The two methods were compared in terms of four quantitative indices intended to assess i) the robot accuracy of the motion performing in the task space and ii) the level of anthropomorphism of the computed motion.

Furthermore, qualitative indices have been introduced to evaluate the user's feeling related to robot motion. In particular, questionnaires have been administered to ten users after seeing the robot moving; they were asked to rate the level of perceived safety and acceptability of the robot motion when the two methods were adopted.

Finally, the system ability to generalize with respect to different object positions and task duration has been assessed by means of the same indices, and robustness of the proposed system against perturbations (i.e. the presence of an obstacle along the path tracked by a couple joints of the robot kinematic chain) has been evaluated in terms of two further quantitative indices. They are i) the distance between the robot joint and the obstacle and ii) the success rate of the task execution.

3.2.5.1 Experimental setup

The proposed Hybrid Joint/Cartesian DMPs approach has been tested on an anthropomorphic robotic arm (i.e. the KUKA Light Weight Robot 4+) during point-to-point reaching tasks in presence of an obstacle (Fig. 3.42). The obstacle was a sphere of radius 0.05 m and was a priori positioned in the middle point of the path that was tracked by the robot fourth joint during the task performing.

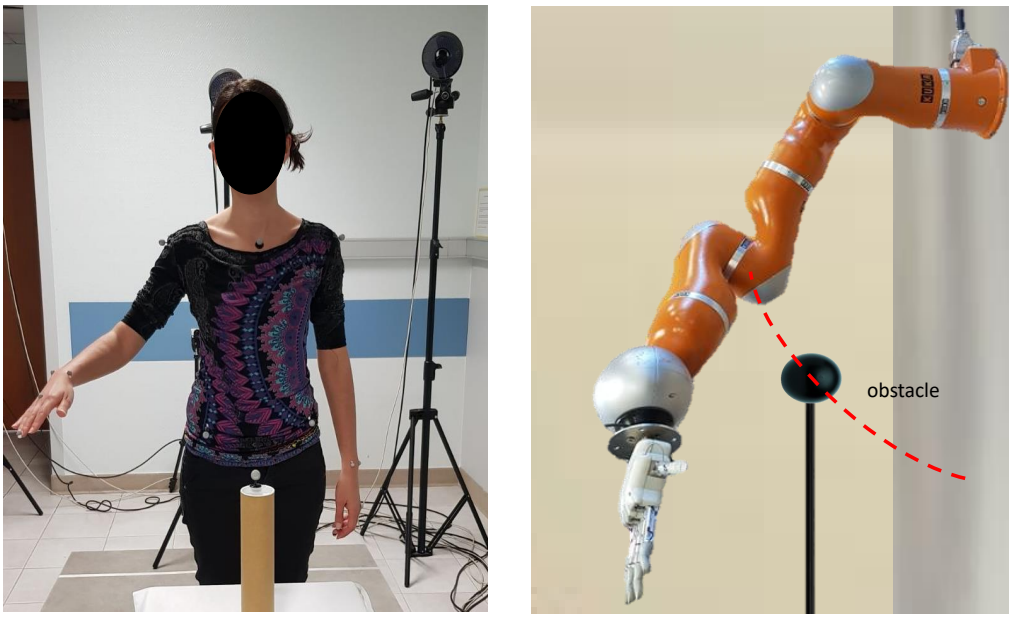

Fig. 3.34 Experimental setup.

The KUKA Light Weight Robot 4+ is a 7 DoFs anthropomorphic robotic arm with position and torque sensors at joints. The communication between the robot and a remote PC is guaranteed by the Fast Research Interface (FRI) Library, which runs, under the Robot Operating System (ROS), on a remote PC connected to the KUKA Robot Controller via a UDP communication protocol.

Human motion recording have been performed by means of the optoelectronic system BTS SMART-D Motion Capture System, [20]. It is a 8-camera motion analysis system with an acquisition rate of 60 Hz and an accuracy less than 0.1mm over a 2x2m area. The 3D Cartesian positions of retroreflective markers attached to the human subject upper-limb joints and a link model of the subject arms and trunk have been reconstructed with the BTS Smart Analyzer software package.

3.2.5.2 Experimental protocol

The experimental validation consisted of two phases, named in the following a) Offline database building and b) DMP computation.The 1^{st} phase aimed at recording a normative motion from a sample of healthy subjects and to subsequently extract from this normative motion the set of DMP parameters to be stored in the database.The 2^{nd} phase was intended to validate the proposed Hybrid Joint/Cartesian DMPs on the anthropomorphic robot and consisted of a comparative analysis between the proposed method and the one presented in [88] based on Cartesian DMPs and IK.

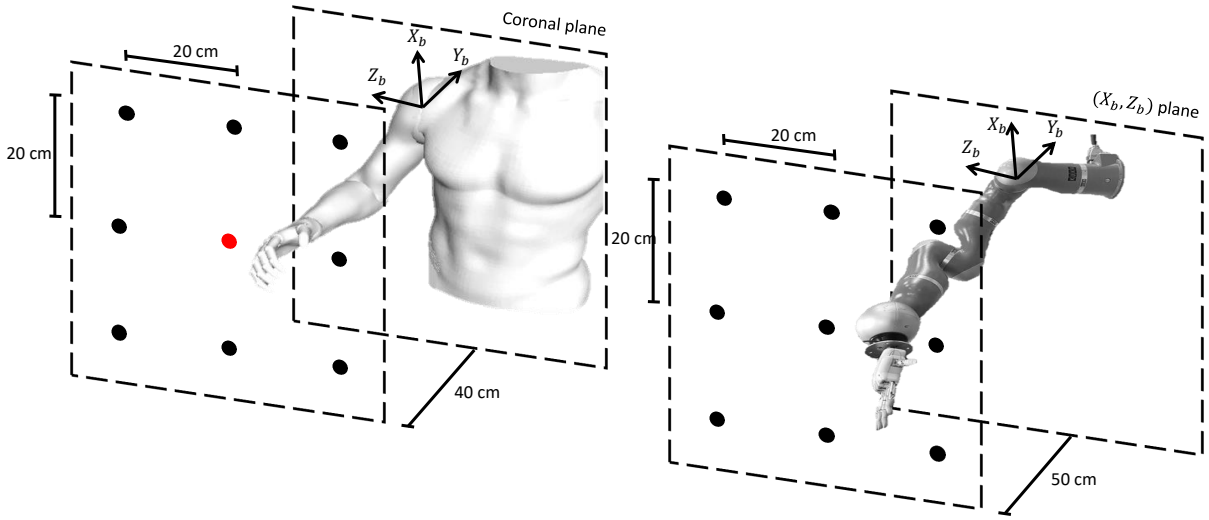

Fig. 3.35 A graphical illustration of the 9 points reached by the recruited subjects (on the left) and reached by the kuka robot (on the right). The red dot is the position reached by the subjects that was used to computed the DMPs parameters during the Generalization Capability assessment.

Offline database building Eight healthy subjects volunteered to participate in the experimental validation. They have been asked to perform 9 point-to-point reaching tasks with their right arm. The 9 points reached by the recruited subjects were placed in a plane parallel to the coronal one as shown in Fig. 3.35. Each of the 9 point-to-point reaching tasks was performed by the subjects 5 times. The recruited subjects were also asked to perform an activity of daily living, i.e. the pouring task, five times, for 9 different positions of the bottle and the glass (as shown in Fig. 3.36).

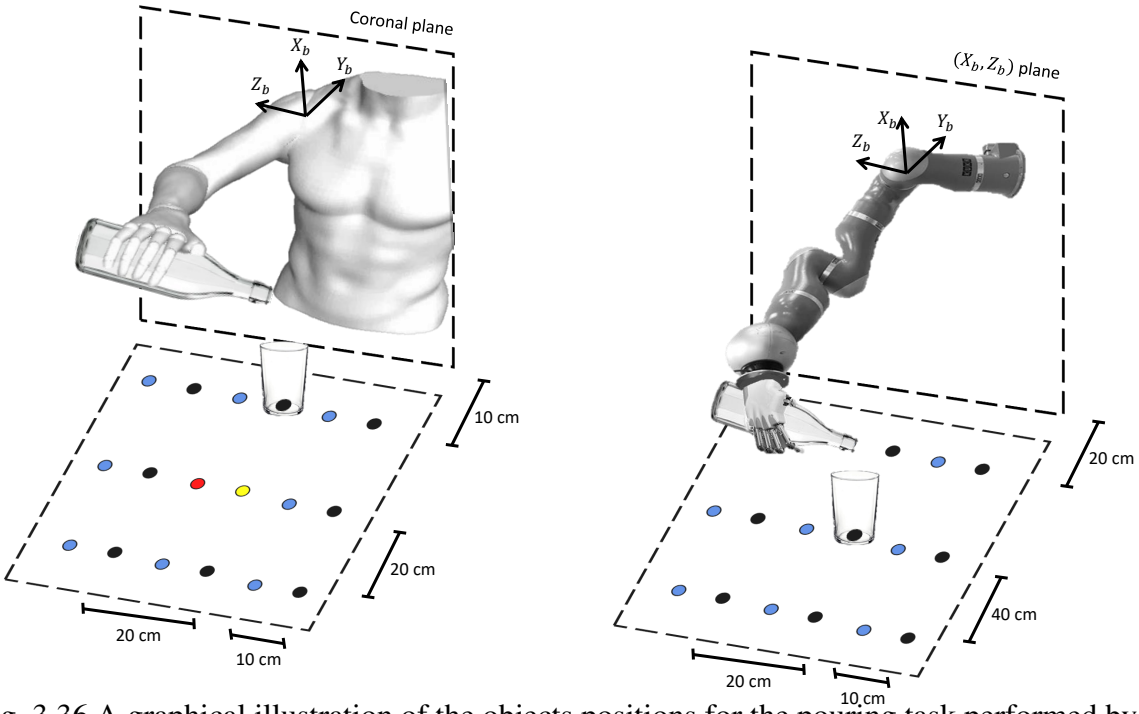

Fig. 3.36 A graphical illustration of the objects positions for the pouring task performed by the recruited subjects (on the left) and by the kuka robot (on the right). Blue and black dots illustrate the 9 positions of the bottle and the glass, respectively, during the task fulfilment. Red and yellow dots are the positions of the bottle and the glass, respectively, used to compute the DMPs parameters during the Generalization Capability assessment.

Human joint motions were recorded by means of the BTS optoelectronic system. 17 retroreflective markers were positioned on the subject trunk and upper limb anatomical landmarks by following the kinematic protocol proposed in [96]. The 3D Cartesian Coordinates of the markers positioned on the subjects have been reconstructed by using the BTS Smart Analyzer software.

Starting from these 3D Cartesian Coordinates of the markers acquired by the BTS, a kinematic model has been constructed for each subject by adopting the method introduced in [96]. The sensitivity of the method to inaccuracies in joint center estimation implies an error in the upper limb joint angles estimation less than 5 *deg* [96]. This error is fully compatible with the application envisaged in this work.

The so obtained center of the joints are adopted to build reference frames for each arm joint (i.e. shoulder, elbow and wrist) and to extract joint angles by adopting Eulerian sequence about X, Y and Z axes. In particular, the following seven upper-limb joint angles have been computed starting from marker 3D coordinates: abduction/adduction (sA/A), flexion/extension (sF/E) and internal/external rotation (sI/E) of the shoulder, elbow flex-

ion/extension (eF/E) and pronation/supination (wP/s), abduction/adduction (wA/A) and flexion/extension (wF/E) of the wrist.

Mean value of the extracted joint motion was computed on the 8 subjects and 5 trials for each of the 9 point-to-point reaching and 9 pouring tasks. The LWR was subsequently adopted on the average joint motion to compute a set of N_q DMP parameters per joint DoF and task to be stored in the database. The number of parameters N_q was dynamically retrieved by means of a recursive method intended to ensure a motion reconstruction error lower than a certain value, i.e. 5% of $\|\mathbf{q_f} - \mathbf{q_i}\|$ where $\mathbf{q_f}$ and $\mathbf{q_i}$ are the final and initial points of the joint trajectories, respectively (see [65] for more details).

Hence, a forward kinematics was computed on the average joint motion in order to obtain the Cartesian motion of the human wrist, i.e. X, Y and Z and roll, pitch and yaw (expressed in the [XB, YB, ZB] reference frame of Fig. 3.35), during the fulfilment of the 9 point-to-point reaching tasks and 9 pouring tasks. The forward kinematics was computed on an average kinematic chain, with a $0.3m$ arm and a $0.33m$ forearm lengths.

Finally, as for the joint motions, a LWR was adopted in order to compute a set of N_y DMP parameters per Cartesian DoF and task to be stored in the database. The number of parameters N_q was dynamically retrieved by means of the same recursive method used in [65].

DMP computation The second phase of the experimental session was aimed at i) performing the Comparative Analysis between the Hybrid Joint/Cartesian DMPs and the Cartesian DMPs and IK proposed in [88], ii) evaluating the Generalization Capability of the proposed system (i.e. the system ability to generalize with respect to different target positions and different task duration) and iii) assessing its Robustness Against Perturbation, i.e. the presence of an obstacle.

About the Comparative Analysis, the robot arm initial position is shown in Fig. 3.35 and in Fig. 3.36 for the reaching and pouring tasks, respectively. The robot arm was first operated to reach the 9 points shown in Fig. 3.35 and to perform the pouring task for the 9 different objects positions shown in Fig. 3.36 in an obstacle free condition. The robot joint motion during the fulfilment of the 9 reaching and 9 pouring tasks was planned by means of the a) Hybrid Joint/Cartesian DMPs and the b) Cartesian DMPs and IK proposed in [88], and executed on the robot throughout a joint space Inverse Dynamic control in order to perform the Comparative Analysis. In this case, the Cartesian and joint DMP parameters used to compute the DMPs were selected by means of the above mentioned Look-up Table method.

In order to evaluate the system Generalization Capability with respect to the different target positions, the Cartesian and joint parameters used to compute the DMPs were the one

extracted by the average trajectories performed to reach the middle point of Fig. 3.35 and to perform the pouring task for the objects position highlighted in Fig. 3.36 (i.e. red and yellow points). Moreover, in order to assess the Generalization Capability with respect to the task duration, the system was tested for 3 different duration of the 9 reaching and pouring tasks, i.e. 10 s, 15 s and 20 s.

For assessing robustness against perturbation, the robot was operated to reach the same 9 points illustrated in Fig. 3.35 and to perform the pouring task for the 9 different object positions illustrated in Fig. 3.36 in presence of obstacles. As an example, the obstacles were placed along the path of the 4^{th} and 7^{th} robot joints (i.e. the origin of the 4^{th} and 7^{th} link reference frame). The obstacle, i.e. a sphere of 0.05 m radius, was positioned in 6 a priori known positions for each task (i.e. 25%, 50% and 75% of the path tracked by the 4^{th} and 7^{th} robot joint (i.e. the end-effector). In order to fulfill the 9 reaching tasks and 9 pouring tasks, the robot motion was planned, in this case, only by means of the Hybrid Joint/Cartesian DMPs. As for the other phases, the robot was piloted by means of a joint space Inverse Dynamic control.

In order to evaluate if the proposed Hybrid Joint/Cartesian DMPs makes the robot move in a safe and accepted fashion, ten healthy subjects were asked to observe the robot motion while pouring water in a glass. The task was repeated twice, with an anthropomorphic and a non-anthropomorphic configuration. The subjects were then asked to fill in a questionnaire in order to rate the what extent the robot moved in a safe and effective manner.

Performance indices Four performance indices were computed based on the trajectories executed by the robot in order to perform the Comparative Analysis between the Hybrid Joint/Cartesian DMPs and the method based on Cartesian DMPs and IK and to asses the Generalization Capability of the proposed system. They are listed in the following: i) Position error, ii) Orientation error, iii) Convex hull, and iv) physiological joint limits (PhJL). They are meant to evaluate the accuracy of the movement execution in the task space and the distance between the robot joint motion and the recorded human joint motion (i.e. level of anthropomorphism).

Moreover, in addition to Position error, Orientation error and PhJL, other two indices have been computed in order to assess robustness against perturbation. They are: i) the joint distance from the obstacle ($Joint - Obstacle$) and ii) the Success Rate of the task execution.

Position Error and Orientation Error are defined as follows

$$Position\ Error = \frac{1}{2}\sqrt{(x-x_m)^2+(y-y_m)^2+(z-z_m)^2} \tag{3.76}$$

$$Orientation\ Error = \frac{1}{2}\sqrt{(\phi-\phi_m)^2+(\theta-\theta_m)^2+(\psi-\psi_m)^2} \tag{3.77}$$

x, y, z, ϕ, θ and ψ are the coordinates of the Cartesian DMP computed for each task and x_m, y_m, z_m, ϕ_m, θ_m and ψ_m are the coordinates of the related Cartesian motion obtained by calculating the FK on the joint motion computed by means of the two methods, i.e. Hybrid Joint/Cartesian DMPs and Cartesian DMPs and IK. The above mentioned orientation coordinates are expressed according the Euler ZYZ angles.

The distance from the recorded human joint motion is evaluated by means of the Convex Hull and the PhJL. The Convex Hull metric is widely used in literature to measure the "distance" between the robot and the human's kinematic chain, i.e. to assess the robot functional anthropomorphism. It is defined, on a set of points (Q), the smallest convex polygon P for which each point in Q is either on the boundary of P or in its interior. In this study we computed the Convex Hull on the set of points illustrated in Fig 3.37, namely the human and robot shoulder (A and B), the human and robot elbow (C and D), and the common end-effector (E), by using a well known quick hull algorithm for convex hulls [9].

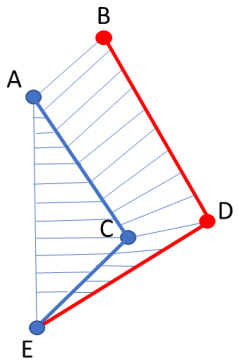

Fig. 3.37 Convex hull created by the human arm (blue line) and the robot arm (red line).

The PhJL is the distance from the physiological joint limits and is expressed as

$$PhJL = \left\| \frac{2(q_i - \bar{q}_i)}{q_{iM} - q_{im}} \right\| \tag{3.78}$$

where q_i is the actual position of the i-th joint, q_{iM} and q_{im} are the upper and lower physiological limit of the i-th joint and $\bar{q}_i$ is the mean value between q_{iM} and q_{im}. An acceptable value of $PhJL$ for the considered tasks ranges in between 0 and 1. The PhJL joint limits of the human subject, expressed in radiants, are: limit1 = [-0.5236, 1.92]; limit2 = [-0.1745, 1.57]; limit3 = [0.5236, 1.92]; limit4 = [-0.1745, -1.92]; limit5 = [1.57, 3.14]; limit6 = [-1.57, 1.57]; limit7 = [-0.6981, 0.1745].

About the Robustness Against Perturbation, the minimum distance of the 4^th and 7^th robot joint from the obstacle (i.e. $Joint - Obstacle$) during the task is expressed as $Joint - Obstacle = min\left(\|\mathbf{Y_{ji}} - \mathbf{o}\|\right)$ where $\mathbf{Y_{ji}}$ is the Cartesian position of the 4^th or 7^th robot joint and $\mathbf{o}$ is the Cartesian position of the obstacle.
The success rate of the task execution is evaluated as

$$Success\ rate = \frac{N_{succ}}{N_{tot}} * 100 \tag{3.79}$$

where N_{succ} is the number of trials successfully accomplished and N_{tot} is the number of all the performed trials. A task is considered as successfully accomplished if all the following conditions are satisfied:

- $Joint - Obstacle > 0.1 \quad m$
- $Position\ Err < 0.005 \quad m$
- $Orientation\ Err < 0.02 \quad rad$

Finally, qualitative indices were extracted in order to assess whether the users prefer an anthropomorphic (generated by the proposed Hybrid Joint/Cartesian DMPs motion planner) or a non-anthropomorphic motion of the robot (generated by the traditional approach). The questionnaire was administered to ten people after observing the robot motion. Users were asked to rate to what extent they agreed with the following statements (Strongly agree; Agree; Neither agree nor disagree; Disagree; Strongly disagree):

- The robot motion is unsafe
- The robot motion is smooth
- I am afraid of the robot while moving in this way
- I would feel comfortable to interact with the robot while moving in this way
- I would feel nervous while collaborating with a robot that moves like this.
- I would prefer the robot to move in this way

To get a quantitative measure of the evaluator rating, their answers were mapped into numerical values. In particular, the Likert scale was adopted in order to retrieve quantitative values from their responses: Strongly agree = 5, Agree= 4, Neither agree nor disagree=3, Disagree = 2, and Strongly disagree = 1. Furthermore, the ten volunteers were asked to fill in the part of the Godspeed Questionnaire Series (GQS) related to anthropomorphism

and perceived safety. GQS is one of the most frequently used questionnaire in the field of Human-Robot Interaction [13].

Statistical analysis Mean value and Standard Deviation (SD) of the all previously described indices have been computed on the 9 point-to-point reaching tasks and 9 pouring tasks, both for the Hybrid Joint/Cartesian DMPs and Cartesian DMPs and IK. Since the data were not normally distributed, a statistical analysis based on Wilcoxon paired-sample test has been performed ($p-value < 0.05$) in order to carry out the comparative analysis between the a) Hybrid Joint/Cartesian DMPs and the b) Cartesian DMPs and IK proposed in [88].

3.2.5.3 Results and discussions

The results of the comparative analysis between the Hybrid Joint/Cartesian DMPs and the Cartesian DMPs + IK are reported in Table. 3.12. Mean value and SD of the *Position Error*, *Orientation Error*, *Convex Hull* and *PhJL* have been calculated on the 9 reaching tasks and 9 pouring tasks for both the Hybrid Joint/Cartesian DMPs and the Cartesian DMPs + IK. As shown in Table. 3.12, the performance of the two approaches in terms of Position and Orientation error are comparable both for the reaching and pouring tasks since the $p-value$ obtained from the performed statistical analysis is > 0.05. This result is achieved thanks to the multi-priority coupling equation, used to combine the Joint and Cartesian DMPs, that ensures the convergence of the *Position Error* and *Orientation Error* to zero with high priority. Conversely, it is worth noticing that the Hybrid Joint/Cartesian DMPs outperforms the Cartesian DMPs + IK in terms of *Convex Hull* and *PhJL*. These differences are statistically significant with a $p-value < 0.05$. The results obtained about the *Convex Hull*, demonstrate that the proposed approach gives the robot the capacity of moving in a way similar to the human demonstrator also in the joint space.

In Fig. 3.41 the users' impressions and emotional states when the robot motion is planned by means of the Hybrid Joint/Cartesian DMPs and the Cartesian DMPs + IK are reported. From the users ratings it is evident that the robot motion is regarded as more natural, human-like, and elegant when the Hybrid Joint/Cartesian DMPs is adopted (the differences are statistically significant $p-value < 0.05$). Moreover, users were more relaxed and calm ($p-value < 0.05$). Finally, from the questionnaire (Table 4.1) it emerges that the users consider the anthropomorphic motion safer and more pleasant than a non anthropomorphic one and think that they can feel more comfortable and less nervous to interact with a robot that moves in a human-like fashion.

In Fig. 3.38 the motion of robot 5^{th} joint during task 1 is reported for i) the Hybrid Joint/Cartesian DMPs, ii) the Cartesian DMPs + IK and iii) the recorded motion. As

expected, the joint angles obtained with the Hybrid Joint/Cartesian DMPs are not exactly the same as the recorded one. This is due to the different link lengths of the robot and the human demonstrator. Nevertheless, it is worth observing that the joint motion obtained by means of the proposed method, i.e. Hybrid Joint/Cartesian DMPs, is more similar to the recorded one, with respect to the one obtained through the Cartesian DMPs + IK. Furthermore, the joint values obtained with the proposed approach always respect the PhJL, while the one obtained with the Cartesian DMP + IK sometimes overcome the PhJL, as it happens for the 5^th joint in Fig.6. Therefore, the Hybrid Joint/Cartesian DMPs guarantee a higher level of anthropomorphism of the motion with respect to the traditional methods. For the sake of brevity, only the behaviour of the 5^th joint during task 1 is shown, but similar results have been achieved for the other joints and tasks.

In Table 3.13, the mean value and SD of the Position Error, Orientation Error, $Convex\,Hull$ and $PhJL$ computed during the performing of the 9 reaching tasks and the 9 pouring tasks, for 3 different duration i.e. 10 s, 15 s and 20 s, are reported in order to show the system generalization capability. For this experimental session, the Cartesian and joint parameters used to compute the DMPs were the one extracted by the average trajectories performed to reach the middle point of Fig. 3.35 and to perform the pouring task for the objects position highlighted in Fig. 3.36 (i.e red and yellow points).

In Table 3.14, the mean value and SD of the Position Error, Orientation Error, $PhJL$ and $Joint-Obstacle$ computed during the 9 reaching tasks and the 9 pouring tasks in presence of obstacles are shown. The obstacles were placed in 6 different positions for each of the 18 tasks (i.e. 25%, 50% and 75% of the path tracked by the robot 4^th and 7^th joints). The success rate of the task execution is 100%, as confirmed by the $Joint-Obstacle$ value that is always greater than the minimum value to avoid collision between obstacle and link (i.e. 0.1 m) by preserving, anyway, an acceptable level of the Cartesian accuracy ($Position\ error < 0.005\ m$) and ($Orientation\ error < 0.02\ m$). It is worth reminding that the $Position\ error$ and $Orientation\ error$ are metrics introduced to evaluate how well the robot redundancy is exploited in order to make the robot kinematic chain avoid the obstacle. They are not affected when the end-effector Cartesian trajectory is changed for collision avoidance. Additionally, in Fig. 3.39 a graphical illustration of how the obstacle is avoided by the 4^{th} robot joint during the fulfilment of task 1 is reported. One can notice that, even when the system tries to avoid an obstacle placed on path of the robot 4^{th} joint, the operational space tracking is achieved with high accuracy.

Table 3.12 Experimental results obtained for comparative analysis

		Hybrid Joint/Cart DMPs		
Task	Position Error [mm]	Orientation Error [rad]	Convex Hull [m^3]	PhJL
Reaching	0.3 ± 0.1	0.016 ± 0.001	0.0077 ± 0.0006	0.6 ± 0.1
Pouring	0.5 ± 0.2	0.017 ± 0.002	0.0081 ± 0.0005	0.7 ± 0.1
Mean and SD	0.4 ± 0.1	0.017 ± 0.002	0.0079 ± 0.0006	0.7 ± 0.1
		Cartesian DMPs + IK		
Task	Position Error [mm]	Orientation Error [rad]	Convex Hull [m^3]	PhJL
Reaching	0.3 ± 0.1	0.016 ± 0.001	0.0089 ± 0.0004	1.0 ± 0.2
Pouring	0.5 ± 0.2	0.017 ± 0.002	0.0092 ± 0.0006	1.2 ± 0.2
Mean and SD	0.4 ± 0.1	0.017 ± 0.002	0.0091 ± 0.0006	1.1 ± 0.2
p-value	0.92	0.94	0.02	0.03

Table 3.13 Experimental results obtained for generalization capability

	Hybrid Joint/Cartesian DMPs			
Task	Position Error [mm]	Orientation Error [rad]	Convex Hull [m^3]	PhJL
Reaching	0.4 ± 0.2	0.015 ± 0.001	0.0082 ± 0.0007	0.6 ± 0.1
Pouring	0.6 ± 0.1	0.016 ± 0.002	0.0084 ± 0.0007	0.5 ± 0.3
Mean and SD	0.5 ± 0.2	0.015 ± 0.002	0.0083 ± 0.0007	0.6 ± 0.3

3.2.6 Experimental validation 4

The approach proposed in Sect.3.2.2.4 was tested on the Tiago robot during the fulfilment of 1 Activity of Daily living (ADL), i.e. the pouring task and the obtained results were compared to the one achieved by using the original formulation of the DMPs [49] [123]. The comparative analysis were performed by means of a quantitative index aimed at evaluating the success rate of the task execution.

3.2.6.1 Experimental setup

The proposed DMP-based motion planning was tested on the Tiago robot developed by PAL Robotics S.L. The main robot components used to carried out the experimental validation are showed in Fig. 3.42. They are: i) the RGB-D camera, ii) the lifting torso, iii) the 7 Dof arm and iv) Pal gripper. The RGB-D camera, i.e. the Astra S manufactured by Orbbec, is embedded in the TIAGo's head and is a short-range version of the Orbbec Astra pro camera. It has a range of $[0.4\ m; 2\ m]$. TIAGo's torso is the structure that supports the robot's arm and

Table 3.14 Experimental results obtained for robustness against perturbation

	Hybrid Joint/Cartesian DMPs			
Task	Position Error [mm]	Orientation Error [rad]	PhJL	$Joint-Obstacle[mm]$
Reaching	0.3 ± 0.2	0.018 ± 0.001	0.7 ± 0.1	16 ± 3
Pouring	0.6 ± 0.1	0.019 ± 0.002	0.8 ± 0.1	13 ± 2
Mean and SD	0.3 ± 0.2	0.019 ± 0.002	0.8 ± 0.1	15 ± 3
Success rate [%]	100			

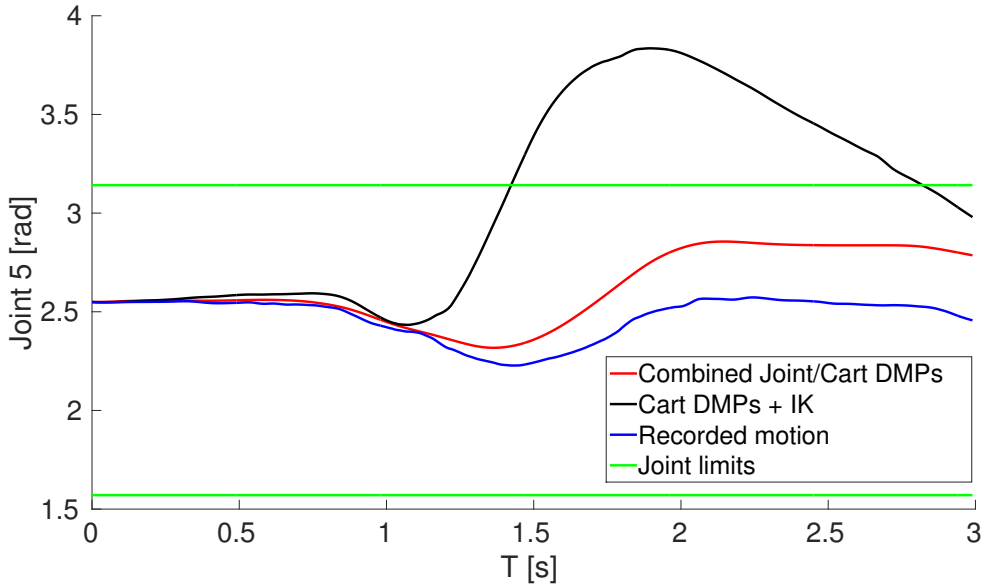

Fig. 3.38 Joint motion during the fulfilment of task 1

head, and is equipped with an internal lifter mechanism which allows the user to change the height of the robot. The lifter is able to move at 50 mm/s and has a RoM of 350 mm. The minimum and maximum height of the robot is 1.10 m and 1.45 m, respectively. TIAGo's arm is a 7 DoF anthropomorphic arm, composed of four M90 modules and one 3 DoF wrist. The Pal gripper contains two motors, each controlling one of the fingers. Each finger has a linear range of 4 cm.

3.2.6.2 Experimental protocol

The experimental validation consisted of two phases, named in the following a) Offline database building and b) DMP computation. The 1^{st} phase was aimed to record the motion from a demonstrator during the execution of an ADL, i.e. the pouring task, and to subsequently extract from this motion the set of DMP parameters to be stored in the database. The

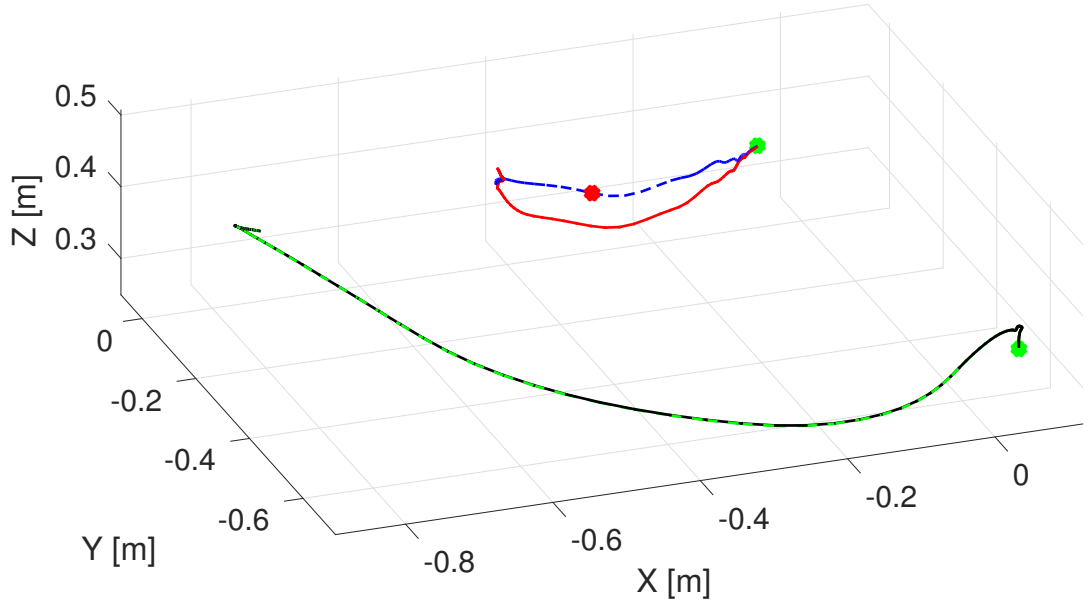

Fig. 3.39 Graphical illustration of the path tracked by the 4^{th} robot joint with and without the presence of an obstacle (red and blue lines, respectively). The path tracked by the 7^{th} robot joint with and without the presence of an obstacle are also shown in black and green lines. The red and green dots are the obstacle and the target position, respectively.

set of DMP parameters were extracted both by means of the proposed approach, grounded on Lie theory and Dynamic Parameterization (i.e. DMP/Lie theory + DP) and the original formulation proposed in [123] without dynamic parameterization (i.e. DMP/Lie theory without DP). The 2^{nd} phase was intended to compute DMPs from database built by means of the two approaches and to subsequently execute the computed DMPs on the robotic platform.

Offline database building In the 1^{st} phase of the experimental validation a human subject was asked to teach the robot how to perform an ADL, namely the pouring task, by means of a hands-on approach. In other words, the subject was required to passively move the robot arm

Table 3.15 Questionnaire

Question	Hybrid Joint/Cartesian DMPs	Cartesian DMPs + IK
The robot motion is unsafe	1.5 ± 0.6	2.8 ± 0.9
The robot motion is smooth	3.6 ± 0.9	2 ± 1
I am afraid of the robot while moving in this way	1.5 ± 0.8	3 ± 1
I would feel comfortable to interact with the robot while moving in this way	4 ± 0.9	1.9 ± 0.8
I would feel nervous while collaborating with a robot that moves like this	1.7 ± 0.7	2 ± 1
I would prefer the robot to move in this way	4.5 ± 0.7	1.8 ± 0.9

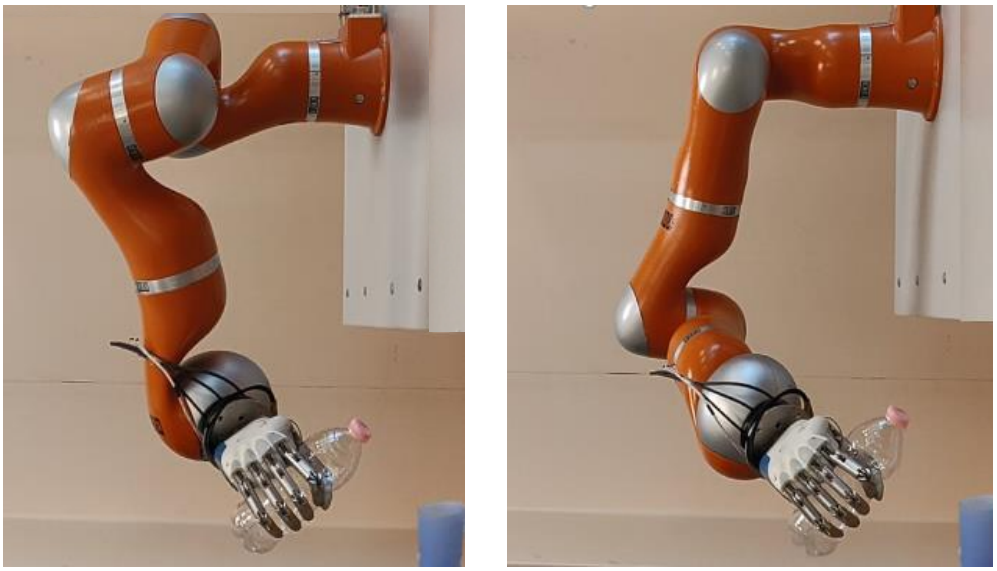

Fig. 3.40 A graphical illustration of the robot joint configuration while performing the pouring task when the traditional approach (left) and the hybrid Joint/Cartesian DMP (right) is adopted.

in order to accomplish the task. During the task execution, the robot was piloted throughout a gravity compensation control and the sensors embedded in the robot, i.e. the encoders, were used to record the joints motion. The task was performed for nine different positions of the objects, i.e. the bottle and the glass. These positions are reported in Fig. 3.43.

Subsequently, Cartesian trajectories were computed by means of the robot Forward Kinematics (FK), by adopting the Unit quaternion representation for the orientation. Finally, a set of DMP parameters were computed for each objects position, by using the proposed DMP/Lie theory + DP and the original DMP/Lie theory without DP.

DMP computation The 2^{nd} phase of the experimental validation was aimed at computing DMPs by using parameters extracted throughout the two approaches and to subsequently execute the computed DMPs on the robotic platform. The robot was operated to perform the pouring task for the 9 different objects positions shown in Fig. 3.43.

Performance indices The success rate of the task execution was evaluated as

$$Success\ rate = \frac{N_{succ}}{N_{tot}} * 100 \tag{3.80}$$

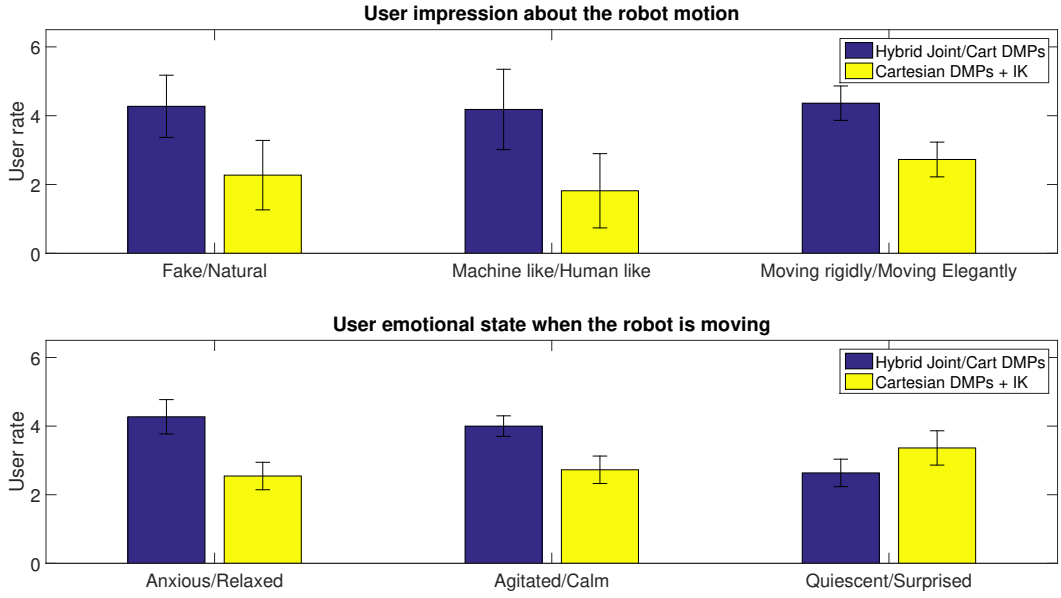

Fig. 3.41 Users feelings related to the robot motion

where N_{succ} is the number of trials successfully accomplished and N_{tot} is the number of all the performed trials.

3.2.6.3 Results and discussion

A success rate of 100% was achieved by the proposed DMP/Lie theory + DP; conversely a success rate of 66.66% was achieved when the original DMP/Lie theory without DP was adopted. Hence, the obtained results demonstrated the effectiveness of the proposed approach, grounded on Lie theory and Dynamic Parameterization, in solving singularity issues.

Fig. 3.42 Experimental setup.

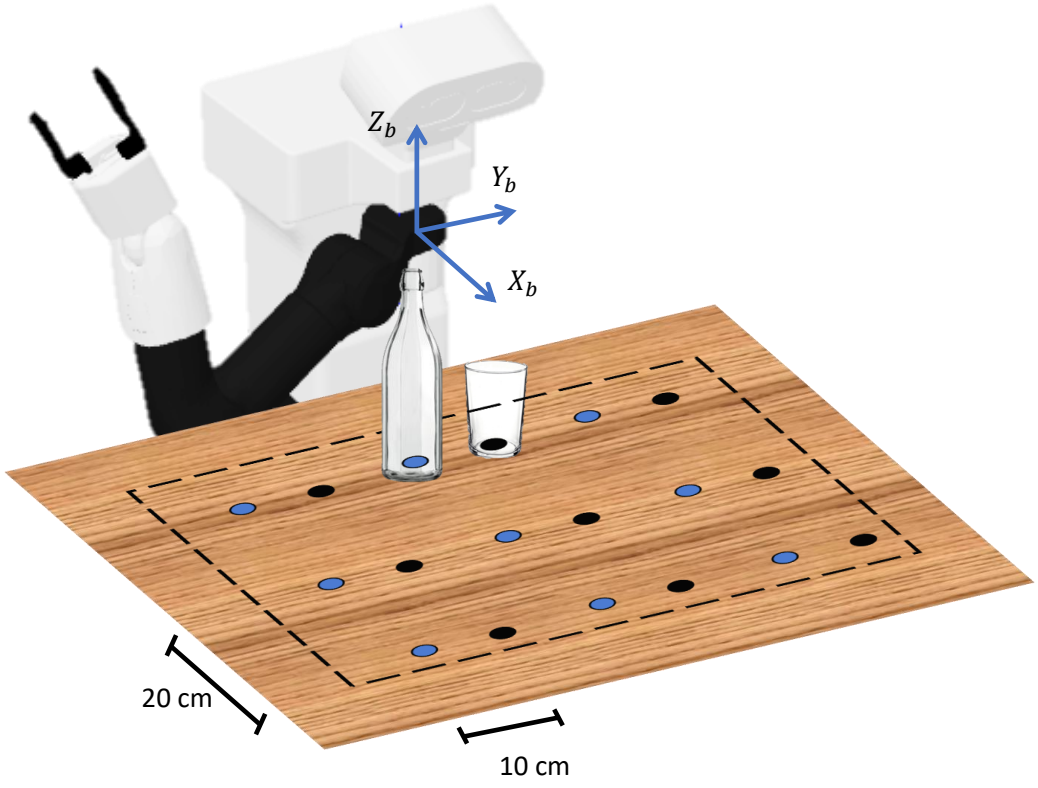

Fig. 3.43 A graphical illustration of the objects positions for the pouring task during the offline database building

Chapter 4

Sensory feedback to improve postural control during robot-aided rehabilitation

4.1 Introduction

The adoption of robotic technologies in rehabilitation is widely increased in the recent years, since they have the ability to deliver highly intensive, repeatable and accurate motion therapy and contemporary to measure the clinical outcome [7, 82]. Various approaches for robot-aided rehabilitation have been presented in the literature to allow varying the level of assistance based on patient state and his/her performance. However, repetitive and intensive exercises during robot-aided rehabilitation treatments may expose patients to inappropriate and unsafe spine postures that could cause neck and back pain as well as some other negative effects, both physically and mentally. Improper posture conditions have in fact a long-term negative influence on internal functioning of the body like breathing, blood flow and digestion and also result in higher stress levels [99].

Patients who perform exercises under the supervision of a physiotherapist assume less dangerous configurations and experience less pain during the treatment compared to the unsupervised ones [31]. Although there is a great evidence supporting the benefits of patient supervision during the treatment, an objective posture evaluation and a constant monitoring of the patient behavior is difficult to achieve since physiotherapists are usually required to control multiple aspects of a rehabilitation session (e.g. correctness of motion, patient involvement, feeling and progresses).

Several systems have been proposed in literature to objectively evaluate the patient's behaviour during a rehabilitation session and provide them with a feedback related to the correctness of the exercise. Sensory feedback has an important role in rehabilitation; it

promotes a higher level of user participation in the task accomplishment than traditional therapy, thanks to the stimuli the user is provided with. In fact, the feedback on the results and/or performance achieved during the robotic training simplifies the execution of the target movement and promotes subject involvement in the rehabilitation exercise [125].
Patient body motion can be monitored by means of motion capture systems, such as opto-electronic systems, cameras [19], or wearable sensors such as magneto-inertial and electromyographic sensors [64], or smart textile [104]. They are valuable solutions to provide a quantitative measure of the patient posture during a rehabilitation treatment as well as to assess the correctness of the exercise execution, differently from the simple qualitative visual observation used in clinical practice by therapists.
Once an incorrect position is detected or the exercise is assessed as improperly performed during the rehabilitation treatment, the patient can be provided with a feedback in order to stimulate a better posture control and improve the exercise performance.
In [6], bend sensors are adopted to detect the flexion/extension angle of the knee during a rehabilitation treatment. The acquired information is used to give a visual notification of the bend progression as the patient performs knee extensions. In [61], a system providing the user with continuous visual feedback and guidance to improve quality of motion performance during the rehabilitation treatment is proposed. Vision is assessed to be the most important sensory modality during the interaction with the environment. For perceiving information with high resolution, vision dominates other senses [26]. However, visual feedback uses an important sensory channel that is essential for a successful accomplishment of the task. Hence, when the patient is focused on a complex task, visual feedback may be perceived as cumbersome or confusing since visual perceptual channel becomes overloaded[114].
To overcome this drawback, auditory feedback was introduced in the rehabilitation treatment in order to convey important information to the patient related to the performed task. In [89] and [122], it was demonstrated that auditory feedback is a valuable mean to provide information about spine posture of post-stroke patients during the execution of reaching tasks. However, there could be a delay between the time when the incorrect spine posture is detected and the time when the warning feedback is transmitted to the patients by means of words.
Haptic feedback could be a valid solution to face this issue. Haptic refers to the sense of touch, and haptic interfaces are meant to provide force or tactile feedback by applying pressure, vibrations, forces. Although a great number of haptic feedback devices could be employed during the rehabilitation session to correct the patient's posture, there are some drawbacks that cannot be neglected. For instance, electrotactile systems can cause pain on

the skin and fatigue [54]. Force feedback systems can be cumbersome and have limited spatial resolution on the patient skin [29].
Vibrotactile feedback (VtF) systems can be considered to be safe and have an acceptable spatial resolution [67] in comparison to the other tactile solutions. In [51], VtF was used to train post stroke patients suffering from hemiplegia to perform lower-limb rehabilitative tasks. In [103], VtF was delivered to the palm and the fingers of post stroke patients while training to hold and manipulate objects. In [39], VtF was proposed to teach post stroke patients how to perform Activities of Daily living (ADLs).
Despite the wide use of VtF in many fields, this kind of feedback seems not to be suitable for applications that require long term usages [34]. Indeed, it is well known in the literature that an extended vibrotactile stimulation of the fast adapting sensory receptors on the user skin induces sensory adaptation effects in the patient. However, this does not apply to rehabilitation sessions that may expose patients only to short and infrequent stimuli.

Progress beyond the state of art From an in-depth analysis of the literature emerged that VtF feedback can enhance motor learning and performance and is preferred by users over visual or auditory feedback [2] [59] [117]. However, there is poor attention to the type of feedback preferred by the users, in terms of acceptability and comfort, for correcting spine posture while performing activities in sitting positions [131]. Moreover, to the best of our knowledge, there are no previous studies in literature that investigate which type of feedback could be effectively and efficiently employed during robot-aided rehabilitation treatments to improve patient spine postures.
The literature confirms that both VF and VtF could be suitable tools to correct patient postures in robot-aided rehabilitation treatments. Therefore, this work aims at in-depth investigating the two feedback modalities in experimental conditions by comparing their i) effectiveness to improve patients posture in robot-aided rehabilitation treatments, ii) acceptability and iii) comfort.
This work presents an extended version of the robotic platform for upper limb rehabilitation already presented in [107]. In particular, visual and vibrotactile feedback modules are added to provide information about incorrect neck and trunk posture.

Ten healthy subjects were asked to perform 3D reaching tasks with the aid of the robotic platform composed of i) an anthropomorphic robotic arm attached to the subject's wrist and used to help subjects perform 3D reaching tasks, ii) a motorized arm weight support, which provides a support level variable on the basis of muscular fatigue, iii) a virtual reality environment, which shows to the subjects the activity to be performed and the motion of their avatar, iv) a posture assessment module, and v) a visual and a vibrotactile feedback module

for posture improvement. Quantitative indicators, such as reaction time and trunk and neck angles, are extracted and a questionnaire was submitted to the subjects to understand the utility of the feedback and subject preference between VF and VtF.

The robotic platform for upper limb rehabilitation

In this work, a variation of the robotic platform for upper limb rehabilitation proposed in [107] is adopted. The original platform was composed of three modules:

I. An anthropomorphic 7-DoFs (Degrees of Freedom) robotic arm, i.e. the Kuka Light Weight Robot 4+, connected to the user wrist by means of a purposely developed flange. The robotic arm is driven by means of a Cartesian impedance control with variable level of stiffness and task duration on the basis of biomechanical indicators related to patient performance (see [110] for more details).

II. A motorized arm-weight support for the patient impaired limb. It is composed of i) a brushless Maxon Motor (EC-max 40), ii) a planetary gearhead Maxon (GP 42-C 74:1), iii) a Maxon encoder (HEDL-5540), and iv) a Maxon EPOS2 50/5 control unit. The arm-weight support is controlled by means of a torque control with gravity compensation [109] and provides a variable support level of the patient limb on the basis of muscular fatigue. To assess user muscular fatigue, the Dimitrov Index [23] is computed on electromyographic (EMG) data acquired at 1 kHz with surface EMG electrodes (i.e. Delsys Trigno wireless sensors) positioned on the following muscles: upper trapezius, posterior deltoid, lateral deltoid, anterior deltoid, pectoralis major, biceps brachii and lateral triceps.

III. A virtual reality environment (VR), ad-hoc developed in Unity 3D, to show the patient the task to be performed.

In addition to these modules, the modules shown in Fig. 4.1 were developed for i) monitoring the patient posture and ii) conveying to the user warning stimuli when an incorrect position is detected, during the robot-aided rehabilitation treatment. In the following, some theoretical details about the modules of posture evaluation and stimulation feedback are given.

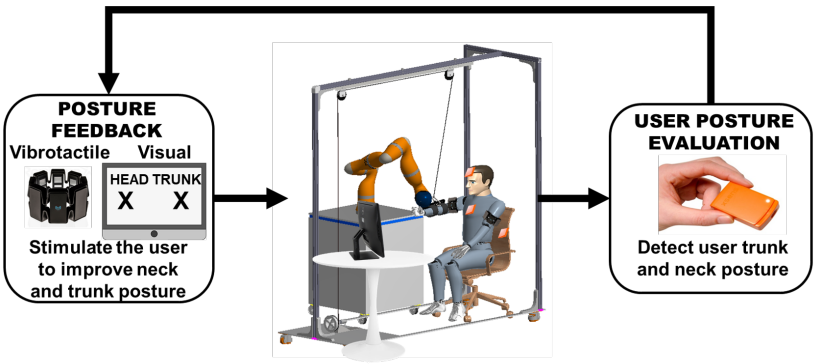

Fig. 4.1 The proposed platform: during the rehabilitation session performed with the aid of the robotic platform, the subject posture is monitored by means of M-IMU sensors. The obtained information are used to provide visual/vibrotactile feedback to the user if an incorrect posture is assumed.

Posture Evaluation

Three magneto-inertial measurement units (M-IMUs, XSens MTw) were used to assess subject posture during the rehabilitation treatment. As shown in Fig. 4.2, the M-IMU sensor S1 was positioned on the chair where the subjects were seated during the treatment; the sensor S2 was located on the subject's trunk and S3 was fixed on the subject's head. The sensor placed on the chair acted as reference for the sensors positioned on the subject's trunk and head, while the other two sensors were used to measure trunk and head flexion/extension (F/E) (Fig. 4.3), respectively.

Let R^G_{chair}, R^G_{trunk}, and R^G_{head} be the rotation matrices that express the orientation of the three M-IMUs with respect to the earth-fixed reference coordinate system G. In order to evaluate trunk F/E (α_{trunk}) and head F/E (β_{head}), the inverse problem of the RPY Euler angles was solved, starting from the rotation matrices R^{chair}_{trunk} and R^{trunk}_{head} calculated as follows

$$R^{chair}_{trunk} = (R^G_{chair})^{-1} R^G_{trunk} \tag{4.1}$$

$$R^{trunk}_{head} = (R^G_{trunk})^{-1} R^G_{head} \tag{4.2}$$

The M-IMUs are synchronised through an Awinda Station that checks the reception of wireless data from the M-IMUs at 100 Hz.

The Rapid Upper Limb Assessment (RULA) scale was adopted to establish appropriate thresholds for the trunk and head F/E angles. The RULA is a tool to assess the exposure to ergonomic risk factors during working tasks. Briefly, it allows to detect any ergonomically incorrect postures through a score from 1 to 7.In our case, in which the head and trunk F/E

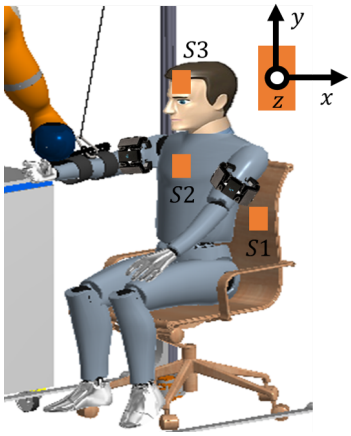

Fig. 4.2 Positioning of the M-IMU sensors on the subject body. Sensor S1 is positioned on the chair and acts as a reference, sensors S2 and S3 are positioned on the trunk and on the head of the subject, respectively.

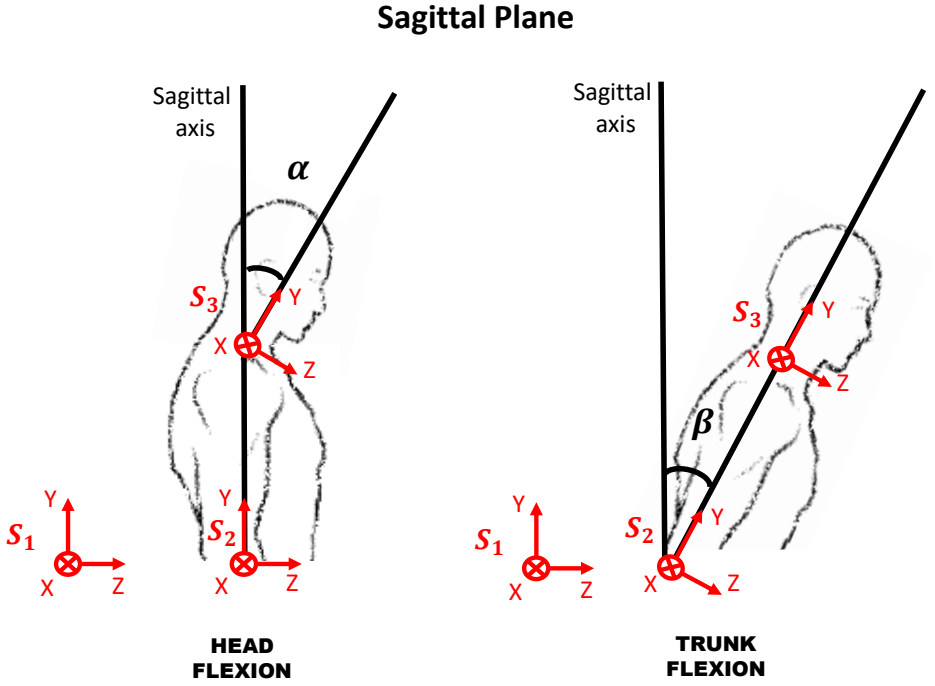

Fig. 4.3 Head and Trunk F/E angles considered to provide feedback

angles (α_{head} and β_{trunk}) are monitored, the upper and lower thresholds for both angles were conventionally set at 0.17 and 0 rad, respectively, i.e. the first thresholds that determines an increase in the score for the head and trunk districts in the RULA test.

4.2 Stimulation feedback for posture improvement

The VR module has been developed in order to allow the user to perform pick and place tasks in nine predefined positions in the 3D virtual reality space. The subject hand position, monitored by the sensors embedded in the robotic arm, was reconstructed in the Virtual Environment. The positions the subject hand has to reach were located at three different heights (i.e. 0 m, 0.19 m and 0.38 m) and at three different angles (i.e. -0.21 rad, 0 rad, $+0.21$ rad with respect to the starting position, i.e. where the subject avatar holds the object to be moved with 0 rad shoulder abduction angle and $\pi/2$ rad elbow flexion angle). In Fig. 4.4, the virtual environment seen by the subjects during the whole rehabilitation session by means of a video screen positioned in front of them is shown. The object to be picked and placed is a brown box initially located in the starting position (circled in red). Once picked, the object should be moved with point to point movements up to the 9 white balls (i.e. the target positions) passing through the starting position each time the target position is changed.

The user is provided with two types of feedback, namely the visual (VF) and the vibrotactile (VtF) feedback, to allow him/her to maintain a correct posture during the rehabilitation session. A posture is considered correct as long as the trunk and head angles are within the thresholds defined in Sect. 4.1.

1. The Visual feedback (VF) is integrated in the VR module and consists of showing to the user some warning visual stimuli when the user trunk and neck are considered to be in unsafe positions. In particular, two warning indicators are shown on the screen for each of the considered Degrees of Freedom, i.e. the trunk and head F/E. When the user is considered to be in a correct position, the indicators are black. Otherwise, when the user overcomes the preset Range of Motion (RoM) limits with the trunk and/or the neck, the indicator related to the specific DoF become red accordingly. The red indicator visualized by the subjects is continuous if $\alpha_{head} > 0.17$ rad or $\beta_{trunk} > 0.17$ rad, whereas it is blinking if $\alpha_{head} < 0$ rad or $\beta_{trunk} < 0$ rad.

2. The Vibrotactile feedback (VtF) is provided by two light-weighted vibrating actuators integrated in two Myo Armbands (Thalmic Labs, CDN) positioned on the arms of the subject. The vibration of the Myo Armband on the right/left arm of the subject is activated when the subject head/trunk exceeds the correct posture range defined in

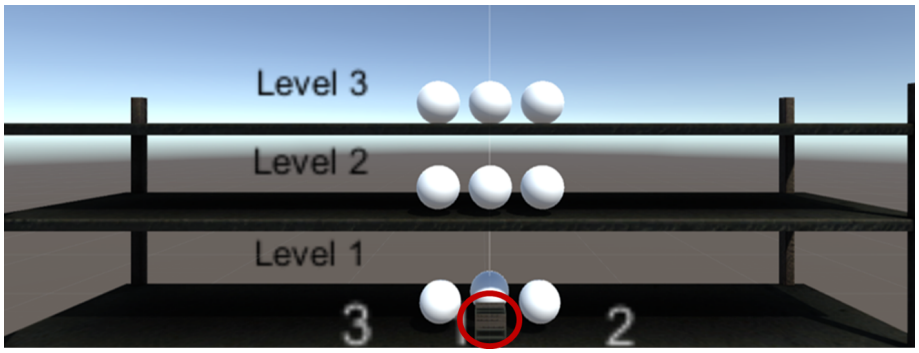

Fig. 4.4 The proposed VR module with nine target positions on three different levels and with angles of 0.21 rad with respect to the starting position (circled in red).

Sect. 4.1. The vibration supplied to the subjects is continuous if $\alpha_{head} > 0.17$ rad or $\beta_{trunk} > 0.17$ rad, whereas the vibration is intermittent if $\alpha_{head} < 0$ rad or $\beta_{trunk} < 0$ rad.

4.3 Experimental validation

4.3.1 Experimental setup and protocol

Ten healthy subjects were recruited for participating in the study (28.7 ± 4.7 years old) after providing written informed consent. They were asked to test the overall platform (Fig. 4.5) by performing two consecutive repetitions of the nine 3D reaching movements with the aid of the robotic platform and the feedback modules. The subjects seated on a chair in front of a screen projecting the VR and had the right wrist attached to the robot arm end-effector by means of the connection flange and the right arm supported by the arm-weight support. In order to determine the level of support to be provided by the robotic arm and the arm-weight support, an initial evaluation session was performed. During it, the subjects were asked to reach the 9 target positions with the robotic arm and the arm-weight support modules passive (i.e. the two modules did not provide assistance to the subjects) and without any feedback about posture. After the evaluation session, biomechanical indicators and muscular fatigue were computed. As expected, being the subjects healthy, it was confirmed that no assistance is needed and therefore, a low value of robot arm stiffness (i.e. $K = 0.1N/m$) and a level equal to 0 of arm gravity support were obtained. A null arm gravity support level is also due to the very short duration of the trial, which not generates muscular fatigue on healthy subjects. As demonstrated in [110], a long duration of the trial could generate muscular

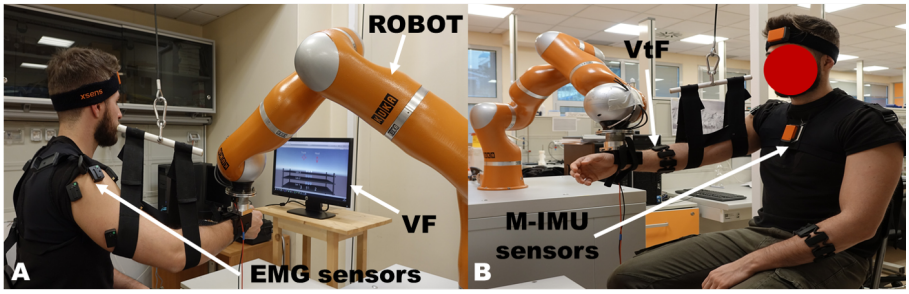

Fig. 4.5 A representative subject is performing the required tasks with the aid of the rehabilitative platform. He is receiving information about his posture by means of A) Visual Feedback, B) Vibrotactile Feedback.

fatigue, therefore requiring a level of arm gravity support different from 0 even on healthy subjects.

Robot end-effector position was represented in the VR by a hand avatar holding a virtual box; hence, the users were able to move the virtual box in the VR by using the robot end-effector as input device. The users were asked to move the virtual box to reach the nine virtual balls positioned at different distances and heights into a virtual shelf and to push them outside the shelf as shown in Fig.4.4.

The experimental session was divided into 3 phases, where the subjects were required to perform the tasks without feedback, with VtF and with VF. The enrolled subjects were randomized into two groups, called Group 1 and Group 2, composed of five people each. Both groups performed the 9 movements twice without getting any feedback about the correctness of their trunk and neck posture (No FB phase). Subsequently, Group 1 executed the 9 movements twice: with the visual feedback first (VF phase) and later with vibrotactile feedback (VtF phase) to improve their trunk and neck posture. Group 2 performed the same movements of Group 1 but with the feedback modalities inverted. A washout period among the different phases was considered for all the subjects.

Performance indices

Data from the sensors integrated in the whole platform were collected for each trial, phase and subject in order to extract quantitative indices to evaluate the task performance. They are:

- Normalized Incorrect Posture Time ($NIPT$), defined as

$$NIPT = \frac{IPT}{T_{tot}} \tag{4.3}$$

Table 4.1 The administered questionnaire to evaluate the platform.

Questions about Visual Feedback
I did not notice the Visual Feedback
The Visual Feedback was pleasant
The Visual Feedback motivated me to maintain a correct posture
The Visual Feedback was difficult to follow
I found useful the information provided by the Visual Feedback
Questions about Vibrotactile Feedback
I did not notice the Vibrotactile Feedback
The Vibrotactile Feedback was pleasant
The Vibrotactile Feedback motivated me to maintain a correct posture
The Vibrotactile Feedback was difficult to follow
I found useful the information provided by the Vibrotactile Feedback

where IPT is the time in which the users trunk and neck are outside the RoM limits defined in Sect. 4.1 and T_{tot} is the completion time of the trial.

- Mean Reaction Time (MRT). It represents the mean time, computed on the whole trial, needed by the subject to return in a correct posture after receiving the feedback, and is defined as

$$MRT = \frac{1}{N}\sum_{i=0}^{N} |T^i_{thr} - T^i_{peak}| \tag{4.4}$$

where N is the number of times the user exceeds the trunk and head RoM limits defined in Sect. 4.1, T^i_{thr} is the i_{th} time instant the user exceeds the limits and T^i_{peak} is the i_{th} time instant when the derivative over time of trunk and head F/E changes sign.

Moreover, one questionnaire was administered to the recruited subjects after testing the whole platform during the VF and VtF phase. The questionnaire was aimed to assess the users' preferences about the two types of feedback. The questionnaire is shown in Table 4.1. The users could express their satisfaction in a Likert scale from 1 to 5 where: Strongly agree = 5, Agree= 4, Neither agree nor disagree=3, Disagree = 2, and Strongly disagree = 1. Hence, a synthetic indicator of the user answers, i.e. the Mean Rate (MR), was computed, on average, for each statement and subject.

Statistical Analysis

Mean value and standard deviation (SD) of the aforementioned performance indices were computed on the ten subjects and each phase, i.e. No FB, VF and VtF phase. A statistical analysis based on a Wilcoxon paired-sample test was performed for the following three

comparisons: No feedback vs. VF, No feedback vs. VtF and VF vs. VtF. A Bonferroni correction was applied, so the p-value was modified and statistical significance was obtained for $p - value < 0.017$.

4.3.2 Results and discussion

Figures 4.6, 4.7 and 4.9 show the behaviour of trunk and head F/E angles reached by a representative subject belonging to Group 2 during the No feedback, VF and VtF phases. In figures 4.8 and 4.10 the angle behaviour of one representative subject belonging to Group 1 during VF and VtF phases are shown.

In Figs. 4.7, 4.8 and 4.9, 4.10 it can be noted that when the defined trunk and neck thresholds are exceeded, the user corrects his/her posture thanks to the Visual or Vibrotactile feedback. Conversely, in absence of feedback (Fig. 4.6), the user overcomes very often the trunk and neck RoM limits without clear attempts of corrections. By comparing the behaviour of the two groups it is evident that the type of feedback adopted for first does not influence the results. It is also confirmed by the results of the statistically analysis performed on the NIPT value computed for the two groups ($p - value > 0.05$).

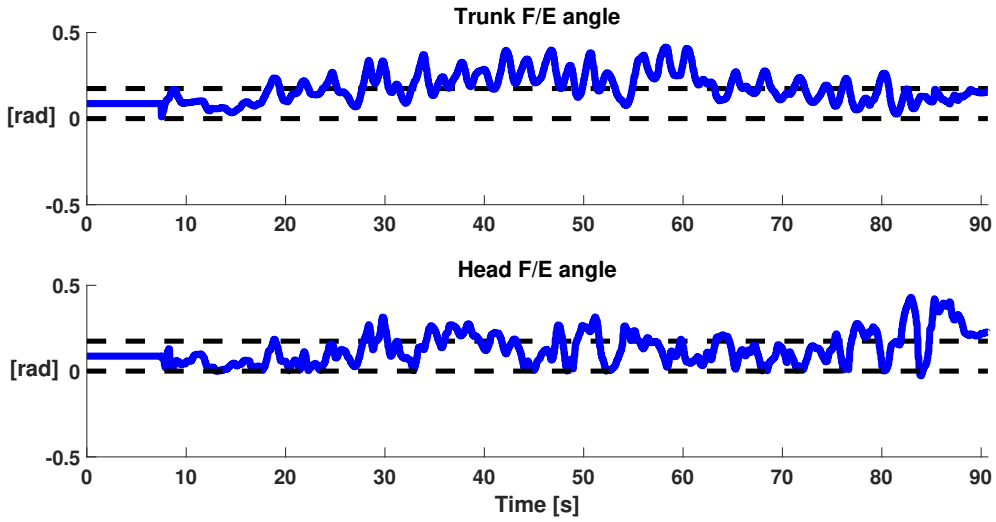

Fig. 4.6 Trend of trunk and head F/E angles during task execution without feedback. The angle behaviour is shown in blue, the angle thresholds (i.e. 0 and 0.17 rad) are in black.

In Figs. 4.11 and 4.12 the NIPT for head and trunk computed on all the subjects, independently of the group they belong to, is shown for the three described conditions, i.e. No FB, VF and VtF. The statistically significant differences are outlined with an asterisc. As evident, when some kind of feedback is provided to the subjects, NIPT is reduced both for head and trunk with respect to the absence of feedback. These differences are statistically

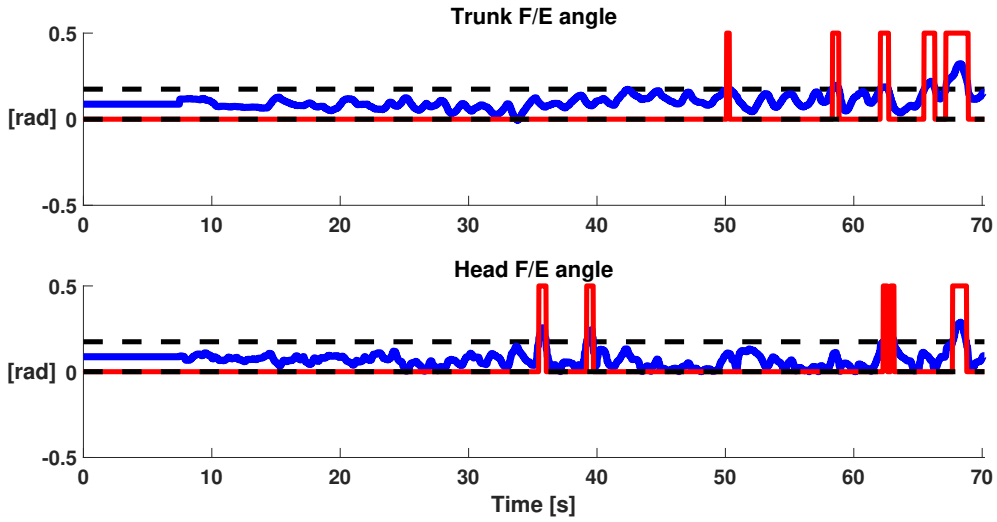

Fig. 4.7 Trend of trunk and head F/E angles reached by one representative subject belonging to Group 2 during task execution with VF. The angle behaviour is shown in blue, the angle thresholds (i.e. 0 and 0.17 rad) are in black and the VF provided to the subjects when they exceed the thresholds is outlined in red.

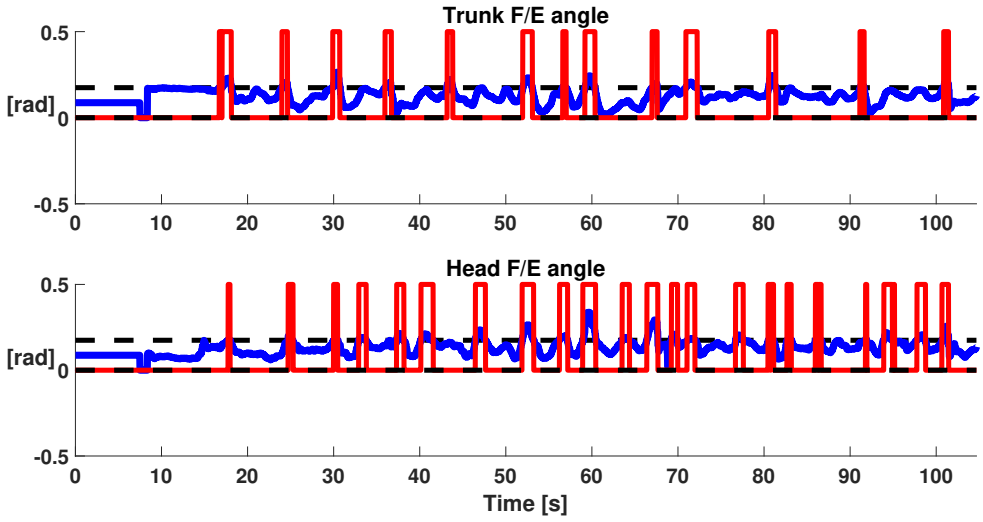

Fig. 4.8 Trend of trunk and head F/E angles reached by one representative subject belonging to Group 1 during task execution with VF. The angle behaviour is shown in blue, the angle thresholds (i.e. 0 and 0.17 rad) are in black and the VF provided to the subjects when they exceed the thresholds is outlined in red.

significant for No FB vs VF and for No FB vs VtF ($p-value<0.017$) for both the angles. No statistically significant differences are obtained for NIPT between the two types of feedback (i.e. VF vs VtF) ($p-value>0.017$). NIPT mean values and standard deviations are also listed in Tab. 4.2 with the statistical significance. These results confirm the feasibility

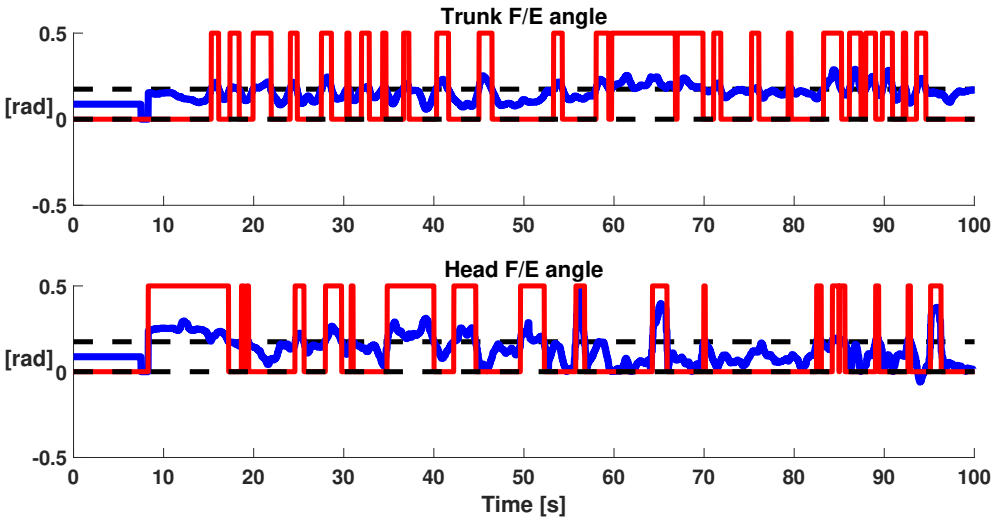

Fig. 4.9 Trend of trunk and head F/E angles reached by one representative subject belonging to Group 2 during task execution with VtF. The angle behaviour is shown in blue, the angle thresholds (i.e. 0 and 0.17 rad) are in black and the VF provided to the subjects when they exceed the thresholds is outlined in red.

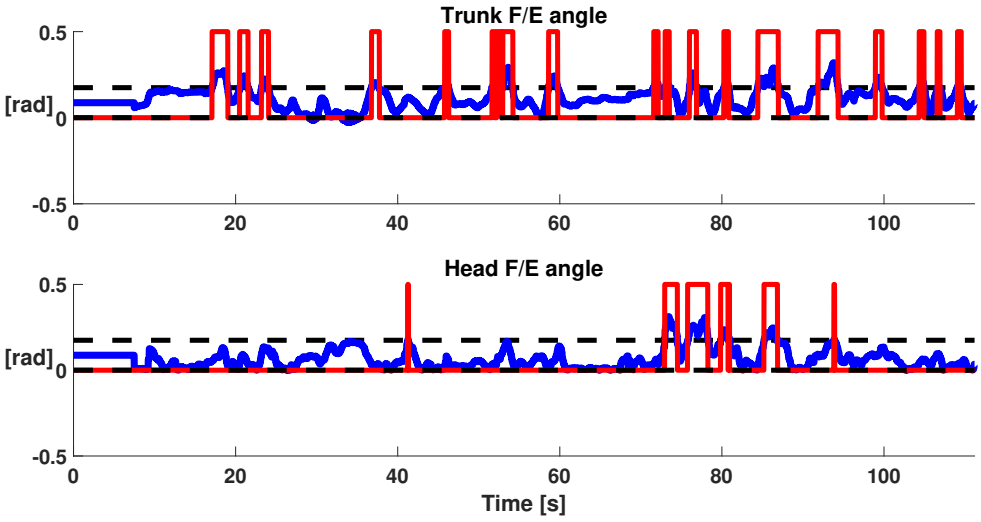

Fig. 4.10 Trend of trunk and head F/E angles reached by one representative subject belonging to Group 1 during task execution with VtF. The angle behaviour is shown in blue, the angle thresholds (i.e. 0 and 0.17 rad) are in black and the VF provided to the subjects when they exceed the thresholds is outlined in red.

and utility of providing feedback to the patients for correcting postures during robot-aided rehabilitation and therefore for improving the outcome of the therapy.

In Fig.4.13 the reaction time is reported for each type of feedback provided to the users. More in detail, the mean reaction time for VF computed on all the subjects, independently of

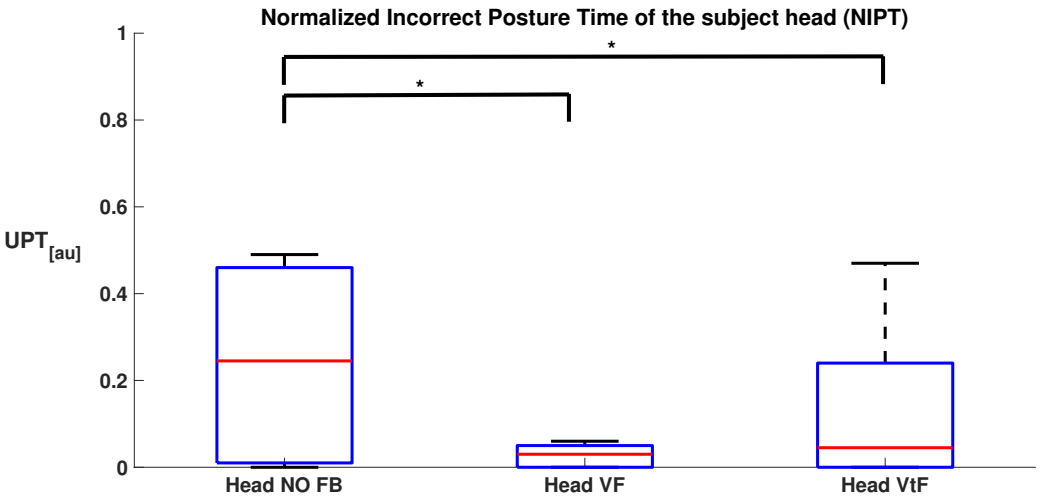

Fig. 4.11 Normalized Incorrect Posture Time (NIPT) of subject head.

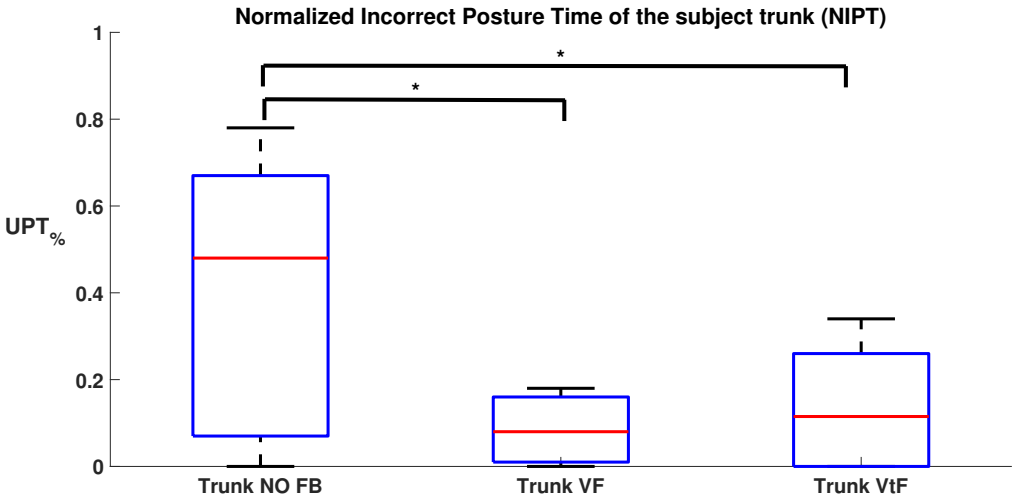

Fig. 4.12 Normalized Incorrect Posture Time (NIPT) of subject trunk.

	No FB [au]	VF [au]	VtF [au]
Head	0.24 ± 0.21	$(0.03 \pm 0.03)^*$	$(0.13 \pm 0.19)^*$
Trunk	0.41 ± 0.32	$(0.1 \pm 0.08)^*$	$(0.14 \pm 0.13)^*$

Table 4.2 Mean and std of NIPT for head in trunk in the three described conditions.

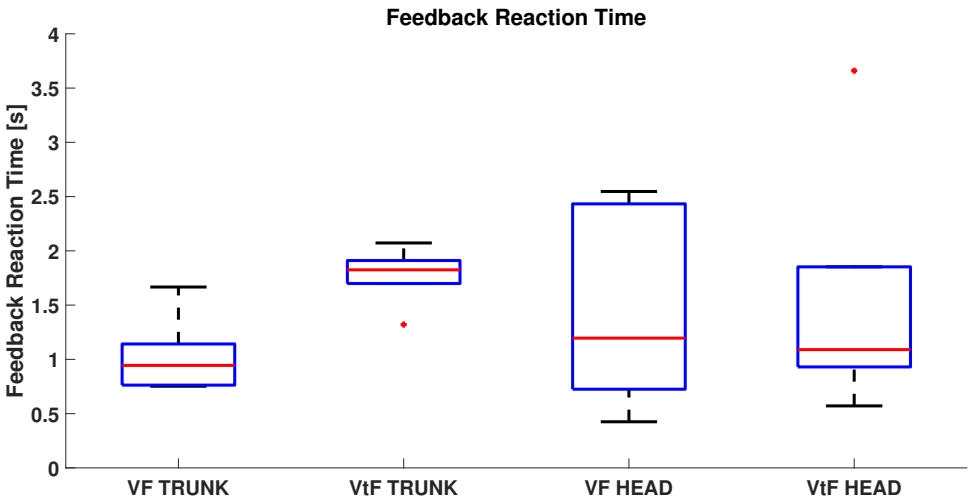

Fig. 4.13 Reaction time for VF and VtF reported for the head and trunk.

the group they belong to, is 1.48 ± 1.06 s for the head and 1.02 ± 0.60 s for the trunk. In the case of VtF, the average reaction time is 1.77 ± 0.84 s for the head and 1.52 ± 1.26 s for the trunk. Statistical analysis revealed that the difference in the reaction time obtained with the VF and the VtF for both the head and trunk is statistically significant ($p - value < 0.05$). It means that the subjects require less time to react to the VF with respect to the VtF.
Table 4.3 reports the users' answers to the questionnaire in terms of how much the subjects strongly disagreed, disagreed, neither agreed nor disagreed, agreed and strongly agreed with the statements about the VF and the VtF reported in Tab 4.1. Their evaluation can range from 1 (strongly disagree) to 5 (strongly agree). The first 5 columns contain the percentage of subjects who answered in a certain manner with respect to the total number of subjects. In the last column, the mean and standard deviation computed on all the subjects who answered to one question is shown. A statistical analysis was performed to understand if the subjects preferred one feedback modality to another. The results revealed that there are not statistically significant differences between the subjective evaluation of the two feedback modalities ($p - value > 0.05$ for the five statements). From these results it is evident that both the VF and VtF are accepted and are considered to be useful by the subjects involved in the study.

Table 4.3 Users' answers to the questionnaires, Strongly Disagree (SD) = 1 , Disagree (D) = 2, Neither agree nor disagree (N) = 3, Agree (A) = 4, Strongly Agree (SA) = 5. Results are reported as a percentage of the total subjects.

	SD	D	N	A	SA	Mean rate±std
Results about Visual Feedback						
I did not notice the Visual Feedback	20	50	30	0	0	2.1±0.2
The Visual Feedback was pleasant	0	0	40	60	0	3.6±0.3
The Visual Feedback motivated me to maintain a correct posture	0	0	0	60	40	4.4±0.3
The Visual Feedback was difficult to follow	0	60	40	0	0	2.3±0.3
I found useful the information provided by the Visual Feedback	0	0	20	70	10	3.9±0.3
Results about Vibrotactile Feedback						
I did not notice the Vibrotactile Feedback	20	40	10	30	0	2.5±0.2
The Vibrotactile Feedback was pleasant	0	20	20	50	10	3.5±0.2
The Vibrotactile Feedback motivated me to maintain a correct posture	0	0	30	70	0	3.7±0.3
The Vibrotactile Feedback was difficult to follow	30	20	20	30	0	2.5±0.1
I found useful the information provided by the Vibrotactile Feedback	0	0	20	60	20	4±0.3

Chapter 5

Conclusions and future work

In this work a bidirectional interface for rehabilitation and assistive robots that is shaped on the patient's needs was designed and developed. The interface is i) adaptable to the user's residual functional and motor capabilities and ii) works well in unstructured environments and with different robot types (e.g. manipulators, exoskeletons or prostheses). It is composed of two main modules, namely the human-machine interface for the device control and the interface for sensory feedback.

The human-machine interface for the device control was first designed to be used by trans-humeral upper-limb amputees. A novel control interface grounded on the combination of the data acquired by two M-IMUs, placed on the user trunk and stump, and two superficial EMG electrodes, positioned on the the user biceps and triceps, was proposed. The proposed approach allows the user to control prosthetic elbow and wrist movements by exploiting the two shoulder DoFs monitored by means of the M-IMUs, when the biceps and triceps are co-contracted. Otherwise, the user could control grasp and release of the hand by contracting biceps and triceps, respectively; elbow and wrist joints will not move, in this case, since the target muscles are not co-contracted.

It is interesting to note that this approach allows performing simultaneous movements and improving trans-humeral amputee performance in activities of daily living, differently from the commercially available amplitude-based control that enables only sequential movements. The proposed control interface was experimentally validated on eight healthy subjects in a virtual environment reproducing four activities of daily living, i.e. reaching and grasping virtual objects differently placed on a virtual table. A comparative analysis with the traditional EMG control was carried out by means of three quantitative indices capable of describing the subject's performance: completion time, average rotational speed and success rate. From the experimental results emerged that the savings in terms of completion time, when the novel

control strategy is adopted, are significant: at worst, the duration of the task performing is reduced of 5 seconds.

Subsequently, adaptability of the proposed control interface to patients with different levels of disability and different robot types were demonstrated. Indeed, the proposed interface was tested on people with severe motor disability to control their robotic rehabilitation/assistive device, such as a manipulator or an upper-limb exoskeleton. The M-IMUs were positioned on the subject head and trunk in order to allow the user to control the robotic device my means of the head motion. Involuntary movement of the robot were avoided by means EMG superficial electrodes positioned on the subject arm that allow him/her to enable the robot motion. Two control modalities were implemented in order to modulate the frequency of the user's intervention in the robot control depending on the user's preference and cognitive/physical state. They are the M-IMUs/EMG continuous control and M-IMUs/EMG trigger control. Two experimental sessions were carried out in order to i) compare the M-IMUs/EMG interface with a standard interface made of the voice recognizer for continuously controlling the motion of a arm-hand robotic system for assistive purposes and iii) compare the M-IMUs/EMG continuous control and the M-IMUs/EMG trigger control in terms of usability and user acceptance. About the first experimental session, sixteen healthy subjects took part to the experiments; they were randomized in two groups: 8 subjects used the combined M-IMU/EMG interface, while the other ones used the voice recognizer for moving the robotic system during a drinking task. Performance indices have been extracted and questionnaires have been submitted to the subjects in order to evaluate performance and the usability of the interfaces. The obtained results pointed out that performance and level of acceptance were higher for the combined M-IMU/EMG interface with respect to the voice control.

About the second experimental session, six subjects with different upper-limb impairment conditions were asked to perform one activity of daily living, i.e. drinking, and 2 tasks belonging to the SHAP clinical test, i.e. pouring and reaching-grasping-moving-releasing a sphere, with the aid of a robotic upper-limb exoskeleton piloted by the means of both the M-IMU/EMG continuous control and M-IMU/EMG trigger control. System performance has been evaluated in terms of success rate (i.e. number of times that the activity has been correctly carried out) and by means of questionnaires about the subjective assessment of the users stress status. The obtained results demonstrated a high patient involvement in using a M-IMU/EMG continuous control, but better performance, in terms of success rate, has been achieved with the trigger-based control.

When the M-IMU/EMG trigger control is adopted, the user is only required to send a start signal to the robot and it will autonomously accomplish the task. Hence, a motion planning

system was proposed in order to make the robot perform the task in a way that is safe and accepted by the user. In this work a Motion Planning System for rehabilitation and assistive robotics, grounded on LbD approach, has been proposed. The LbD algorithm presented in this work is grounded on DMPs as in [49], but it is improved in terms of i) accuracy of the trajectory reconstruction, ii) adaptability of the DMPs to different subjects anthropometry and robotic device (e.g. manipulators or exoskeletons) ii) ability to reproduce human-like movements, iii) ability to solve orientation singularity in the DMP equations and iv) generalization capabilities with respect to different target positions. Four experimental sessions were carried out in order to assess the motion planner performance.

The first experimental session was aimed to test the proposed motion planning on eight healthy subjects who were asked to perform three activities of daily living i.e. drinking, pouring and eating with the aid of a robotic manipulator attached to their wrist. The achieved results showed that significant savings in terms of size of the database to be recorded, being equal the accuracy in the reproduction of user personal motion style could be obtained when the proposed motion planning is adopted compared to the one proposed in [49]. It is particularly important in daily living scenarios where several amount of ADLs should be learned.

The second experimental session was aimed to preliminary validate the proposed motion planner in simulation and later to experimentally validate it on 4 patients with Limb girdle muscular dystrophys, who used the combined M-IMU/EMG interface for controlling an upper-limb exoskeleton. The validation session was aimed to: i) assess performance of the proposed motion planning system by means of quantitative indicators and compare it with traditional methods used to operate upper-limb exoskeletons, which are based on path planning and inverse kinematics (IK inverse Jacobian and IK swivel angle); (ii) investigate the generalization level of the proposed approach with respect to the variability in the experimental scenario, given for example by different anthropometry of the patients and different object positions. The results achieved for the comparative analysis showed that the DMP based control guarantees a 100% success rate in the task fulfillment, with an acceptable position and orientation error for the targeted application. Moreover, it also ensures that the exoskeleton always has configurations within the physiological joint limits, differently from methods based on path planning and inverse kinematics. Furthermore, the computational time required by the proposed approach is lower than the one required by the IK algorithm with inverse Jacobian and comparable with the IK with swivel angle. Finally, the results achieved in simulation as well as in the experimental setting also showed a high generalization level of the DMP based motion planning with respect to the different object positions and subjects anthropometries. A success rate of 100% for all tasks was reported.

The third experimental session was aimed to test the proposed motion planner on a 7-DoF anthropomorphic manipulator and assess its capability in i) performing movement in a way similar to the human demonstrator both in the joint and Cartesian space and ii) avoiding obstacles. The offline database was built on healthy subjects performing 9 reaching and pouring tasks and was used to extract the Cartesian and joint DMPs. The proposed approach was experimentally tested on an anthropomorphic robot arm and a comparative analysis with a literature method based on Cartesian DMPs and IK was performed. The obtained performance indices, i.e. position error, orientation error, convex hull and PhJL, demonstrated that the proposed approach guarantees a robot anthropomorphic behaviour (always respecting the PhJL) and a robot motion similar to the one of the human demonstrator both in the Cartesian and in the joint space. Moreover, the analysis of the questionnaire results has shown that the users prefer the anthropomorphic motion planned through the proposed approach with respect to the non-anthropomorphic one planned by means of the Cartesian DMPs and IK. This supports out hypothesis that the proposed motion planner well matches needs coming from application to social contexts where the interaction between human and robots is thigh. The system generalization capability with respect to different target positions and task duration, and the robustness of the proposed approach against perturbation (i.e. obstacles along the robot kinematic chain path) has also been tested. A success rate of 100% in avoiding obstacles positioned near the robot kinematic chain and a high Cartesian accuracy ($Position\ err < 0.005\ m$ and $Orientation\ err < 0.02\ m$) was reported.

The fourth experimental session was aimed to test the ability of the proposed motion planning in solving singularity issues. To this end, the proposed motion planning was used to teach the Tiago robot how to fulfill an Activity of Daily living (ADL), i.e. the pouring task, and the obtained results were compared to the one achieved by using the original formulation of the DMPs [49] [123]. The comparative analysis were performed by means of a quantitative index aimed at evaluating the success rate of the task execution. The obtained results demonstrated the effectiveness of the proposed approach in solving singularity issues that outperformed the one proposed in [49] [123].

The interface for sensory feedback was designed and developed in order to improve user's postural control during robot-aided daily living activities, both in standing and in sitting position. The proposed approach is grounded on the combined use of magneto-inertial sensors, and vibrotactile actuators. Magneto-inertial sensors are used to detect user's incorrect posture conditions. Conversely, vibrotactile actuators are used to convey to the user information about his/her posture and hence make him/her to correct it. The proposed vibrotactile stimulation feedback was employed, during robot-aided rehabilitation, to correct patients' spine posture. Three inertial sensors were used in order to measure trunk and neck

flexion/extension (F/E) and information about user's incorrect posture were provided by two lightweight vibrating actuators located on the user's arms. Performance of the proposed stimulation feedback was evaluated by comparing it to a typical approach used in literature to notify incorrect posture to the users, i.e. visual feedback. The system performance was assessed in terms of effectiveness to improve the posture of the subject, acceptability and user's comfort. The stimulation feedback was tested on 10 healthy subjects performing 3D reaching movements with the aid of the visual and vibrotactile feedback and without any information about the correctness of his/her posture. The obtained results revealed that the user had a more correct posture while performing the task with the aid of the visual and vibrotactile feedback compared to a no feedback condition.
Future works will be mainly addressed to:

- increase the number of robot degrees of freedom that could be driven by means of the proposed control interface and test it on a greater number of assistive tasks
- test the proposed motion planning on a higher number of patients and assistive tasks, and extend the approach also to the motion planning of hand exoskeletons
- test the proposed vibrotactile stimulation feedback on a larger number of patients (e.g. patients suffering from musculoskeletal disorders.) Moreover, the proposed stimulation feedback will be combined with the proposed control interface based on M-IMUs and EMG electrodes in order to close the control loop of upper-limb prostheses by restoring tactile sensory feedback in amputees and hence fostering a more fine control of the prosthetic device.

References

[1] Adams, J. A. (2002). Critical considerations for human-robot interface development. In *Proceedings of 2002 AAAI Fall Symposium*, pages 1–8.

[2] Akamatsu, M., MacKenzie, I. S., and Hasbroucq, T. (1995). A comparison of tactile, auditory, and visual feedback in a pointing task using a mouse-type device. *Ergonomics*, 38(4):816–827.

[3] Albu-Schäffer, A., Haddadin, S., Ott, C., Stemmer, A., Wimböck, T., and Hirzinger, G. (2007). The dlr lightweight robot: design and control concepts for robots in human environments. *Industrial Robot: an international journal*, 34(5):376–385.

[4] Alexandrova, S., Cakmak, M., Hsiao, K., and Takayama, L. (2014). Robot programming by demonstration with interactive action visualizations. In *Robotics: science and systems*. Citeseer.

[5] An, C. H. (1988). Model-based control of a robot manipulator.

[6] Ananthanarayan, S., Sheh, M., Chien, A., Profita, H., and Siek, K. (2013). Pt viz: towards a wearable device for visualizing knee rehabilitation exercises. In *Proceedings of the SIGCHI Conference on Human Factors in Computing Systems*, pages 1247–1250. ACM.

[7] Babaiasl, M., Mahdioun, S. H., Jaryani, P., and Yazdani, M. (2016). A review of technological and clinical aspects of robot-aided rehabilitation of upper-extremity after stroke. *Disability and Rehabilitation: Assistive Technology*, 11(4):263–280.

[8] Baker, J. J., Scheme, E., Englehart, K., Hutchinson, D. T., and Greger, B. (2010). Continuous detection and decoding of dexterous finger flexions with implantable myoelectric sensors. *IEEE Transactions on Neural Systems and Rehabilitation Engineering*, 18(4):424–432.

[9] Barber, C. B., Dobkin, D. P., and Huhdanpaa, H. (1996). The quickhull algorithm for convex hulls. *ACM Transactions on Mathematical Software (TOMS)*, 22(4):469–483.

[10] Barea, R., Boquete, L., Mazo, M., and López, E. (2002). Wheelchair guidance strategies using eog. *Journal of intelligent and robotic systems*, 34(3):279–299.

[11] Barreto, A., Scargle, S., and Adjouadi, M. (2000). A practical emg-based human-computer interface for users with motor disabilities.

[12] Barry, D. T., Leonard, J. A., Gitter, A. J., and Ball, R. D. (1986). Acoustic myography as a control signal for an externally powered prosthesis. *Archives of physical medicine and rehabilitation*, 67(4):267–269.

[13] Bartneck, C., Croft, E., and Kulic, D. (2008). Measuring the anthropomorphism, animacy, likeability, perceived intelligence and perceived safety of robots. In *Metrics for HRI workshop, technical report*, volume 471, pages 37–44. Citeseer.

[14] Bell, C. J., Shenoy, P., Chalodhorn, R., and Rao, R. P. (2008). Control of a humanoid robot by a noninvasive brain–computer interface in humans. *Journal of neural engineering*, 5(2):214.

[15] Chen, J. R. (2005). Constructing task-level assembly strategies in robot programming by demonstration. *The International Journal of Robotics Research*, 24(12):1073–1085.

[16] Chevalley, C. (2018). *Theory of Lie groups*. Courier Dover Publications.

[17] Ciancio, A. L., Cordella, F., Barone, R., Romeo, R. A., Bellingegni, A. D., Sacchetti, R., Davalli, A., Di Pino, G., Ranieri, F., Di Lazzaro, V., et al. (2016). Control of prosthetic hands via the peripheral nervous system. *Frontiers in neuroscience*, 10:116.

[18] Cordella, F., Ciancio, A. L., Sacchetti, R., Davalli, A., Cutti, A. G., Guglielmelli, E., and Zollo, L. (2016). Literature review on needs of upper limb prosthesis users. *Frontiers in neuroscience*, 10:209.

[19] Cordella, F., Di Corato, F., Loianno, G., Siciliano, B., and Zollo, L. (2013). Robust pose estimation algorithm for wrist motion tracking. In *IEEE/RSJ International Conference on Intelligent Robots and Systems*, pages 3746–3751. IEEE.

[20] Cordella, F., Di Corato, F., Siciliano, B., and Zollo, L. (2017). A stochastic algorithm for automatic hand pose and motion estimation. *Medical & biological engineering & computing*, 55(12):2197–2208.

[21] Crea, S., Cempini, M., Moisè, M., Baldoni, A., Trigili, E., Marconi, D., Cortese, M., Giovacchini, F., Posteraro, F., and Vitiello, N. (2016). A novel shoulder-elbow exoskeleton with series elastic actuators. In *Biomedical Robotics and Biomechatronics (BioRob), 2016 6th IEEE International Conference on*, pages 1248–1253. IEEE.

[22] Dario, P., Guglielmelli, E., and Laschi, C. (2001). Humanoids and personal robots: Design and experiments. *Journal of robotic systems*, 18(12):673–690.

[23] Dimitrov, G. V., Arabadzhiev, T. I., Mileva, K. N., Bowtell, J. L., Crichton, N., and Dimitrova, N. A. (2006). Muscle fatigue during dynamic contractions assessed by new spectral indices. *Medicine and science in sports and exercise*, 38(11):1971.

[24] Dipietro, L., Sabatini, A. M., Dario, P., et al. (2008). A survey of glove-based systems and their applications. *IEEE Trans. Systems, Man, and Cybernetics, Part C*, 38(4):461–482.

[25] Duffy, B. R. (2003). Anthropomorphism and the social robot. *Robotics and autonomous systems*, 42(3-4):177–190.

[26] Eimer, M. (2004). Multisensory integration: how visual experience shapes spatial perception. *Current biology*, 14(3):R115–R117.

[27] Evans, D. J. (1977). On the representatation of orientation space. *Molecular Physics*, 34(2):317–325.

[28] Fajen, B. R. and Warren, W. H. (2003). Behavioral dynamics of steering, obstable avoidance, and route selection. *Journal of Experimental Psychology: Human Perception and Performance*, 29(2):343.

[29] Fan, R. E., Culjat, M. O., King, C.-H., Franco, M. L., Boryk, R., Bisley, J. W., Dutson, E., and Grundfest, W. S. (2008). A haptic feedback system for lower-limb prostheses. *IEEE Transactions on Neural Systems and Rehabilitation Engineering*, 16(3):270–277.

[30] Flash, T. and Hogan, N. (1985). The coordination of arm movements: an experimentally confirmed mathematical model. *Journal of neuroscience*, 5(7):1688–1703.

[31] Friedrich, M., Cermak, T., and Maderbacher, P. (1996). The effect of brochure use versus therapist teaching on patients performing therapeutic exercise and on changes in impairment status. *Physical Therapy*, 76(10):1082–1088.

[32] Fukuda, O., Tsuji, T., Kaneko, M., and Otsuka, A. (2003). A human-assisting manipulator teleoperated by emg signals and arm motions. *IEEE Transactions on Robotics and Automation*, 19(2):210–222.

[33] Fukuda, O., Tsuji, T., Ohtsuka, A., and Kaneko, M. (1998). Emg-based human-robot interface for rehabilitation aid. In *Robotics and Automation, 1998. Proceedings. 1998 IEEE International Conference on*, volume 4, pages 3492–3497. IEEE.

[34] Gescheider, G. A. and Wright, J. H. (1968). Effects of sensory adaptation on the form of the psychophysical magnitude function for cutaneous vibration. *Journal of experimental psychology*, 77(2):308.

[35] Gorostiza, J. F., Barber, R., Khamis, A. M., Malfaz, M., Pacheco, R., Rivas, R., Corrales, A., Delgado, E., and Salichs, M. A. (2006). Multimodal human-robot interaction framework for a personal robot. In *ROMAN 2006-The 15th IEEE International Symposium on Robot and Human Interactive Communication*, pages 39–44. IEEE.

[36] Griffin, W. B., Findley, R. P., Turner, M. L., and Cutkosky, M. R. (2000). Calibration and mapping of a human hand for dexterous telemanipulation. In *ASME IMECE 2000 Symposium on Haptic Interfaces for Virtual Environments and Teleoperator Systems*, pages 1–8.

[37] Grigorescu, S. M., Lüth, T., Fragkopoulos, C., Cyriacks, M., and Gräser, A. (2012). A bci-controlled robotic assistant for quadriplegic people in domestic and professional life. *Robotica*, 30(3):419–431.

[38] Hegel, F., Krach, S., Kircher, T., Wrede, B., and Sagerer, G. (2008). Understanding social robots: A user study on anthropomorphism. In *Robot and Human Interactive Communication, 2008. RO-MAN 2008. The 17th IEEE International Symposium on*, pages 574–579. IEEE.

[39] Held, J. P., Klaassen, B., van Beijnum, B.-J. F., Luft, A. R., and Veltink, P. H. (2017). Usability evaluation of a vibrotactile feedback system in stroke subjects. *Frontiers in bioengineering and biotechnology*, 4:98.

[40] Higgins, W. T. (1975). A comparison of complementary and kalman filtering. *IEEE Transactions on Aerospace and Electronic Systems*, (3):321–325.

[41] Hoc, J.-M. (2000). From human–machine interaction to human–machine cooperation. *Ergonomics*, 43(7):833–843.

[42] Hochberg, L. R., Bacher, D., Jarosiewicz, B., Masse, N. Y., Simeral, J. D., Vogel, J., Haddadin, S., Liu, J., Cash, S. S., van der Smagt, P., et al. (2012). Reach and grasp by people with tetraplegia using a neurally controlled robotic arm. *Nature*, 485(7398):372.

[43] Hocking, C. (1999). Function or feelings: factors in abandonment of assistive devices. *Technology and Disability*, 11(1, 2):3–11.

[44] Hoffmann, H., Pastor, P., Park, D.-H., and Schaal, S. (2009). Biologically-inspired dynamical systems for movement generation: automatic real-time goal adaptation and obstacle avoidance. In *Robotics and Automation, 2009. ICRA'09. IEEE International Conference on*, pages 2587–2592. IEEE.

[45] Hoozemans, M. J. and Van Dieen, J. H. (2005). Prediction of handgrip forces using surface emg of forearm muscles. *Journal of electromyography and kinesiology*, 15(4):358–366.

[46] House, B., Malkin, J., and Bilmes, J. (2009). The voicebot: a voice controlled robot arm. In *Proceedings of the SIGCHI Conference on Human Factors in Computing Systems*, pages 183–192. ACM.

[47] Howcroft, J., Lemaire, E. D., Kofman, J., and Kendell, C. (2016). Understanding responses to gait instability from plantar pressure measurement and the relationship to balance and mobility in lower-limb amputees. *Clinical Biomechanics*, 32:241–248.

[48] iARM (2016). Exact dynamics. www.exactdynamics.nl/site/?page=iarm. Accessed: 2016.

[49] Ijspeert, A. J., Nakanishi, J., Hoffmann, H., Pastor, P., and Schaal, S. (2013). Dynamical movement primitives: learning attractor models for motor behaviors. *Neural computation*, 25(2):328–373.

[50] Jackson, A. and Zimmermann, J. B. (2012). Neural interfaces for the brain and spinal cord—restoring motor function. *Nature Reviews Neurology*, 8(12):690.

[51] Jaffe, D. L., Brown, D. A., Pierson-Carey, C. D., Buckley, E. L., and Lew, H. L. (2004). Stepping over obstacles to improve walking in individuals with poststroke hemiplegia. *Journal of Rehabilitation Research & Development*, 41.

[52] Jentsch, F. (2016). *Human-robot interactions in future military operations*. CRC Press.

[53] Jiang, L., Shisheie, R., Cheng, M. H., Banta, L. E., and Guo, G. (2013). Moving trajectories and controller synthesis for an assistive device for arm rehabilitation. In *Automation Science and Engineering (CASE), 2013 IEEE International Conference on*, pages 268–273. IEEE.

[54] Kaczmarek, K. A., Webster, J. G., Bach-y Rita, P., and Tompkins, W. J. (1991). Electrotactile and vibrotactile displays for sensory substitution systems. *IEEE Transactions on Biomedical Engineering*, 38(1):1–16.

[55] Kairy, D., Lehoux, P., Vincent, C., and Visintin, M. (2009). A systematic review of clinical outcomes, clinical process, healthcare utilization and costs associated with telerehabilitation. *Disability and rehabilitation*, 31(6):427–447.

[56] Kiguchi, K., Tanaka, T., and Fukuda, T. (2004). Neuro-fuzzy control of a robotic exoskeleton with emg signals. *IEEE Transactions on fuzzy systems*, 12(4):481–490.

[57] Kim, D.-J., Lovelett, R., and Behal, A. (2009). Eye-in-hand stereo visual servoing of an assistive robot arm in unstructured environments. In *Robotics and Automation, 2009. ICRA'09. IEEE International Conference on*, pages 2326–2331. IEEE.

[58] Kim, H., Miller, L. M., Byl, N., Abrams, G. M., and Rosen, J. (2012). Redundancy resolution of the human arm and an upper limb exoskeleton. *IEEE Transactions on Biomedical Engineering*, 59(6):1770–1779.

[59] Koritnik, T., Koenig, A., Bajd, T., Riener, R., and Munih, M. (2010). Comparison of visual and haptic feedback during training of lower extremities. *Gait & posture*, 32(4):540–546.

[60] Kuiken, T. A., Li, G., Lock, B. A., Lipschutz, R. D., Miller, L. A., Stubblefield, K. A., and Englehart, K. B. (2009). Targeted muscle reinnervation for real-time myoelectric control of multifunction artificial arms. *Jama*, 301(6):619–628.

[61] Lam, A. W., HajYasien, A., and Kulic, D. (2014). Improving rehabilitation exercise performance through visual guidance. In *Engineering in Medicine and Biology Society (EMBC), 2014 36th Annual International Conference of the IEEE*, pages 1735–1738. IEEE.

[62] Lauretti, C., Cordella, F., , and Zollo, L. (2009). A hybrid joint/cartesian dmp-based approach for obstacle avoidance of anthropomorphic assistive robots. *International Journal of Social Robotics*.

[63] Lauretti, C., Cordella, F., Ciancio, A. L., Trigili, E., Catalan, J. M., Badesa, F. J., Crea, S., Pagliara, S. M., Sterzi, S., Vitiello, N., et al. (2018). Learning by demonstration for motion planning of upper-limb exoskeletons. *Frontiers in neurorobotics*, 12:5.

[64] Lauretti, C., Cordella, F., di Luzio, F. S., Saccucci, S., Davalli, A., Sacchetti, R., and Zollo, L. (2017a). Comparative performance analysis of m-imu/emg and voice user interfaces for assistive robots. In *Rehabilitation Robotics (ICORR), 2017 International Conference on*, pages 1001–1006. IEEE.

[65] Lauretti, C., Cordella, F., Guglielmelli, E., and Zollo, L. (2017b). Learning by demonstration for planning activities of daily living in rehabilitation and assistive robotics. *IEEE Robotics and Automation Letters*, 2(3):1375–1382.

[66] Lauretti, C., Davalli, A., Sacchetti, R., Guglielmelli, E., and Zollo, L. (2016). Fusion of m-imu and emg signals for the control of trans-humeral prostheses. In *Biomedical Robotics and Biomechatronics (BioRob), 2016 6th IEEE International Conference on*, pages 1123–1128. IEEE.

[67] Lauretti, C., Pinzari, G., Ciancio, A. L., Davalli, A., Sacchetti, R., Sterzi, S., Guglielmelli, E., and Zollo, L. (2017c). A vibrotactile stimulation system for improving postural control and knee joint proprioception in lower-limb amputees. In *Robot and Human Interactive Communication (RO-MAN), 2017 26th IEEE International Symposium on*, pages 88–93. IEEE.

[68] Lee, J. and Moray, N. (1992). Trust, control strategies and allocation of function in human-machine systems. *Ergonomics*, 35(10):1243–1270.

[69] Lee, W., Kang, S., Kim, M., and Park, M. (2004). Robhaz-dt3: teleoperated mobile platform with passively adaptive double-track for hazardous environment applications. In *Intelligent Robots and Systems, 2004.(IROS 2004). Proceedings. 2004 IEEE/RSJ International Conference on*, volume 1, pages 33–38. IEEE.

[70] Liarokapis, M. V., Artemiadis, P. K., and Kyriakopoulos, K. J. (2012). Functional anthropomorphism for human to robot motion mapping. In *RO-MAN, 2012 IEEE*, pages 31–36. IEEE.

[71] Lourakis, M. I. (2005). A brief description of the levenberg-marquardt algorithm implemented by levmar. *Foundation of Research and Technology*, 4(1).

[72] Lund, A. M. (2001). Measuring usability with the use questionnaire12. *Usability interface*, 8(2):3–6.

[73] Lv, X., Zhang, M., and Li, H. (2008). Robot control based on voice command. In *Automation and Logistics, 2008. ICAL 2008. IEEE International Conference on*, pages 2490–2494. IEEE.

[74] Magermans, D., Chadwick, E., Veeger, H., and Van Der Helm, F. (2005). Requirements for upper extremity motions during activities of daily living. *Clinical biomechanics*, 20(6):591–599.

[75] Maheu, V., Archambault, P. S., Frappier, J., and Routhier, F. (2011). Evaluation of the jaco robotic arm: Clinico-economic study for powered wheelchair users with upper-extremity disabilities. In *Rehabilitation Robotics (ICORR), 2011 IEEE International Conference on*, pages 1–5. IEEE.

[76] Marchal-Crespo, L. and Reinkensmeyer, D. J. (2009). Review of control strategies for robotic movement training after neurologic injury. *Journal of neuroengineering and rehabilitation*, 6(1):20.

[77] Meier, R. and Atkins, D. (2007). Functional restoration of adults and children with upper extremity amputation. *Res Trends for the Twenty-First Century*, 30(30):353–360.

[78] Merlo, A., Longhi, M., Giannotti, E., Prati, P., Giacobbi, M., Ruscelli, E., Mancini, A., Ottaviani, M., Montanari, L., and Mazzoli, D. (2013). Upper limb evaluation with robotic exoskeleton. normative values for indices of accuracy, speed and smoothness. *NeuroRehabilitation*, 33(4):523–530.

[79] Mihelj, M. (2006). Human arm kinematics for robot based rehabilitation. *Robotica*, 24(3):377–383.

[80] Miller, N., Jenkins, O. C., Kallmann, M., and Mataric, M. J. (2004). Motion capture from inertial sensing for untethered humanoid teleoperation. In *Humanoid Robots, 2004 4th IEEE/RAS International Conference on*, volume 2, pages 547–565. IEEE.

[81] Murphy, R. R., Nomura, T., Billard, A., and Burke, J. L. (2010). Human–robot interaction. *IEEE robotics & automation magazine*, 17(2):85–89.

[82] Nordin, N., Xie, S. Q., and Wünsche, B. (2014). Assessment of movement quality in robot-assisted upper limb rehabilitation after stroke: a review. *Journal of neuroengineering and rehabilitation*, 11(1):137.

[83] Novak, D. and Riener, R. (2015). A survey of sensor fusion methods in wearable robotics. *Robotics and Autonomous Systems*, 73:155–170.

[84] Okamura, A. M. (2004). Methods for haptic feedback in teleoperated robot-assisted surgery. *Industrial Robot: An International Journal*, 31(6):499–508.

[85] Orsag, M., Korpela, C., Oh, P., and Bogdan, S. (2018). Coordinate systems and transformations. In *Aerial Manipulation*, pages 19–31. Springer.

[86] Pagel, A., Arieta, A. H., Riener, R., and Vallery, H. (2016). Effects of sensory augmentation on postural control and gait symmetry of transfemoral amputees: a case description. *Medical & biological engineering & computing*, 54(10):1579–1589.

[87] Papaleo, E., Zollo, L., Garcia-Aracil, N., Badesa, F. J., Morales, R., Mazzoleni, S., Sterzi, S., and Guglielmelli, E. (2015). Upper-limb kinematic reconstruction during stroke robot-aided therapy. *Medical & biological engineering & computing*, 53(9):815–828.

[88] Park, D.-H., Hoffmann, H., Pastor, P., and Schaal, S. (2008). Movement reproduction and obstacle avoidance with dynamic movement primitives and potential fields. In *Humanoid Robots, 2008. Humanoids 2008. 8th IEEE-RAS International Conference on*, pages 91–98. IEEE.

[89] Parker, J., Mountain, G., and Hammerton, J. (2011). A review of the evidence underpinning the use of visual and auditory feedback for computer technology in post-stroke upper-limb rehabilitation. *Disability and rehabilitation: Assistive technology*, 6(6):465–472.

[90] Pastor, P., Hoffmann, H., Asfour, T., and Schaal, S. (2009). Learning and generalization of motor skills by learning from demonstration. In *Robotics and Automation, 2009. ICRA'09. IEEE International Conference on*, pages 763–768. IEEE.

[91] Perrin, S., Cassinelli, A., and Ishikawa, M. (2004). Gesture recognition using laser-based tracking system. In *Automatic Face and Gesture Recognition, 2004. Proceedings. Sixth IEEE International Conference on*, pages 541–546. IEEE.

[92] Peterka, R. J., Wall Iii, C., and Kentala, E. (2006). Determining the effectiveness of a vibrotactile balance prosthesis. *Journal of Vestibular Research*, 16(1, 2):45–56.

[93] Prensilia (2016). http://www.prensilia.com/index.php?q=en/node/40. Accessed: 2016.

[94] Provenzale, A., Cordella, F., Zollo, L., Davalli, A., Sacchetti, R., and Guglielmelli, E. (2014). A grasp synthesis algorithm based on postural synergies for an anthropomorphic arm-hand robotic system. In *Biomedical Robotics and Biomechatronics (2014 5th IEEE RAS & EMBS International Conference on*, pages 958–963. IEEE.

[95] Pulliam, C. L., Lambrecht, J. M., and Kirsch, R. F. (2011). Emg-based neural network control of transhumeral prostheses. *Journal of rehabilitation research and development*, 48(6):739.

[96] Rab, G., Petuskey, K., and Bagley, A. (2002). A method for determination of upper extremity kinematics. *Gait & posture*, 15(2):113–119.

[97] Rai, A., Meier, F., Ijspeert, A., and Schaal, S. (2014). Learning coupling terms for obstacle avoidance. In *Humanoid Robots (Humanoids), 2014 14th IEEE-RAS International Conference on*, pages 512–518. IEEE.

[98] Riener, R., Frey, M., Bernhardt, M., Nef, T., and Colombo, G. (2005). Human-centered rehabilitation robotics. In *Rehabilitation Robotics, 2005. ICORR 2005. 9th International Conference on*, pages 319–322. IEEE.

[99] Riskind, J. H. and Gotay, C. C. (1982). Physical posture: Could it have regulatory or feedback effects on motivation and emotion? *Motivation and Emotion*, 6(3):273–298.

[100] Rodríguez-Angeles, A., Guzmán-Gutiérrez, J. L., and Cruz-Villar, C. (2010). User wearable interface based on inertial sensors for unilateral master-slave robot teleoperation. In *Electrical Engineering Computing Science and Automatic Control (CCE), 2010 7th International Conference on*, pages 458–463. IEEE.

[101] Rogalla, O., Ehrenmann, M., Zollner, R., Becher, R., and Dillmann, R. (2002). Using gesture and speech control for commanding a robot assistant. In *Robot and Human Interactive Communication, 2002. Proceedings. 11th IEEE International Workshop on*, pages 454–459. IEEE.

[102] Roggen, D., Calatroni, A., Rossi, M., Holleczek, T., Förster, K., Tröster, G., Lukowicz, P., Bannach, D., Pirkl, G., Ferscha, A., et al. (2010). Collecting complex activity datasets in highly rich networked sensor environments. In *Networked Sensing Systems (INSS), 2010 Seventh International Conference on*, pages 233–240. IEEE.

[103] Rosado, C. and Simone, L. (2007). Translational haptic feedback for post-stroke rehabilitation. In *Bioengineering Conference, 2007. NEBC'07. IEEE 33rd Annual Northeast*, pages 259–260. IEEE.

[104] Sardini, E., Serpelloni, M., Pasqui, V., et al. (2015). Wireless wearable t-shirt for posture monitoring during rehabilitation exercises. *IEEE Trans. Instrumentation and Measurement*, 64(2):439–448.

[105] Schaal, S. and Atkeson, C. G. (1998). Constructive incremental learning from only local information. *Neural computation*, 10(8):2047–2084.

[106] Scheme, E. and Englehart, K. (2011). Electromyogram pattern recognition for control of powered upper-limb prostheses: state of the art and challenges for clinical use. *Journal of Rehabilitation Research & Development*, 48(6).

[107] Scotto di Luzio, F., Cordella, F., Lauretti, C., Simonetti, D., Sterzi, S., Draicchio, F., and Zollo, L. (2019a). A bio-cooperative robotic system to ensure ergonomic postures during upper limb rehabilitation in occupational contexts. In *Advances in Intelligent Systems and Computing*, pages 327–336. Springer.

[108] Scotto di Luzio, F., Lauretti, C., Cordella, F. C., Draicchio, F., and Zollo, L. (2019b). Visual vs vibrotactile feedback for posture assessment during upper-limb robot-aided rehabilitation. *Applied ergonomics*.

[109] Scotto di Luzio, F., Simonetti, D., Cordella, F., Carpino, G., Draicchio, F., and Zollo, L. (2018a). An adaptive arm-weight support platform for 3d upper limb robot-aided neuro-rehabilitation. In *2018 7th IEEE International Conference on Biomedical Robotics and Biomechatronics (Biorob)*, pages 426–431. IEEE.

[110] Scotto di Luzio, F., Simonetti, D., Cordella, F., Miccinilli, S., Sterzi, S., Draicchio, F., and Zollo, L. (2018b). Bio-cooperative approach for the human-in-the-loop control of an end-effector rehabilitation robot. *Frontiers in neurorobotics*, 12.

[111] Shi, F., Cao, Q., Leng, C., and Tan, H. (2010). Based on force sensing-controlled human-machine interaction system for walking assistant robot. In *2010 8th World Congress on Intelligent Control and Automation*, pages 6528–6533. IEEE.

[112] Siciliano, B., Sciavicco, L., Villani, L., and Oriolo, G. (2009). Robotics–modelling, planning and control. advanced textbooks in control and signal processing series.

[113] Siciliano, B., Sciavicco, L., Villani, L., and Oriolo, G. (2010). *Robotics: modelling, planning and control*. Springer Science & Business Media.

[114] Sigrist, R., Rauter, G., Riener, R., and Wolf, P. (2013). Augmented visual, auditory, haptic, and multimodal feedback in motor learning: a review. *Psychonomic bulletin & review*, 20(1):21–53.

[115] Simon, A. M., Hargrove, L. J., Lock, B. A., and Kuiken, T. A. (2011). The target achievement control test: Evaluating real-time myoelectric pattern recognition control of a multifunctional upper-limb prosthesis. *Journal of rehabilitation research and development*, 48(6):619.

[116] Spataro, R., Chella, A., Allison, B., Giardina, M., Sorbello, R., Tramonte, S., Guger, C., and La Bella, V. (2017). Reaching and grasping a glass of water by locked-in als patients through a bci-controlled humanoid robot. *Frontiers in human neuroscience*, 11:68.

[117] Sun, M., Ren, X., and Cao, X. (2010). Effects of multimodal error feedback on human performance in steering tasks. *Journal of Information Processing*, 18:284–292.

[118] Svinin, M. M., Goncharenko, I. A., Hosoe, S., and Osada, Y. (2010). *Optimality Principles and Motion Planning of Human-Like Reaching Movements*. INTECH Open Access Publisher.

[119] Tan, H., Erdemir, E., Kawamura, K., and Du, Q. (2011). A potential field method-based extension of the dynamic movement primitive algorithm for imitation learning with obstacle avoidance. In *Mechatronics and Automation (ICMA), 2011 International Conference on*, pages 525–530. IEEE.

[120] Tan, J., Xing, Y., Fan, W., and Hong, P. (2018). Smooth orientation interpolation using parametric quintic-polynomial-based quaternion spline curve. *Journal of Computational and Applied Mathematics*, 329:256–267.

[121] Tangsuksant, W., Aekmunkhongpaisal, C., Cambua, P., Charoenpong, T., and Chanwimalueang, T. (2012). Directional eye movement detection system for virtual keyboard controller. In *Biomedical Engineering International Conference (BMEiCON), 2012*, pages 1–5. IEEE.

[122] Thielman, G. (2010). Rehabilitation of reaching poststroke: a randomized pilot investigation of tactile versus auditory feedback for trunk control. *Journal of Neurologic Physical Therapy*, 34(3):138–144.

[123] Ude, A., Nemec, B., Petrić, T., and Morimoto, J. (2014). Orientation in cartesian space dynamic movement primitives. In *Robotics and Automation (ICRA), 2014 IEEE International Conference on*, pages 2997–3004. IEEE.

[124] Van der Meijden, O. A. and Schijven, M. P. (2009). The value of haptic feedback in conventional and robot-assisted minimal invasive surgery and virtual reality training: a current review. *Surgical endoscopy*, 23(6):1180–1190.

[125] van Vliet, P. and Wulf, G. (2006). Extrinsic feedback for motor learning after stroke: what is the evidence?. *Disability and Rehabilitation*, 28(13–14):831–840.

[126] Wall Iii, C. and Kentala, E. (2005). Control of sway using vibrotactile feedback of body tilt in patients with moderate and severe postural control deficits. *Journal of Vestibular Research*, 15(5, 6):313–325.

[127] Yap, H. K., Mao, A., Goh, J. C., and Yeow, C.-H. (2016). Design of a wearable fmg sensing system for user intent detection during hand rehabilitation with a soft robotic glove. In *2016 6th IEEE International Conference on Biomedical Robotics and Biomechatronics (BioRob)*, pages 781–786. IEEE.

[128] Yin, Y. H., Fan, Y. J., and Xu, L. D. (2012). Emg and epp-integrated human–machine interface between the paralyzed and rehabilitation exoskeleton. *IEEE Transactions on Information Technology in Biomedicine*, 16(4):542–549.

[129] Young, A. J., Smith, L. H., Rouse, E. J., and Hargrove, L. J. (2013). Classification of simultaneous movements using surface emg pattern recognition. *IEEE Transactions on Biomedical Engineering*, 60(5):1250–1258.

[130] Young, A. J., Smith, L. H., Rouse, E. J., and Hargrove, L. J. (2014). A comparison of the real-time controllability of pattern recognition to conventional myoelectric control for discrete and simultaneous movements. *Journal of neuroengineering and rehabilitation*, 11(1):5.

[131] Zheng, Y. and Morrell, J. B. (2013). Comparison of visual and vibrotactile feedback methods for seated posture guidance. *IEEE transactions on haptics*, 6(1):13–23.